NTNU

Norwegian University of
Science and Technology

Modelling and estimation of ocean wave induced error in pressure measurement

Eirik Ariansen Haaland

Master of Science in Industrial Cybernetics
Submission date: June 2017
Supervisor: Edmund Førland Brekke, ITK
Co-supervisor: Are Baardsgaard Willumsen, Kongsberg Maritime

Norwegian University of Science and Technology
Department of Engineering Cybernetics

Problem Description

The pressure sensor as a depth measuring device is important for underwater vehicles. A good model of the sensor's performance is a vital tool for optimally utilizing the sensor readings in a full navigation system. The assignment will focus on improving the sensor model, testing and verifying the benefits of using the improved model by simulations and on real data.

Preface

This thesis is the academic end product of the course *TTK4900 - Engineering Cybernetics, Master's Thesis*. The course is mandatory for students in *Industrial Cybernetics*. The project was carried out during the spring of 2017. The assignment was presented by control systems engineer Are B. Willumsen at Kongsberg Maritime AS. From him I received consultation, software and test data.

The reader of this paper is expected to understand basic terminology regarding physics, such as pressure. In addition, a familiarity with statistics and estimation processes will add to the understanding of the methods presented here.

Trondheim, 2017-6-06

Eirik A. Haaland

Acknowledgment

I would like to thank Kongsberg Maritime for providing me with real sensor data and the navigation and processing software Navlab.

I would also like to thank the people at my office, Fredrik Ulvin, Oskar Lund and Kristine Elisabeth Aas Herje for lending me the extra computing capacity.

Lastly, I want to thank my supervisors, Edmund F. Brekke and Are B. Willumsen for their dedication and guidance. An extra thanks to Are for making himself so available.

Sammendrag

Undervannsfarkoster benytter trykksensorer til å måle fartøyets dybde. Disse målingene er utsatt for støy fra bølger. En estimatoralgoritme blir benyttet på målingene for å redusere virkning av den bølgeinduserte støyen. Denne algoritmen avhenger av matematiske modeller som beskriver støydynamikken. Siden bølger er osillatoriske er det naturlig at også bølgestøymodellen er det. Denne osillatoriske prosessen krever et estimat av bølgefrekvensen. En modell som estimererte bølgefrekvens i tillegg til bølgestøy ble utviklet. Modellen fikk data fra simulerte og ekte målinger. Estimatene av målingene ble sammenlignet med estimater fra en etablert estimatormodell. Den osillatoriske modellen ga noe mer nøyaktige dybdeestimater enn den etablerte modellen før parameterjustering. Dette til tross for at den hadde problemer med å finne frekvensen. Etter parameterjustering ble frekvensestimatene mer nøyaktige. Dette førte igjen til mer nøyaktige dybdemålinger.

Abstract

Underwater vehicles use pressure sensors to measure depth. These measurements are subjected to noise from ocean waves. To reduce the impact of the wave induced noise, an estimator algorithm is applied to the measurements. This algorithm relies on mathematical models that describe the noise dynamics. Since waves are oscillatory, the modeled wave noise is as well. The wave frequency must be estimated for this process. A model was developed that estimated the wave frequency in addition to the wave noise. The model was inputted data from simulated and real measurements. The estimates were compared to those of an established estimator model. Before parameter tuning, the oscillatory model provided slightly more accurate depth estimates than the field tested model, but struggled with estimating the frequency. With some tuning, the model was able to estimate the wave frequency accurately and as a consequence the depth estimates were more accurate.

Contents

List of Figures

Chapter 1

Introduction

The ocean floor is a vast and relative uncharted area. Per 2014 the most accurate Global Positioning System (GPS) based mapping had a resolution of 5 kilometers (Copley (2014)). As a contrast, 98% of the planet Venus has been mapped with a resolution of only 100 meters (Dunbar (2007)). Water is much more compact than gases and acts as a veil, hiding the seabed from high resolution satellite imagery (Copley (2014)). Some actors, e.g. the offshore industry, depend on high resolution mapping of the seabed. Luckily for them there are alternatives to satellites, when it comes to mapping. One such solution is to let an underwater vehicle (UV) perform the mapping of the desired seabed area.

Using sound waves the UVs scan the seabed to gather data that can be used to produce maps. However, the scanned data only give information of the scanned area relative to the position of the UV. It is therefore important that the UVs position can be accurately estimated.

The vertical position, depth, is determined with the use of pressure sensors combined with an Inertial Navigation System (INS). The INS consists of gyros and accelerometers. These devices exploit the moment of inertia to determine the acceleration of the UV. However since acceleration must be integrated twice to get position, any error will grow exponentially and cause drift in the depth measurement. The pressure sensor measurement, on the other hand, does not drift, but is subjected to noise from the environment.

To improve the accuracy of the measurements, an estimator algorithm, the *Kalman Filter* (KF) is employed. The KF combines the noise subjected measurement with a predefined mathematical model of the system and outputs an estimate of the depth. A more accurate system

model results in more accurate estimates.

The measured pressure is the sum of hydrostatic and dynamic pressure. The hydrostatic pressure is affected by parameters such as salinity, temperature, density and tidal waves. However these factors are slow varying and Willumsen et al. (2007) make some simple suggestions on how to identify them. Much more troublesome is the dynamic pressure.

Surface waves causes changes in the pressure in the water column. This is the main source of noise attributed to dynamic pressure (Willumsen et al. (2007)). Figure 1.1a shows what effect the waves can have on the pressure sensor when mapping the seabed. In figure 1.1b the KF has been used to produce a better estimate, however wave induced noise is still apparent. One solution, as demonstrated in figure 1.1c is called *smoothing*.

The smoothing algorithm optimizes the estimates based on previous and future data, i.e. the entire dataset (Willumsen and Hegernæs (2009)). The resulting estimate is much more accurate up until the last data points, where it lacks the future data points. For that reason, smoothing can not replace real-time estimates for navigation purposes, and correct navigation is important when mapping.

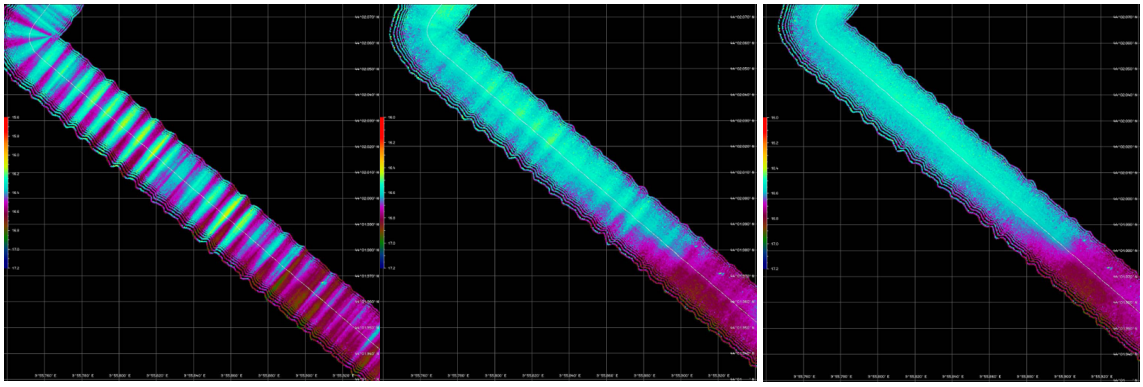

(a) Pressure sensor (b) Real-time filtered (c) Smoothed

Figure 1.1: Mapping of the seabed (Willumsen et al. (2007))

Another method of removing the pressure induced noise is by exploiting other means of depth measurement. Thomson and Emery (2014) mentions echo sounding as an alternative. However the sound waves must be reflected by the surface of the ocean, and are therefore just as vulnerable to surface waves. Other concepts are discussed in Olsen (2015), but these are not practical to implement in the ROV environment.

The wave induced noise creates a bias in the measurements. However, unlike most types of bias, the wave induced bias is oscillatory. The standard industry approach does not model for oscillations. Haaland (2016) demonstrated that by modeling the wave bias as an oscillatory process the KF depth estimates became more accurate. However, this system model required that the wave frequency was known, which is often not the case in real time estimation.

This thesis describes how it is possible to modifying the oscillatory model from Haaland (2016) so that it can be used without prior knowledge of any wave parameters. The model should also perform better than the ones being used in the industry. These were the two primary objectives of this thesis.

Chapters 2 describes concepts that are important for understanding the estimation procedures in later chapters. In chapter 3, properties of waves are examined and modeled. A wave simulation model is developed in chapter 4. The purpose of this model is to supply test data for the development of the estimators. To create a benchmark on performance, chapter 5 describes how a field tested industry estimator model is studied and tested on the simulated wave data. The model developed in Haaland (2016) is also studied and tested on the simulation model. This is described in chapter 6. The extensions to the oscillatory model is developed in chapter 7. A summary, conclusion and final notes are presented in chapter 9. Acronyms and symbols are listed in appendix A.

Chapter 2

Important mathematical and estimation concepts

The reader might not be familiar with some of the terms and methods presented in chapters 4-9. Some of these are explained here. The chapter is based on Haaland (2016).

2.1 Estimation

Some times the observations of states can be of quite uncertain. A noisy depth measurement of an UV is an example of this. By supplementing the observation with a mathematical description (a model) of the state dynamics, an estimate is produced. Given a that the state model was well defined, the estimate is statistically closer to the true value than the observation. Often it can be practical to let the system being estimated be presented on *State Space form*. In this way the system can be described by a set of first order differential equations and measurement equations. In this thesis, the models of the systems will be described by the following equations:

$$\dot{x} = Fx + w \tag{2.1a}$$

$$y = Hx + v \tag{2.1b}$$

Equation 2.1a is the process equation and describes the dynamics of the parameters to be measured. The F matrix give the interdependencies of the states, x, while w is noise on the process.

The measurement is given by 2.1b. The H matrix give the relationship between the states and the measurement. v is noise on the measurement. The system is *time invariant*, meaning F and H do not change with time. If all equations contain only linear terms, the system is *Linear*.

As will be discussed in 2.4 a system can either be *continuous* or *discrete*. The latter being a system where variables only change value at certain time instances. The given time instance is denoted by (k). In a continuous system the variables may change value with incremental time steps. The time instances are denoted by (t).

There are different methods of discretization. One such method is *Euler's method*. It is simple, but not *exact*. An exact method is when the discrete representation is equal the continuous at k. This is the case for *Van Loans method*. However the Van Loan method is only exact for linear time invariant systems. The Euler method can be used on close to all systems on state space form.

The state-space equations in 2.1 is said to be *observable* if for any unknown initial state x(0), there exists a finite $t_1 > 0$ such that knowledge of the input u and the output y over $[0, t_1]$ suffices to determine uniquely the initial state x(0). Otherwise, the equation is said to be unobservable (Chen, 2013).

The observability matrix ($\mathcal{O}$) can be used to check for observability.

$$\mathcal{O} = \begin{bmatrix} H \\ HF \\ HF^2 \\ \vdots \\ HF^{n-1} \end{bmatrix} \tag{2.2}$$

n is the size of the dimensions of the square matrix A. If $\mathcal{O}$ has *full column rank*, the system can be shown to be observable (Chen, 2013). Full column rank is achieved if no column can be described by a combination of the others.

Another property that can be investigated is the pole values. This value determines the behavior of the system. For the process in equation 2.1 the poles are given by F.

2.2 Statistical Concepts

A good estimate of a variable is one which is probable. For that reason, statistics is an important part of estimation.

The *autocorrelation function* describes how well a random process, X(t), is correlated with itself. The function can be expressed this way:

$$R_X(\tau) = E[X(t)X(t+\tau)] \tag{2.3}$$

Closely related to the autocorrelation function is the *Power Spectral Density* function (PSD). It is the fourier transform of the autocorrelation function. The PSD present the intensity of different frequencies in the random process (Brown and Hwang, 2012).

As implied, the *the probability density function* (PDF) describes the probability of different outcomes in a random process. The *Gaussian distribution* is an important PDF and is defined by mean (μ) and standard deviation (σ). The standard deviation describes the dispersion of the data.

Variance is the square of the standard deviation and also describe the dispersion of data. The *covariance* describes how a change in one parameter effects another. The *covariance matrix* is a matrix where the off diagonal values show the covariance and the diagonal values the variance of parameters.

A *Gaussian process* is a non-parametric model for functions where each point in the function space is treated as a random variable. The covariance function specifies how the values of different points influences the likelihood of values for other points to take. Every point in the input space is associated with Gaussian distributed random variable. If μ and σ do not change as a function of time, the Gaussian process is said to be *stationary*.

2.3 Noise Estimators

The statistical descriptors discussed so far are used to characterize two models for noise estimation: *white noise* and *Gauss-Markov Process*.

Both models are stationary Gaussian processes. The white noise has an impulse as an au-

tocorrelation function and is equally spread out in the PSD. The Gauss-Markov process, on the other hand, has an exponential autocorrelation function.The Gauss-Markov process results when a first-order LTI system is given white Gaussian input.

2.4 The Kalman Filter

The Kalman filter is an established method for state estimation in linear stochastic systems. Named after its inventor, Rudolf Emil Kàlmàn, it was first published in 1960. The Kalman filter is not to be confused with frequency based filters, e.g. a low-pass filter. This section will:

1. Explain the basic principles and benefits of the Kalman filter
2. Describe the discrete Kalman filter
3. Describe the *Extended Kalmanfilter* (EKF)

The assumptions and equations in section 2.4 are heavily based on Vik (2014) and on Brown and Hwang (2012).

2.4.1 Basic Features of the Kalman Filter

The Kalman filter is an *optimal recursive data processing algorithm.* Data processing is done by combining predictions with observations. The predictions are based on how we believe the system dynamics behave. The observations are measurements. By processing the measurements with a Kalman filter a more accurate estimate is produced. Some benefits of the filter is that it is optimal in the minimum variance sense, that it is unbiased and that it is asymptotically stable. However, the filter requires that:

1. The process noise and the measurement noise are Gaussian and white
2. The initial state is Gaussian
3. The system is linear
4. The system is observable

Discrete Kalman filter

The Kalman filter published by Kàlmàn was the *Discrete Kalman filter*. Like the name implies, the discrete KF operates in discrete time. The algorithm can therefore be computed in a series of steps in an iterative manner. The system is modeled by linear difference equations with the process described by

$$x(k+1) = \Phi(k)x(k) + \Delta(k)u(k) + \Gamma w(k) \tag{2.4}$$

and the measurement given by

$$y(k) = H(k)x(k) + v(k) \tag{2.5}$$

and the covariance matrices Q_d and R_d relating to the noise v and w by

$$E[w(k)w^T(j)] = \begin{cases} Q_d(k) & \text{if } j = k \\ 0 & \text{if } j \neq k \end{cases} \tag{2.6a}$$

$$E[v(k)v^T(j)] = \begin{cases} R_d(k) & \text{if } j = k \\ 0 & \text{if } j \neq k \end{cases} \tag{2.6b}$$

$$E[w(k)v^T(j)] = 0 \tag{2.6c}$$

After identifying the model for the system, an algorithm is used to project ahead states ($\bar{x}(k)$) and the error covariance matrix ($\bar{P}(k)$). These are called *a priori estimates*. The a priori estimates are combined to produce the optimal estimates, the *a posteriori estimates* $\hat{x}(k)$ and $\hat{P}(k)$. The steps of the DKF algorithm is explained below.

Step 0: Identify initial conditions. This is only done once in the algorithm. The initial values of the states ($\bar{x}(0)$)are in some way estimated. The initial values of the covariance matrix ($\bar{P}(0)$) are given by the equation:

$$\bar{P}(0) = [(x(0) - \hat{x})(x(0) - \hat{x}(0))^T] \tag{2.7}$$

Step 1: Update the Kalman gain. The Kalman gain (K) is a blending factor, meaning that the gain determines how much weight is given to the measurement versus the priori estimate.The

Kalman gain is by definition the gain that minimizes the mean square estimation error. The Kalman gain equation is

$$K(k) = \bar{P}(k)H^T(k)[H(k)\hat{P}(k)H^T(k) + R_d(k)]^{-1} \tag{2.8}$$

Step 2: Update the a posteriori estimates. With the current a priori estimates and Kalman gain, the a posteriori estimates are updated. This is done in equation 2.9 and 2.10.

$$\hat{x}(k) = \bar{x}(k) + K(k)[y(k) - H(k)\bar{x}(k)] \tag{2.9}$$

$$\hat{P}(k) = [I - K(k)H(k)]\bar{P}(k)[I - K(k)H(k)]^T + K(k)R_d(k)K^T(k) \tag{2.10}$$

Step 3: Update the a priori estimates. The a priori estimates of the states and error covariance matrix are based on our model of the system and the a posteriori estimates. See equation 2.11 and 2.12.

$$\bar{x}(k+1) = \Phi(k)\hat{x}(k) + \Delta(k)u(k) \tag{2.11}$$

$$\bar{P}(k+1) = \Phi(k)\hat{P}(k)\Phi^T(k) + \Gamma(k)Q_d(k)\Gamma^T(k) \tag{2.12}$$

As shown in figure 2.1 the algorithm is an iterative process that repeat steps 1-3.

2.4.2 Extended Kalmanfilter

As mentioned in section 2.4.1, one of the assumptions that are made when using the Kalman filter is that the system is linear. In real systems, this is often not the case. There are, however, methods of coping with nonlinear systems. The method being used by Navlab is the Extended Kalman Filter (EKF).

The nonlinear system is in the continuous case described by the equation

$$\dot{x}(t) = f(x(t), u(t), t) + \Gamma w(t) \tag{2.13}$$

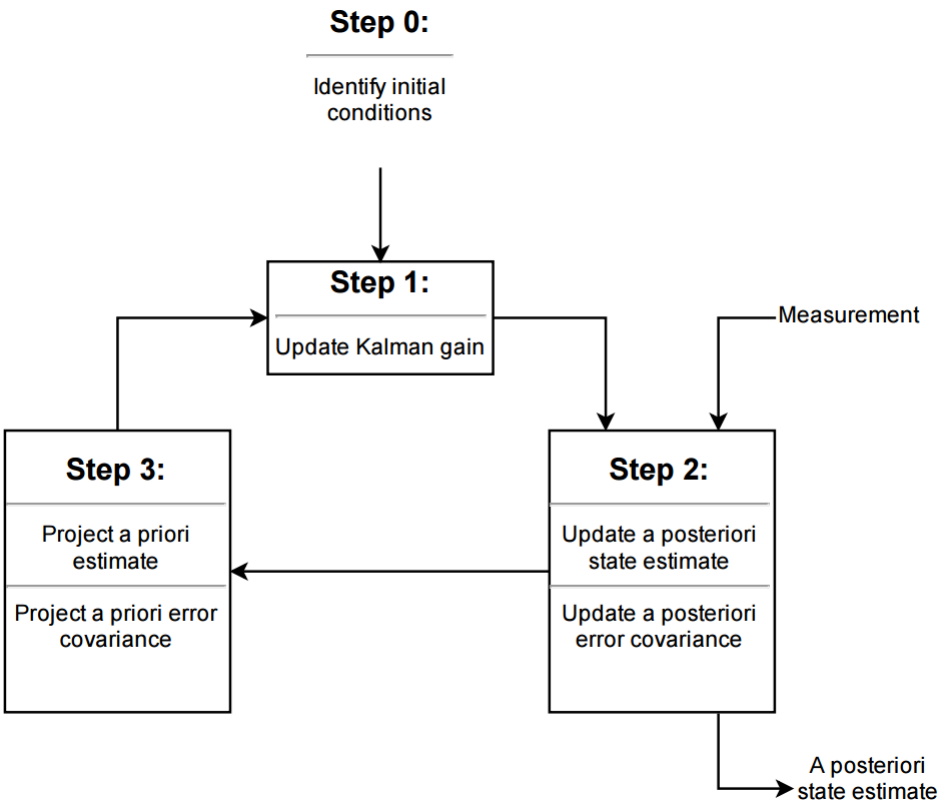

Figure 2.1: The iterative process of a Discrete Kalman filter

and the measurement is given by the equation

$$y(t) = h(x(t), t) + v(t) \tag{2.14}$$

The process noise $w(t)$ and the measurement noise $v(t)$ are assumed Gaussian distributed:

$$w(t) \sim N(0, Q(t)) \tag{2.15a}$$

$$v(t) \sim N(0, R(t)) \tag{2.15b}$$

As shown in figure 2.2 the EKF linearize the system about the computed estimated trajectory at different time instances. The linearization of the process, $F(\hat{x}(t), u(t), t)$, is element wise given by

$$f_{ij}(\tilde{x}(t), u(t), t) = \frac{\delta f_i(x(t), u(t), t)}{\delta x_j(t))}\bigg|_{x=\tilde{x}} \tag{2.16}$$

and the linearizion of the measurement ,$H(\tilde{x}(t),t)$, is given by

$$[h_{ij}] = \frac{\delta f_i(x(t),u(t),t)}{\delta x_j(t))}\bigg|_{x=\tilde{x}} \tag{2.17}$$

$\tilde{x}(t)$ is an approximate of E[x(t)]

The actual trajectory x(t) and estimated trajectory $\tilde{x}$ are shown in figure 2.2. The difference given by $\delta x = x(t) - \tilde{x}$ is the what the EKF actually models in the process and measurement. The process equation given by 2.18 and measurement by 2.19

$$\delta \dot{x} = F(\tilde{x}(t),u(t),t)\delta x(t) + w(t) \tag{2.18}$$

$$\delta y(t) = H(\tilde{x}(t),t)\delta x(t) + v(t) \tag{2.19}$$

In the Navlab interface it is the continuous system that is given. However, Navlab makes the system discrete before running the algorithm, which is similar to the discrete Kalman Filter in section 2.4.1.

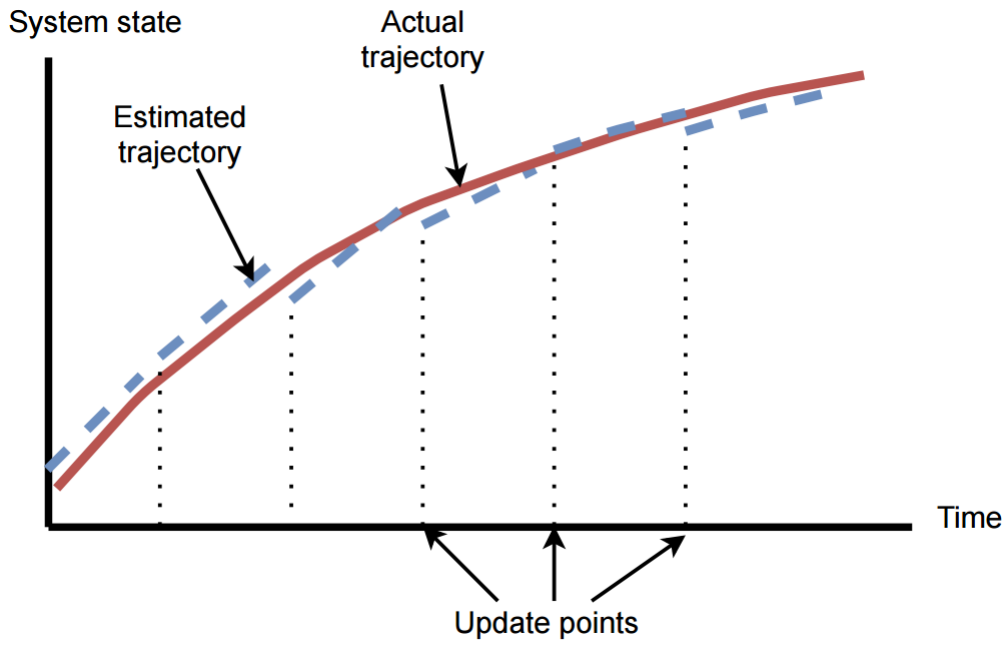

Figure 2.2: The EKF linearization (Brown and Hwang, 2012)

Initiation of the EKF

Unlike the linear case, the EKF is not necessarily asymptotically stable. If $\bar{x}(0)$ has a large error, the linearizion will be off which in turn can cause further divergence.

Another problem occur when a large $\bar{P}(0)$ is combined with a low-noise measurement. This can cause numerical problems. The P matrix might become non-positive definite, and this can cause the estimate to diverge. Without going into detail, there are simple methods that can prevent this.

Chapter 3

Waves

In physics a wave is a transfer of energy through a medium that takes shape as an oscillation. This is also true for ocean waves. For simplicity, *ocean waves* will be referred to as *waves* from this point on. This chapter is dedicated to build an understanding of waves and how to model them. The development of the depth estimator model described in chapter 7 is dependent on good wave simulations. Modeling waves is therefore an important step towards developing the estimator model.

3.1 System of Reference

The system considered in this thesis is in one dimension only, depth. Empirical data justify this simplification (Haaland, 2016). The coordinate system has its origin in the sea surface and positive direction pointing downwards in a direction orthogonal to the horizontal plane. The sea surface is a fixed point. How this point is arrived at is not important for the thesis. It could for instance be the *mean sea level* (MSL), which is the average sea level of a specific place, considering waves and tides.

3.2 Waves and Pressure

As explained in chapter 1, waves have an undesired effect on pressure sensors. The upwards and downwards motion of the water column displaces the UV as illustrated in figure 3.1. The

pressure sensor does not register this change in depth since the pressure is the same. The accelerometer, however, does and the UV stairs itself to the desired depth. This causes the pressure to increase which in turn impacts the depth measurements of the pressure sensor. The closer the UV is to the surface, the greater the wave induced vertical displacement. With high frequency waves, the pressure attenuation is greater. This is due to more waves being present, which increases the interference. In this sense, the water column acts as a low pass filter.

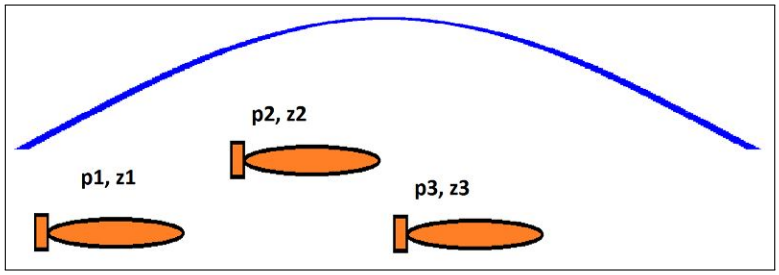

(a) UV being near surface with low frequency wave

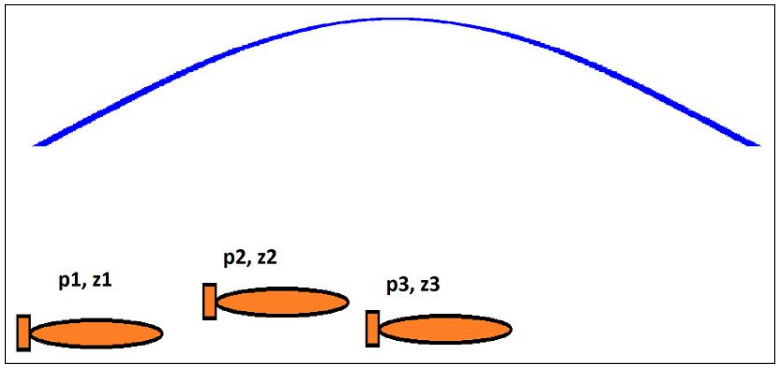

(b) UV being deep with low frequency wave

Figure 3.1: This figure illustrates an UV at different time instances being subjected to a low frequency wave. The wave pulls the UV from depth z1 to z2. The pressure p1 and p2 is the same. To get back to the intended depth the UV steers itself to z3=z1. However the pressure z3 is higher than both z1 and z2. The effect of the waves on the UV is less at deeper waters.

3.3 Wave Nomenclature

Before detailing how to model waves in the following sections, some wave parameters will be explained. Some of these explanations are related to figure 3.2, which show a simple sinusoidal wave.

3.3.1 Single Wave Nomenclature

The expressions described here relate to a single wave.

Crest and through The crest is the top of the wave, while the through is the bottom. See figure 3.2.

Amplitude Denoted by A, this length is half the vertical difference between the crest and through. See figure 3.2. Most waves have crests and throughs that vary in height and depth. Amplitude is therefore more of use in modeling waves than in describing them. The unit of A is [m].

Significant wave height Denoted H_s, the significant height is a more reliable descriptor than amplitude. H_s is approximately the average of the third of waves with the largest height, measured from through to crest. The unit of H_s is [m].

Wave frequency The wave frequency can be used to describe the occurrence of a wave as both as a function of time and as a function of space. As explained in section 3.1, the system is only modeled for one spatial dimension, depth, spatial frequency is irrelevant. All references to wave frequency are therefore regarding time.

The unit for wave frequency in this thesis is given as both [Hz] and [rad/s]. The relationship between these units is purely scalar with [rad/s]=2π[Hz]. The wave frequency parameter ω will be given as $\omega = f_{Hz}2\pi$[rad/s], where f_{Hz} is the frequency in [Hz]. This is due to ω being implemented in [rad/s] but [Hz] being a more intuitive unit.

3.3.2 Sea State Nomenclature

The *sea state* is a description of the waves in an area. It is specified by a *Wave Frequency Spectrum* (WFS) with a given significant wave height and a *Mean Propagation Direction* (MPD). To address *unidirectionality*, a *spreading function* is applied to the WFS Techet (2005). These expressions, and others related to sea state, are explained here.

Wave frequency spectrum The *wave frequency spectrum* (WFS) is a PSD function for the frequencies of a given sea state.

Spectral peak frequency The spectral peak frequency ω_p is the wave frequency at which the WFS has the most energy.

Spectral peak period The spectral peak period T_p is the inverse of the spectral peak frequency.

Wave phase Denoted θ, it is a scalar from 0 to 2π that relates the phases of different waves. See figure 3.2.

Mean propagation direction Waves propagate in different direction along the horizontal plane. The mean propagation direction β is the mean of these directions. The unit of β is [rad], and it is given relative to a coordinate axis of the horizontal plane, counter clockwise.

Unidirectional An unidirectional sea state contains waves that all propagate in the same direction.

Fetch Due to frictional forces, wind blowing over a body of water over a given time will generate ocean waves. The length of water over which the wind blows is important for the development of the sea state. This length is called fetch.

Swell Not all waves are caused by the local winds. Swells are waves created by distant storms that have traveled a long distance.

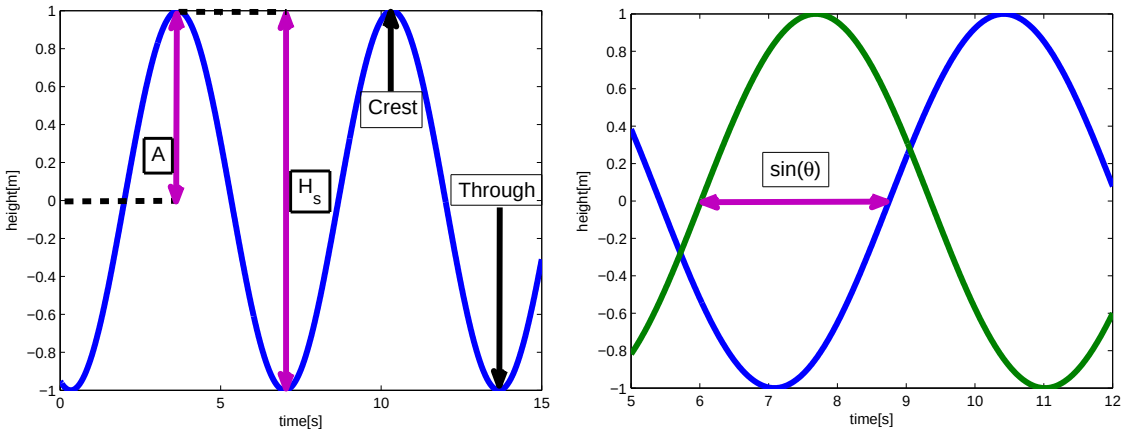

Figure 3.2: This figure illustrates how some wave parameters relates to waves.

3.4 Modeling the Sea State

Since the sea state describes the behavior of waves in an area, an accurate sea state model is a useful tool for modeling waves. *Random wave models* (RWM) can be used for this purpose. A *linear random wave model* (LRWM) is the sum of several waves, each with different amplitude, frequency, direction and phase. A *non-linear random wave model* (NRWM) will in addition take account of parameter value changes caused by non-linear interaction between the wave components. However, NRWM are more complicated than the LRWM. For that reason a LRWM was used instead.

The *linear long-crested wave model* (LLWM) is a simple LRWM. It describes the sea state as the sum of k sinusoidal functions with different parameter values. It is given by:

$$\eta(t) = \sum_{k=1}^{N} A_k cos(\omega_k t + \theta_k) \tag{3.1a}$$

$$E[A_k^2] = 2S(\omega_k)\Delta\omega_k \tag{3.1b}$$

The amplitude of a given wave is in equation 3.1b described as a Rayleigh distributed function of the frequency. $S(\omega)$ is the WFS and $\Delta\omega = (\omega_{k+1} - \omega_{k-1})/2$. k typically will be at least 1000 if properties of extreme waves are to be captured. Figure 3.3 is a LLWM with k=3. It is worth noting that the LLWM is a 2-dimensional model and does not account for sea states with several wave directions.

A further simplification to the model can be made. In Haaland (2016), the waves are modeled as a single frequency sinusoidal. That would reduce the LLWM equation 3.1 to:

$$\eta(t) = cos(\omega_p t + \theta) \tag{3.2a}$$

$$A = H_s \tag{3.2b}$$

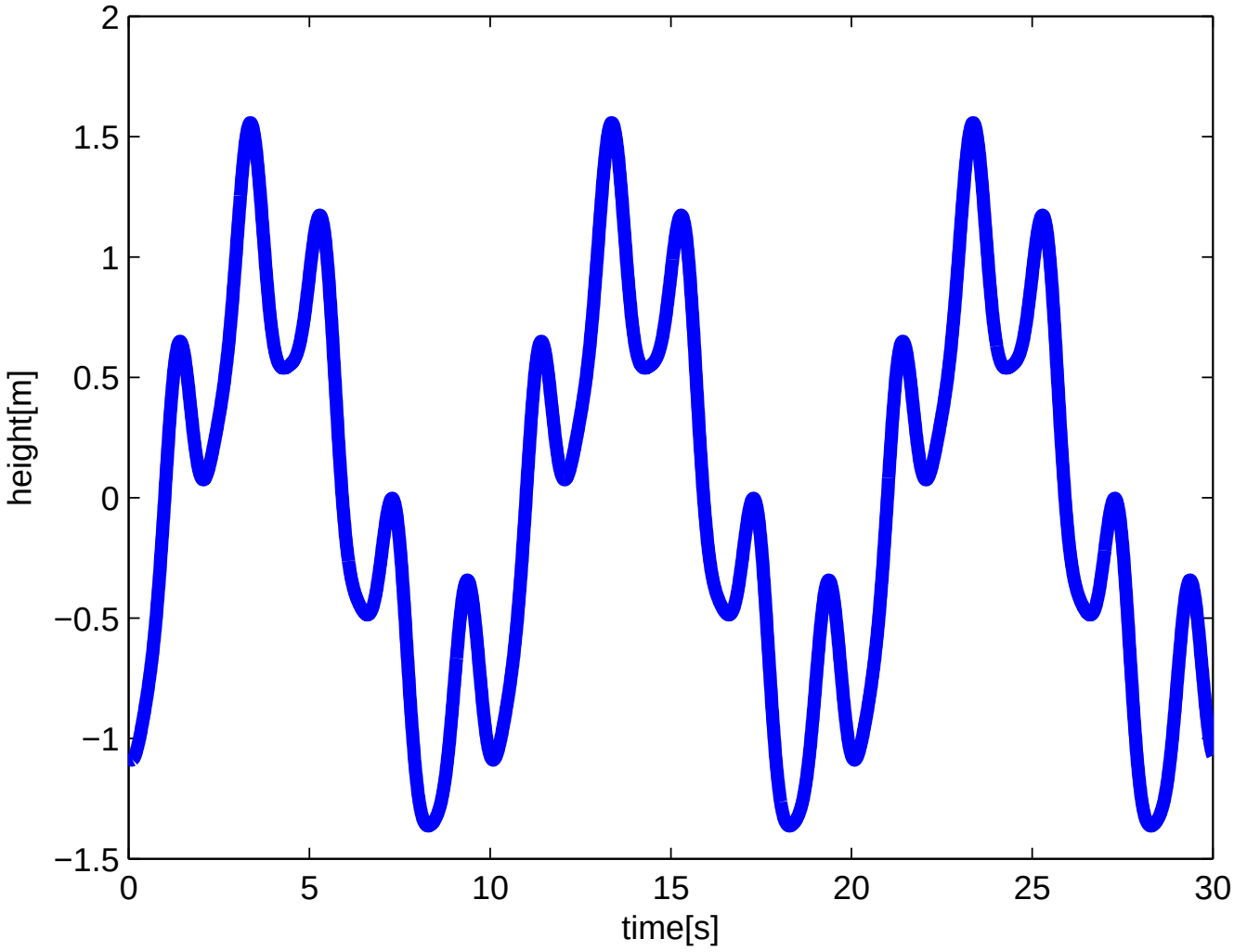

Figure 3.3: This figure illustrates how the sum of waves with different parameters can represent ocean waves. The simulated ocean wave consists of three sinusoidal waves with different amplitude, frequency and phase.

3.5 Wave Frequency Spectrum

To find the peak frequency ω_p and significant wave height H_s for equation 3.2, the WFS must be approximated. This can be a difficult task, due to the effect several parameters have on the frequency. Some of these effects are:

- Swells may be present and have a different directionality than the wind waves. The spreading function cannot account for the presence of swells.

- The fetch and limits to the fetch will set boundaries to how the waves develop.
- Whether the sea is developing or decaying is also important for the WFS.
- Strong currents can significantly impact the wave spectrum.
- Sea depth. Deep water WFS are not valid in shallow water and vice versa.
- Human interference, such as naval traffic.

Fortunately there are some models that can be used to develop the WFS. For wind seas, the *Pierson-Moskowitz Spectrum* (PM) is used to describe the wave spectrum of a fully developed sea. Figure 3.4 show WFS of a PM for certain wind speeds. The relation between peak frequency ω_p and significant wave height H_s and the wind speed is:

$$\omega_p = 0.877g/U_{19.5} \tag{3.3a}$$

$$H_s^2 = 2.74 * 10^{-3} \frac{(U_{19.5})^4}{g^2} \tag{3.3b}$$

where g is the gravitational constant and $U_{19.5}$ is the wind speed at 19.5[m] above mean sea level. According to data from met (2017) wind speeds of more than 17[m/s] only occur a couple of days a year for a given location. Figure 3.5 is a plot of the significant frequency and height for different wind speeds. PM for wind speeds where H_s>0.10[m] was plotted in figure 3.6 and table 3.1.

The *Joint North Sea Wave Observation Project* (JONSWAP) found that due to non-linear interactions between the waves, peak frequency could get even more pronounced. The JONSWAP model is basically the same as the PM, but with a gain that makes the peak frequencies more pronounced.

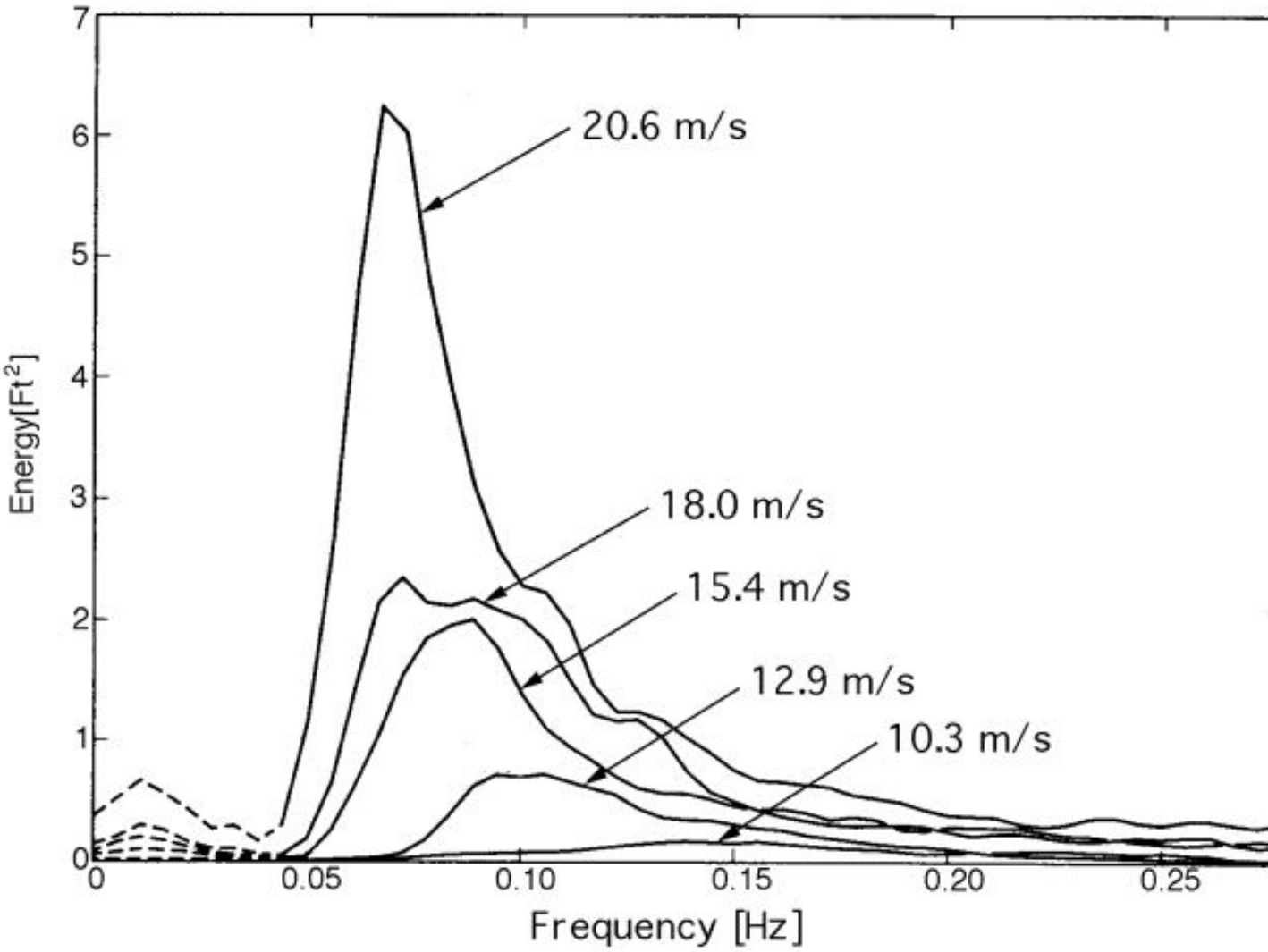

Figure 3.4: Pierson-Moskowitz wave frequency spectrum for a different set of wind speeds. Source: Stewart (1997)

The PM and JONSWAP models only work on fully developed sea states, or close to fully developed in JONSWAPs case. Moderate to low sea states are often composed of both wind waves and swells. Swells typically have a frequency of 0.04-0.10 [Hz]. A two peak wave spectrum may be beneficial in such waters, but for simplicity will not be considered.

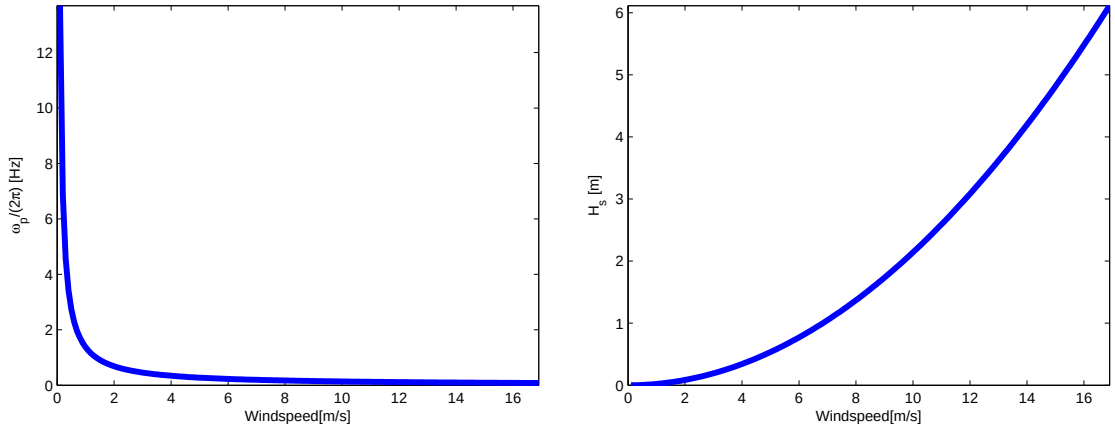

Figure 3.5: Pierson-Moskowitz: Spectral peak frequency ω_p (left) and significant wave height H_s (right) as a function of wind speed.

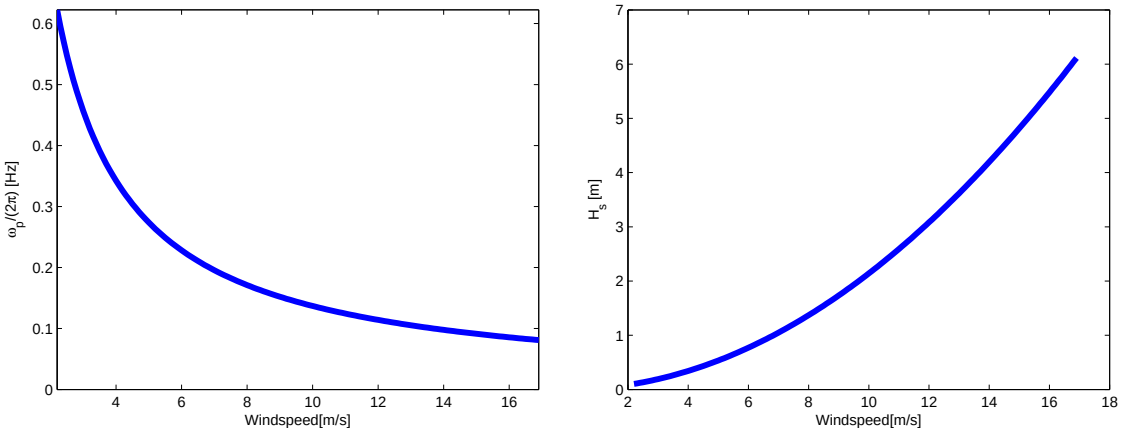

Figure 3.6: Same plot as in figure 3.5, but only for windspeeds that generate a H_s>0.10 [m]

Table 3.1: The minimum and maximum values of PM waves with maximum wave speed 17 [m/s] and minimum significant wave height H_s>0.10[m]

	Min	Max
H_s [m]	0.10	6.11
$\omega_p/(2\pi)$ [rad/s]	0.081	0.622
Wave speed [m/s]	2.2	16.9

3.6 Concluding the Wave Description

Combining the frequency spectrum of wind waves from table 3.1 with the spectrum of the swells, we have a ω_p in the area of 0.04-0.62 $\cdot 2\pi$ [rad/s]. From figure 3.5 it is apparent that the frequency development at low wind speeds is steep. An extra margin was put on the high frequencies. The *peak frequency spectrum* (PFS) is therefore 0.04-1.00 $\cdot 2\pi$ [rad/s]. The significant height can have any value less than 6[m]. In addition, dnv (2012) informs that it is common to assume that the sea surface is stationary for up to 6 hours. The wave frequency will therefore be modeled as time invariant.

Test Frequencies

Some of the figures in this thesis were computationally heavy to calculate with high resolution. For that reason a set of frequencies were picked out for these types of simulations. The frequencies should best represent the PFS and were therefore chosen as the lowest ($0.04 \cdot 2\pi$ [rad/s]) and highest ($1.00 \cdot 2\pi$ [rad/s]) end of the frequency, as well as the logarithmic middle frequency ($0.20 \cdot 2\pi$ [rad/s]). These represent low, middle and high frequencies. In addition a frequency of $0.60 \cdot 2\pi$ [rad/s] was added to the test frequencies. This is close to the highest frequency found in table 3.1.

Chapter 4

Simulation Model

In this chapter, a model that simulates the true states, as well as state measurements, of an UV is developed. Some of the parameter values will be stochastic. As a consequence each simulation will generate a different set of values for states and measurements. In chapters 5-7, the simulations are used as input in the estimation procedure. The objective of the estimators is to accurately estimate the simulated depth. The estimation procedure will normally be done for an ensemble of simulations. This allows for the statistical properties of the estimators to be studied. This method of simulation is known as *Monte Carlo simulation*.

4.0.1 Simulated States

The states vector is as follows:

$$\begin{bmatrix} z \\ v \\ b \\ Dz \\ \psi \\ \omega \end{bmatrix} \tag{4.1}$$

These states are explained in the following paragraphs. The system of reference is given in section 3.1 as a one dimensional system with the positive direction pointing downwards, orthogonal to the horizontal plane.

State 1: Depth (z) Depth is the the vertical position of the UV relative to the sea surface. The estimator's main objective is to estimate depth accurately. Estimation of the other states is only done to improve the depth estimate. The initial depth (z_0) is arbitrary set to 100[m]. This value is of no importance to the simulations. The propagation of z is given by v.

State 2: Depth velocity (v) Depth velocity is the speed of the UV in the vertical column (ascending/descending). The initial depth velocity (v_0) is set to 0 [m/s]. This would be a natural value at the start up. The propagation, described in equation 4.2b is a sinusoidal function. This is so the system continuously will accelerate and decelerate, making sure the velocity stays within reasonable values as well as not having a constant value.

State 3: Accelerometer Bias (b) The accelerometer is subjected to bias in measurements. This bias is modeled as a Gauss-Markov process. The value of the initial accelerometer bias is Gaussian with a STD of σ_b.

State 4: Wave Bias (Dz) The pressure sensor is subjected to a bias in the depth measurements that is caused by ocean waves. In section 3.4 the bias model was derived as a single sinusoidal wave. All values of the wave bias is set by equation 4.2d.

State 5: Wave Bias Velocity (ψ) As the name implies, this state describes the velocity of state 4. All values of the wave bias velocity are given by equation 4.2e.

State 6: Wave Frequency (ω) As explained in section 3.4, the waves can be treated as a time invariant single frequency sinusoidal. The initial frequency (ω_0) will have a value in the peak frequency spectrum (0.04-1.00·2π[rad/s]). The frequency will be time invariant.

Symbols, units and initial values for the different states are summed up in table 4.1. The equations 4.2a-4.2c and 4.2f describe the propagation of respectively z, v, b and ω from the initial

Table 4.1: Simulated states

State	Symbol	Initial value	Unit
Depth	z	100	[m]
Depth velocity	v	0	[m/s]
Accelerometer bias	b	$\mu = 0, STD = \sigma_b$	$[m/s^2]$
Wave bias	Dz	All values given by 4.2d	[m]
Wave bias velocity	ψ	All values given by 4.2e	[m/s]
Wave frequency	ω	$0.04 \cdot 2\pi$ to $1.00 \cdot 2\pi$	[rad/s]

values. Equation 4.2d and 4.2e describe all values of Dz and ψ.

$$\dot{z} = v \tag{4.2a}$$

$$\dot{v} = a \tag{4.2b}$$

$$= 0.1sin(t)$$

$$\dot{b} = -\frac{1}{T_{acc}}b + w_b \tag{4.2c}$$

$$Dz = A_{max}cos(\omega t + \theta) \tag{4.2d}$$

$$\psi = \dot{Dz}$$

$$= \omega A_{max}cos(\omega t + \theta) \tag{4.2e}$$

$$\dot{\omega} = 0 \tag{4.2f}$$

4.0.2 Accelerometer and Pressure Sensor Measurement

The measurements of accelerometer (a_{acc}) is given by equation 4.3a while the pressure sensor measurement (z_{pres}) is given by 4.3b.

$$a_{acc} = a - b - w_{acc} \tag{4.3a}$$

$$z_{pres} = z - Dz + v_z \tag{4.3b}$$

4.0.3 Parameter Values in the Simulation Model

Wave Parameters

θ The initial wave bias will wary as the waves will be in a different phase. This parameter ensures that this also holds true for the simulation. It will have a random value between 0 and 2π.

A_{max} This parameter, the maximum amplitude, is the amplitude of the simulated waves. It is half the significant height H_s, defined in section 3.6). A_{max} must therefore be less than 3[m]. Unless noted otherwise the value of A_{max} in 1[m]. That is so that the Dz would dominate the noise of the pressure sensor, while still not being at the top of the possible amplitude span. [1].

Accelerometer Parameters

For the simulation the accelerometer parameters were set to typical values.

σ_b This is the standard deviation of the accelerometer bias. A typical value for this parameteris $\sigma_b = 25$ [μ g] In SI units: $\sigma_b = 245{,}25$ [$\mu m/s^2$]

T_{acc} This is the time constant of the accelerometer. This value depends on the quality of the accelerometer. A typical values for this parameter is T_{acc}= 3600 [s].

w_{acc} This is the GWN in the a_{acc}. The standard deviation is given by $\sigma_{w_{acc}}$.This value is typically 25 [μg]. In SI units: $\sigma_{w_{acc}} = 245{,}25$ [$\mu m/s^2$]

w_b As explained in section 4.0.1, the bias of the accelerometer is time variant. It also drifts randomly. w_b is a GWN that represents this randomness. σ_{w_b} is calculated as a function of σ_b

[1] At a depth of 100[m] this amplitude might not be realistic. However the simulated depth value has no impact on other states and parameters.

and T_{acc}:

$$\begin{aligned}\sigma_{w_b} &= \sqrt{\frac{2}{T_{acc}}} \cdot \sigma_b \\ &= 5.78[\mu m/s^{\frac{5}{2}}]\end{aligned} \tag{4.4}$$

S_a The accelerometer does not make continuous measurements. Instead it samples at a certain frequency. The accelerometer sample rate was set to a typical value: 100 [Hz].

Pressure Sensor Parameters

v_z Like the w_{acc}, v_z is a GWN that represent random inaccuracies in a measurement instrument, this being the pressure sensor. It is denoted by v since it is apart of the measurement, not the process. σ_v is set to 0.1 [m].

S_p Like the accelerometer, the pressure sensor has a sample rate. This rate is set to 10 [Hz]. The reasoning for this value is discussed in section 5.2.4.

An overview of the current parameters and their values is detailed in table 4.2. The accelerometer parameters, σ_b, T_{acc}, $\sigma_{w_{acc}}$ and σ_{w_b}, have the values of a more exact accelerometer.

Table 4.2: Model 1: GMM parameters

	Variable	Value	Unit	Explanation	Section
Wave-parameters	θ	0-2π	rad	Wave phase	4.0.3
	A_{max}	1	m	Max wave amplitude	4.0.3
Accelero-meter parameters	$\sigma_{w_{acc}}$	245,25	$\mu m/s^2$	STD GWN accelerometer	4.0.3
	σ_b	245,25	$\mu m/s^2$	STD bias accelerometer	4.0.3
	σ_{w_b}	5.78	$\mu m/s^{\frac{5}{2}}$	STD GWN accelerometer bias	4.0.3
	S_a	100	Hz	Sample rate accelerometer	4.0.3
	T_{acc}	3600	s	Time constant accelerometer	4.0.3
P. sensor parameters	S_p	10	Hz	Sample rate pressure sensor	5.2.4
	σ_{v_z}	0.1	m	STD GWN pressure sensor	4.0.3

4.0.4 Verification of Implementation

Before moving on to the estimators, the simulation implementation was inspected to check for errors in the code. Plots shown in this section are from a single simulation with $\omega = 0.04 \cdot 2\pi$. These plots are compared to the model equations and parameter values.

Verification: Simulated True States

The acceleration and the true states, are plotted in figure 4.1. With the exception of the accelerometer bias, the states and acceleration was plotted over 50 [s]. The accelerometer bias was plotted over 600[s] due to its slow dynamics.

The acceleration is given by equation 4.2b. This is a sinusoidal function with an amplitude 0.1 and period 2π [s]. The velocity is given by the initial velocity, $v_0 = 0$ and the integrate of the acceleration. Similarly the depth is given as by $z_0 = 100[m]$ and the integrate of the velocity. The equations for depth and velocity can be rewritten as:

$$\begin{aligned} v =& v_0 + \int_0^t 0.1 sin(t) dt \\ =& 0.1 - 0.1 cos(t) \end{aligned} \tag{4.5a}$$

$$\begin{aligned} z =& z_0 + \int_0^t 0.1 - 0.1 cos(t) dt \\ =& 100 + 0.1t - 0.1 sin(t) \end{aligned} \tag{4.5b}$$

.

The plots for the simulated depth, velocity and acceleration is shown in figures 4.1a, 4.1b and 4.1c. These plots are consistent with the equations 4.5b, 4.5a and 4.2b,

The accelerometer bias, in figure 4.1d is consistent with that of the accelerometer Gauss-Markov process in equation 4.2c. From table 4.1 and 4.2 the following confirmations are made:

- The white noise, $\sigma_{w_{acc}}$, is as large as σ_b. The $-\frac{1}{T_{acc}}\sigma_b$ term is therefore less dominant over short time spans. However over a 600[s] plot, the contribution of the time constant term is noticeable as b goes towards zero.

- The white noise is within the $\sigma_{w_{acc}}$

According to equations for the wave bias, Dz, and its velocity, ψ, 4.2d and 4.2e:

- the amplitude should be 1[m] for Dz and ω[m] for ψ.
- the time period should be $\frac{2\pi}{\omega} = 25[s]$[s] for both Dz and ψ
- the phase difference between Dz (sinus) and ψ (cosinus) should be $\frac{2\pi}{4\omega} = 6.25[s]$.

This checks out when compared to the simulations seen in figures 4.1e and 4.1f.

The last state, ω, is described as having a constant value in equation 4.2f. In this simulation that would be $0.04 \cdot 2\pi \approx 0.2513$[rad/s]. The plot in figure 4.1g verifies that the simulated values are correct.

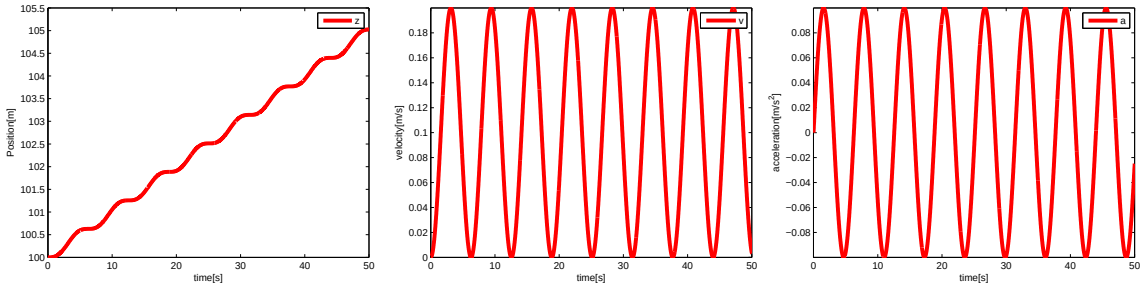

(a) Depth (z) (b) Velocity (v) (c) Acceleration (a)

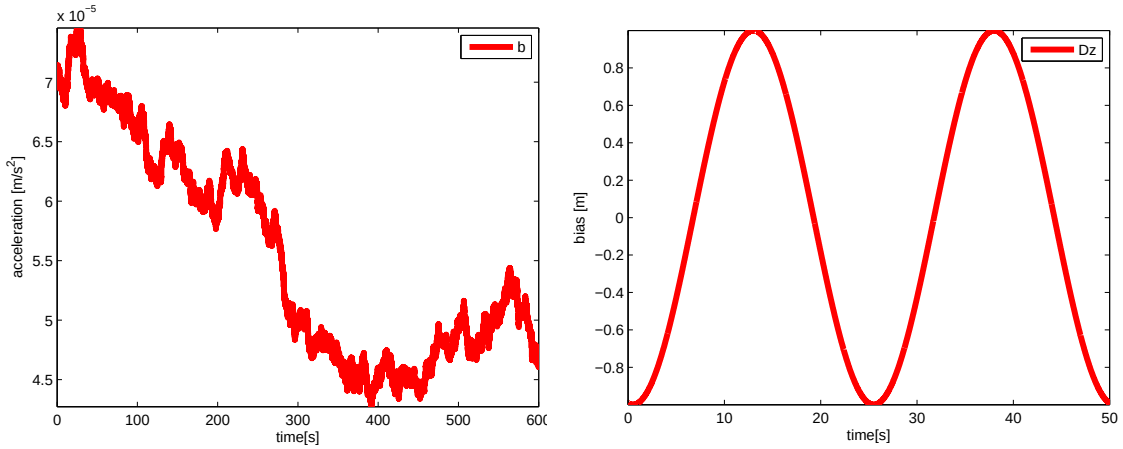

(d) Accelerometer bias (b) (e) Wave bias (Dz)

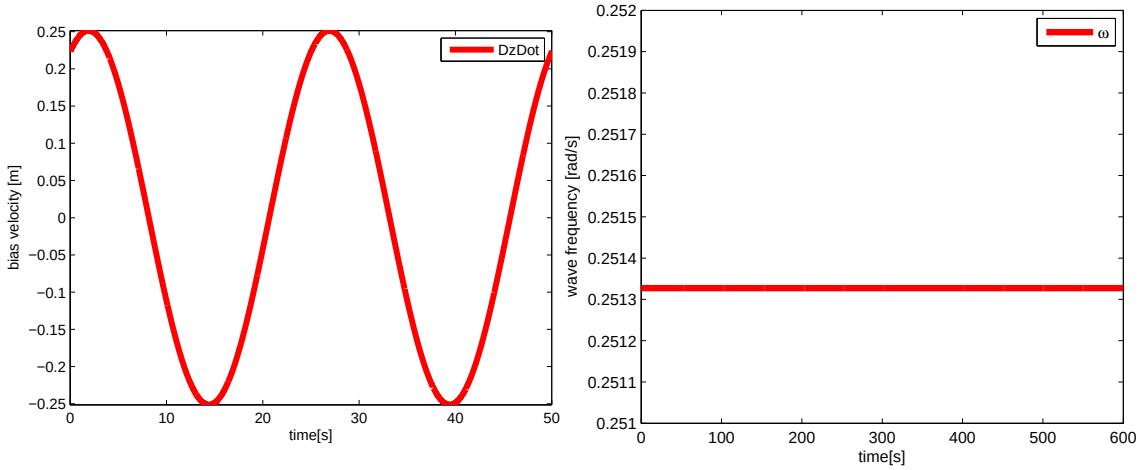

(f) Wave bias velocity (ψ) (g) Wave frequency (ω)

Figure 4.1: Acceleration and true states

Verification: Measurements

The values of the accelerometer bias b and white noise w_{acc} stays low compared to the true acceleration. This is also true in the simulation. See figure 4.2.

The pressure sensor measurements are less accurate as the noise v_{pres} is a larger portion of the signal. Figures 4.2c displays the same dynamics as equation 4.3b. This is made more clear in figure 4.2d where the pressure sensor is plotted against z-Dz.

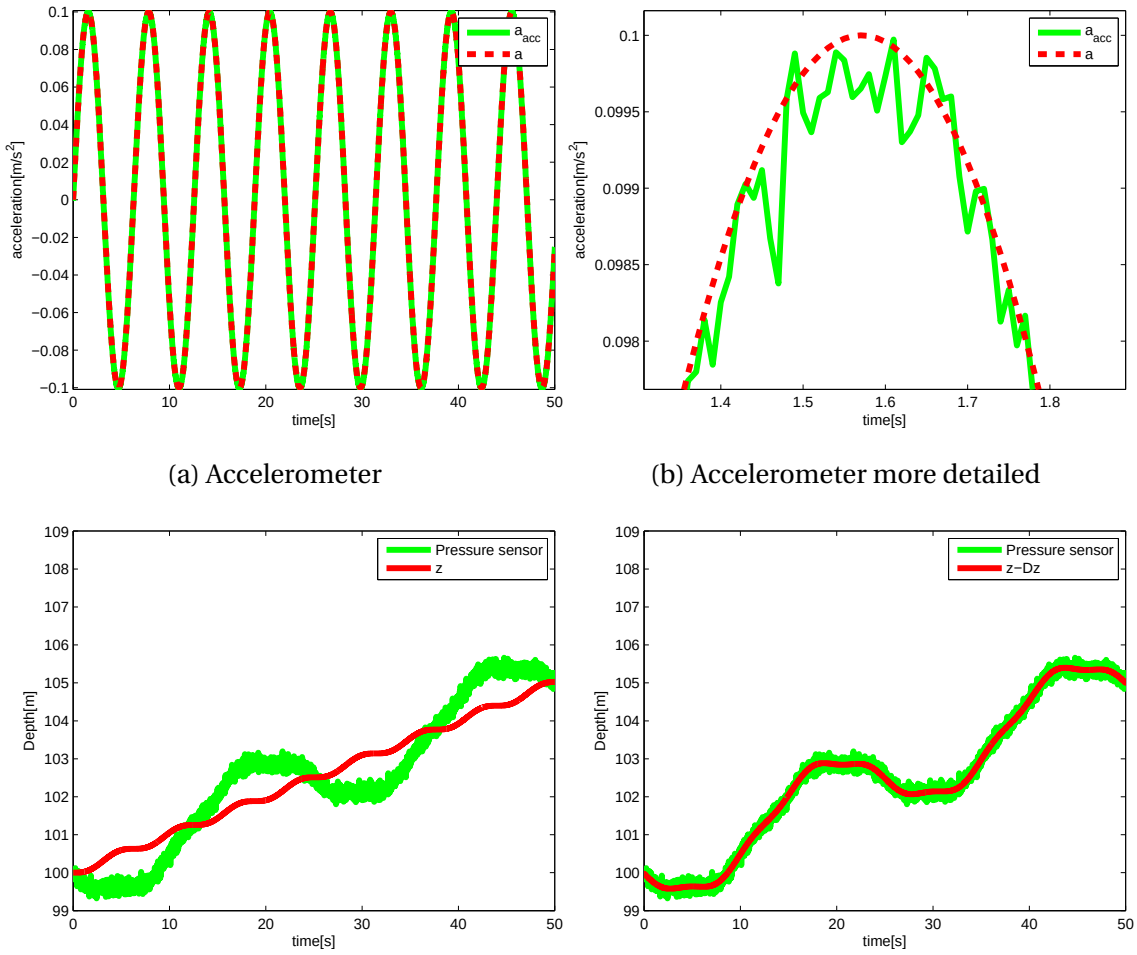

(a) Accelerometer

(b) Accelerometer more detailed

(c) Acceleration (a)

(d) Acceleration (a)

Figure 4.2: Measurements

Chapter 5

Gauss Markov Model

The estimator model discussed in this chapter is based on Gade (1997) and has been used on site in depth estimation. It therefore has some merit and can serve as a benchmark for performance that the estimators developed in chapter 6 and 7 can be compared to. To avoid a mix up, the model in this chapter is referred to as *Gauss Markov Model* (GMM). The name stems from that the wave bias is modeled as a Gauss Markov process.

The bias is not the only state in the estimation process. The state vector for GMM is:

$$\begin{bmatrix} z \\ v \\ b \\ Dz \end{bmatrix} \tag{5.1}$$

The equations for the process are expressed in 5.2 while the measurement is expressed by

equation 5.3.

$$\dot{z} = v \tag{5.2a}$$

$$\dot{v} = a_{acc} + b + w_{acc} \tag{5.2b}$$

$$\dot{b} = -\frac{1}{T_{acc}} b + w_b \tag{5.2c}$$

$$\dot{Dz} = -\frac{1}{T_{Dz}} Dz + w_{Dz} \tag{5.2d}$$

$$\tag{5.2e}$$

$$z_{pres} = z - Dz + v_z \tag{5.3}$$

The system on state space form is:

$$\dot{x} = Ax + Bu + Ew \tag{5.4a}$$

$$y = Cx + v \tag{5.4b}$$

$$\begin{bmatrix} \dot{z} \\ \dot{v} \\ \dot{b} \\ \dot{Dz} \end{bmatrix} = \underbrace{\begin{bmatrix} 0 & 1 & 0 & 0 \\ 0 & 0 & 1 & 0 \\ 0 & 0 & -(\frac{1}{T_{acc}}) & 0 \\ 0 & 0 & 0 & -(\frac{1}{T_{Dz}}) \end{bmatrix}}_{\text{A}} \begin{bmatrix} z \\ v \\ b \\ Dz \end{bmatrix} + \underbrace{\begin{bmatrix} 0 \\ 1 \\ 0 \\ 0 \end{bmatrix}}_{\text{B}} a_{acc} + \underbrace{\begin{bmatrix} 0 & 0 & 0 \\ 1 & 0 & 0 \\ 0 & 1 & 0 \\ 0 & 0 & 1 \end{bmatrix}}_{\text{E}} \begin{bmatrix} w_{acc} \\ w_b \\ w_{Dz} \end{bmatrix} \tag{5.5}$$

$$z_{pres} = \underbrace{\begin{bmatrix} 1 & 0 & 0 & -1 \end{bmatrix}}_{\text{H}} \begin{bmatrix} z \\ v \\ b \\ Dz \end{bmatrix} + v_z \tag{5.6}$$

$$Q = \begin{bmatrix} \sigma^2_{w_{acc}} & 0 & 0 \\ 0 & \sigma^2_{w_b} & 0 \\ 0 & 0 & \sigma^2_{w_{Dz}} \end{bmatrix} \tag{5.7a}$$

$$R = \sigma_{v_z} \tag{5.7b}$$

5.0.1 Parameters in the GMM

Most of the parameters are the same as in section 4.0.3. However, there are two new parameters introduced in the wave bias estimation process, see equation 5.2d. The values of these parameters are have been used for in site depth estimation.

T_{Dz} This is the time constant of the bias caused by the waves. This parameter was set to 100[s].

w_{Dz} This is the contribution of random factors in the wave bias Gauss-Markov process. It is a GWN with standard deviation $\sigma_{w_{Dz}} = 0.15$[m].

These values are appended to table 4.2 to create a, so far, complete overview of parameter values in table 5.1. Since this GMM has the default parameter values, it was called *Default Gauss Markov Model* (DGMM).

Optimized GMM

Haaland (2016) found some other values for the GMM parameters T_{Dz} and $\sigma_{w_{Dz}}$ that improved the measurement accuracy for one set of test data. Further support is found in Hagen and Jalving (2017), where a method of optimizing the GMM parameters, regarding estimate accuracy, is developed. With this model the time constant T_{Dz} was set to 1.28[s]. The optimizer for $\sigma_{w_{Dz}}$, depending on the frequency, is 0.23-5.76[m/s]. Since the GMM-parameters of this model are optimized, it will be referred to as *Optimized Gauss Markov Model* (OGMM).

When comparing the GMM with the models in chapter 6 and 7, the DGMM will represent the least accurate estimator of the GMM, while the OGMM will represent the most accurate. Since

the DGMM is already in use, any new models will have to perform at least as well. Else there is no reason for the industry to adopt the model. If a model performs better than the OGMM, it would indicate that the new estimator is more accurate than GMM all together.

Table 5.1: GMM parameters

	Variable	Value	Unit	Explanation	Section
Wave-parameters	θ	0-2π	rad	Wave phase	4.0.3
	A_{max}	1	m	Max wave amplitude	4.0.3
Accelero-meter parameters	$\sigma_{w_{acc}}$	245,25	$\mu m/s^2$	STD GWN accelerometer	4.0.3
	σ_b	245,25	$\mu m/s^2$	STD bias accelerometer	4.0.3
	σ_{w_b}	5.78	$\mu m/s^{\frac{5}{2}}$	STD GWN accelerometer bias	4.0.3
	S_a	100	Hz	Sample rate accelerometer	4.0.3
	T_{acc}	3600	s	Time constant accelerometer	4.0.3
P. sensor parameters	S_p	10	Hz	Sample rate pressure sensor	5.2.4
	σ_{v_z}	0.1	m	STD GWN pressure sensor	4.0.3
DGMM	$\sigma_{w_{Dz}}$	0.15	m	STD GWN wave bias	5.0.1
	T_{Dz}	100	s	Time constant wave bias	5.0.1
OGMM	$\sigma_{w_{Dz}}$	0.23-5.76	m	STD GWN wave bias	5.0.1
	T_{Dz}	1.28	s	Time constant wave bias	5.0.1

5.1 Linear Kalman Filter

The estimation algorithm of GMM is a Linear Kalman Filter. Section 2.4.1 lists some requirements for this algorithm. They are repeated here, for sake of convenience:

1. The process noise and the measurement noise are Gaussian and white
2. The initial state is Gaussian
3. The system is linear
4. The system is observable

1. Process noise w_{acc}, w_b, w_{Dz} and v_z are all Gaussian and white. See section 4.0.3 and 5.0.1.

2. Initial state z_0, v_0, b_0 and Dz_0 are, as detailed in section 4.0.1, Gaussian.

3. Linear system The state space form of both the GMMs are detailed in equations 5.5 and 5.6. None of the terms presented here are nonlinear, thus the systems are linear.

4. Observable system With equation 2.2 the observability matrix of the GMMs was checked.

Observability GMM

$$\mathcal{O}_{GMM} = \begin{bmatrix} 1 & 0 & 0 & -1 \\ 0 & 1 & 0 & (\frac{1}{T_{Dz}}) \\ 0 & 0 & 1 & -(\frac{1}{T_{Dz}})^2 \\ 0 & 0 & -\frac{1}{T_{acc}} & (\frac{1}{T_{Dz}})^3 \end{bmatrix} \tag{5.8}$$

The time constants are positive by nature. This leaves $\mathcal{O}_{GMM}$ with full rank as long as $T_{acc} \neq T_{Dz}$. This easily be avoided.

5.2 Simulation

To assess the performance of the two methods, they were given input from the simulation described in chapter 4.

5.2.1 Discretization

The GMM system equations as described in 5.2 and 5.3 are given in continuous time. As explained in section 2.4.1, a discrete system is better at lending itself to computational problems. The continuous systems must therefore be discretized.

A, B, Q and R from equations 5.6-5.7 are discretized and symbolized by ϕ, Δ, Q_d and R_d respectively. The Euler method is used for Δ and R_d since these are related to the measurements and are not subjected to feedback. ϕ and Q_d, however are, and the Van Loan method is used instead, since it is exact. The discretization is given by equation 5.9. S_{acc} and S_{pres} are the sampling rates given in table 5.1.

$$\Delta = \frac{1}{S_{acc}} B \tag{5.9a}$$

$$R_d = S_{pres} R \tag{5.9b}$$

$$[\phi(k), Q_d(k)] = VanLoan \tag{5.9c}$$

5.2.2 Verification of the GMM Estimation

To see whether the model was implemented correctly, states and estimates were compared. The plots shown in this section are from a single simulation with $\omega = 0.04 \cdot 2\pi$. This frequency was chosen since the dynamics are slower and easier to observe.

Figures 5.1 and 5.2 show the estimates compared to the true states for DGMM. The same is done for OGMM in figures 5.3 and 5.4. σ_z is the standard deviation in the depth estimate, taken from the diagonal of the P-matrix. The true depth is denoted by z. z_E is the estimate. The difference, in absolute value, of the estimate and the true state is given by the depth error e_z. Dz is the true wave bias.

As expected both models are affected by the wave bias. This becomes especially clear in figures 5.2 and 5.4.

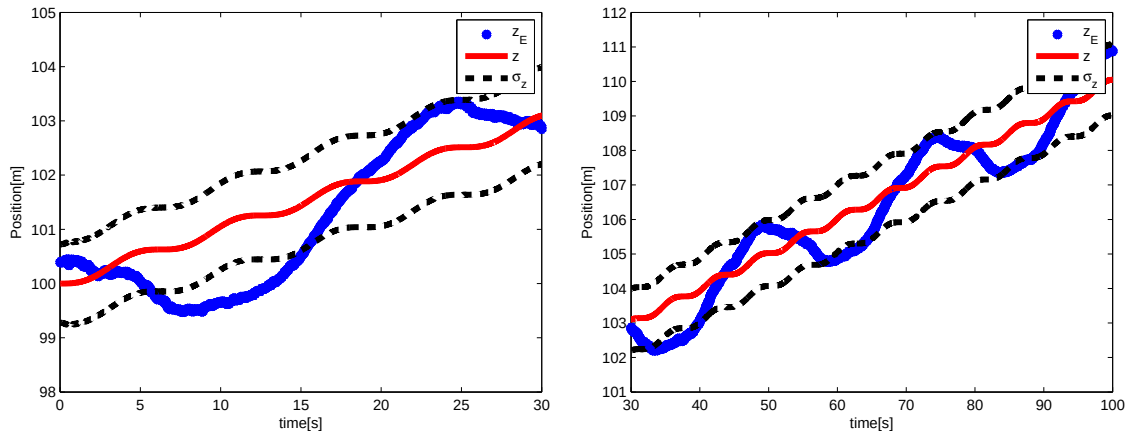

(a) Initiation (b) After initiation (note timespan)

Figure 5.1: DGMM: Estimated and true z

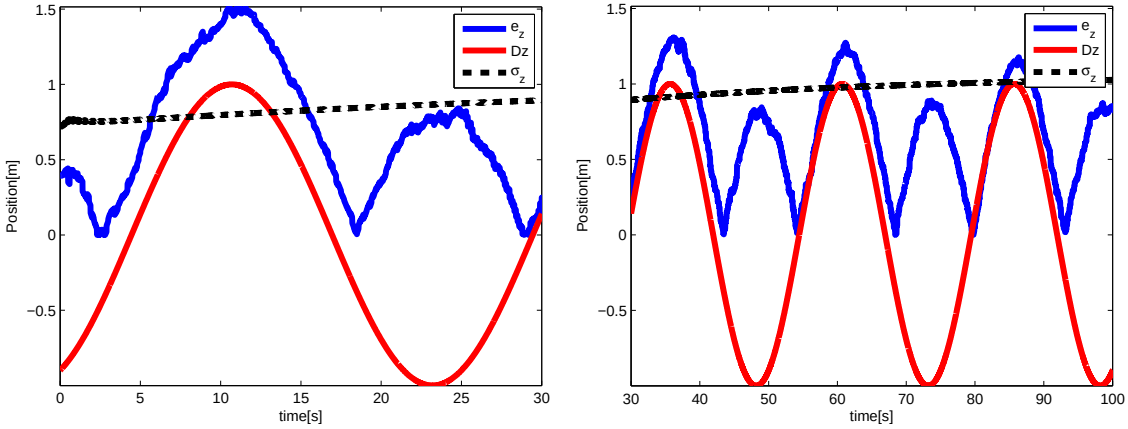

(a) Initiation (b) After initiation

Figure 5.2: DGMM: Error in z estimate (e_z) and wave bias (Dz)

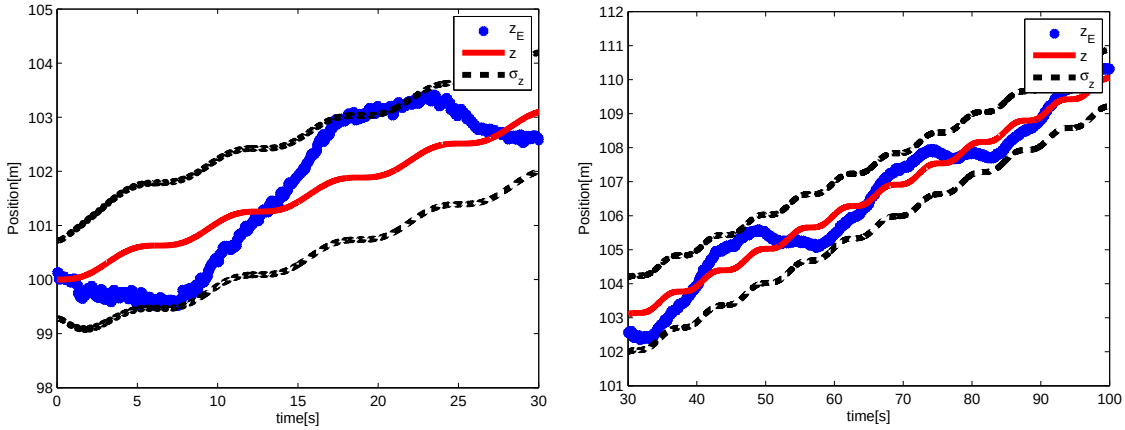

(a) Initiation

(b) After initiation (note timespan)

Figure 5.3: OGMM: Estimated and true z

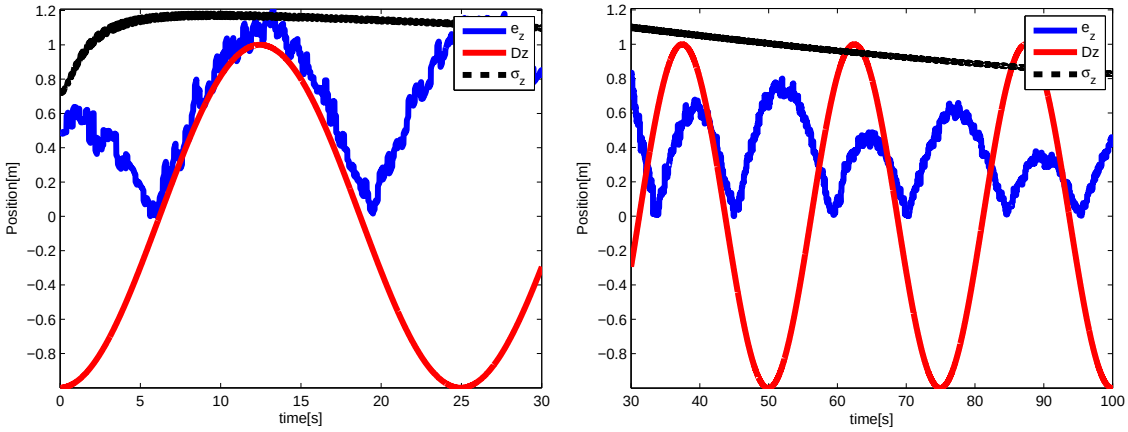

(a) Initiation

(b) After initiation

Figure 5.4: OGMM: Error in z estimate (e_z)

5.2.3 Evaluating GMM

From figures 5.2 and 5.4 it was apparent that the accuracy of both estimators is low during initiation. Measures could be taken to improve the time of convergence. These are not discussed in this thesis. Instead the accuracy was evaluated from a stable state. Figures 5.5-5.6 show e_z and σ_z over a 600[s] simulation. Values were plotted for both low frequencies, ω = 0.04·2π [rad/s], and high frequencies, ω = 1.00·2π[rad/s].

As expected, the estimates reached steady state faster when the frequencies are larger. This partly due to it taking less time to observe the wave bias. For low frequencies OGMM does not reach steady state for σ_z until approximately 500[s] into the simulation. The DGMM converges faster and need 200-250[s] for σ_z to be steady state. When addressing the accuracy of the estimator models, the error will be calculated for 500[s] and onwards. Note that the σ_z is not the standard deviation of e_z. This is because the states are modelled differently in the estimator, see equations 5.2, than in the simulation model, see equations 4.2.

Figure 5.7 show the accuracy of GMM, optimized and not over 600[s] long simulations. A comparison of the μe_z for test frequencies is noted in table 5.2. These values are approximates.

Table 5.2: A comparison of approximate depth errors at different frequencies.

	STD $e_z[m]$	
$\omega/2\pi$ [Hz]	OGMM	DGMM
0.04	0.095	0.53
0.20	0.035	0.41
0.60	0.018	0.20
1.00	0.013	0.13

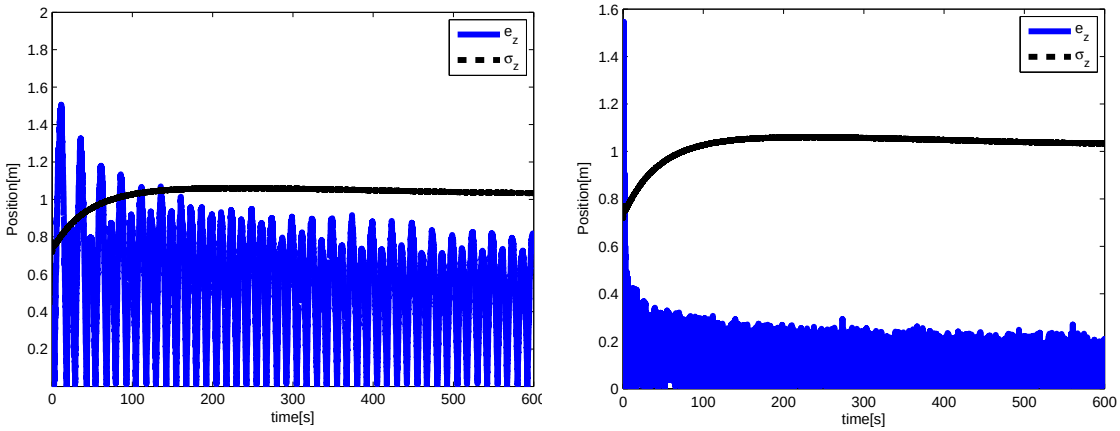

(a) $\omega = 0.04 \cdot 2\pi [rad/s]$ (b) $\omega = 1.00 \cdot 2\pi [rad/s]$

Figure 5.5: DGMM: 600[s] simulation

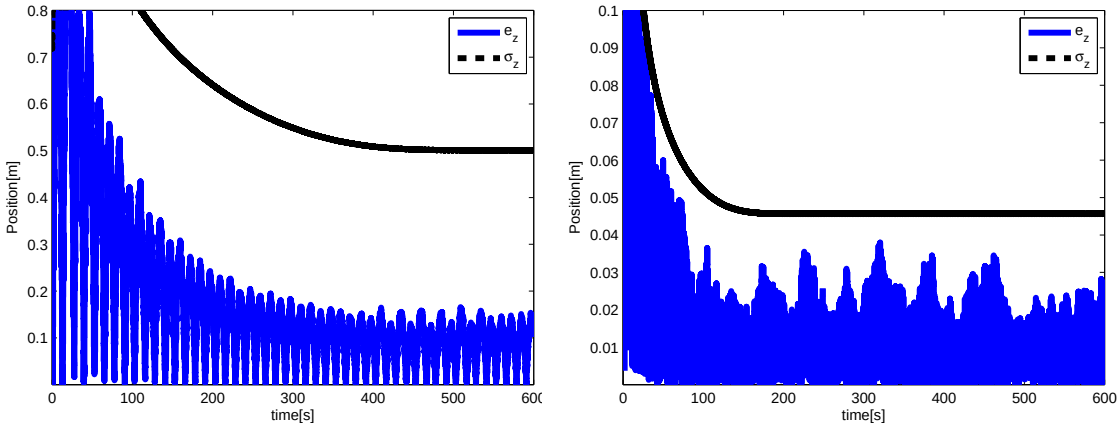

(a) $\omega = 0.04 \cdot 2\pi [rad/s]$ (b) $\omega = 1.00 \cdot 2\pi [rad/s]$

Figure 5.6: OGMM: 600[s] simulation

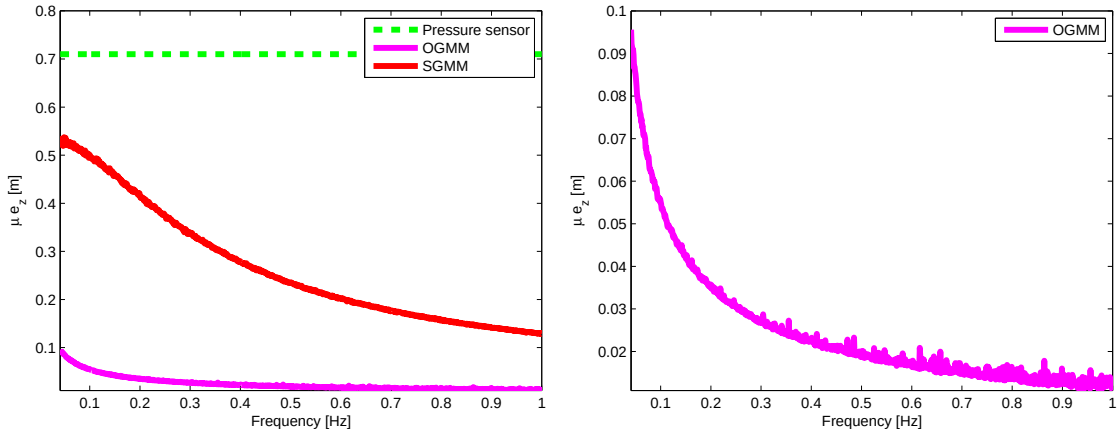

(a) Pressure sensors and estimators

(b) Close up of OGMM

Figure 5.7: GMM: Mean estimation error μe_z at different wave frequencies

5.2.4 Pressure Sensor Sampling Rate

The pressure sensor sampling rate, S_p, is important for the estimation process. All information on the wave bias is taken from the pressure sensor measurements. Figure 5.8 show how the μe_z relates to the frequency when S_p= 1[Hz]. A repeating pattern emerges when looking over a greater range of frequencies, see figures 5.9 and 5.10. The same figure also show a close up of the e_z-dynamics close to the spikes.

Pattern

From figures 5.9 and 5.10 the following patterns are observed:

- Both estimation methods repeat a pattern for every N [Hz], where N is any given integer larger than zero.
- For both DGMM and OGMM spikes occur in and around 0.5N [Hz].
- The μe_z gets larger close to N[Hz], but gets small again at the center of the spike.
- Of all frequencies, the estimates are most exact at 0.5 [Hz] for GMM.

The Nyquist Sampling Theorem (NST) lends an explanation to this pattern. The estimates get more accurate until 0.5 [Hz]. At which point the Nyquist sampling rate of more than twice

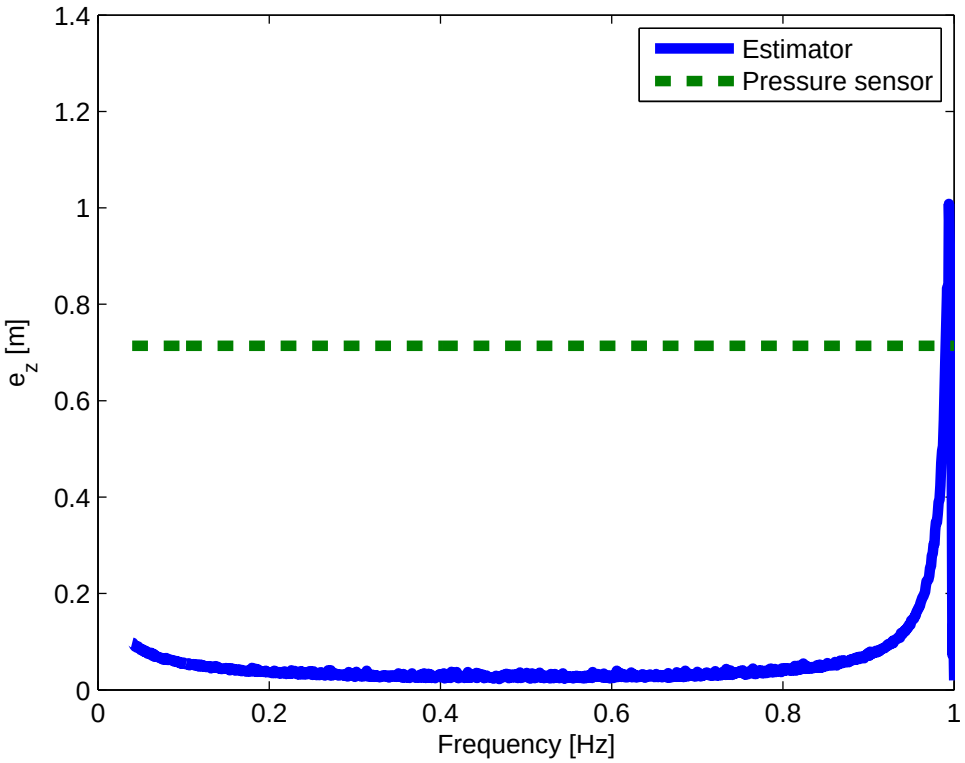

(a) OGMM

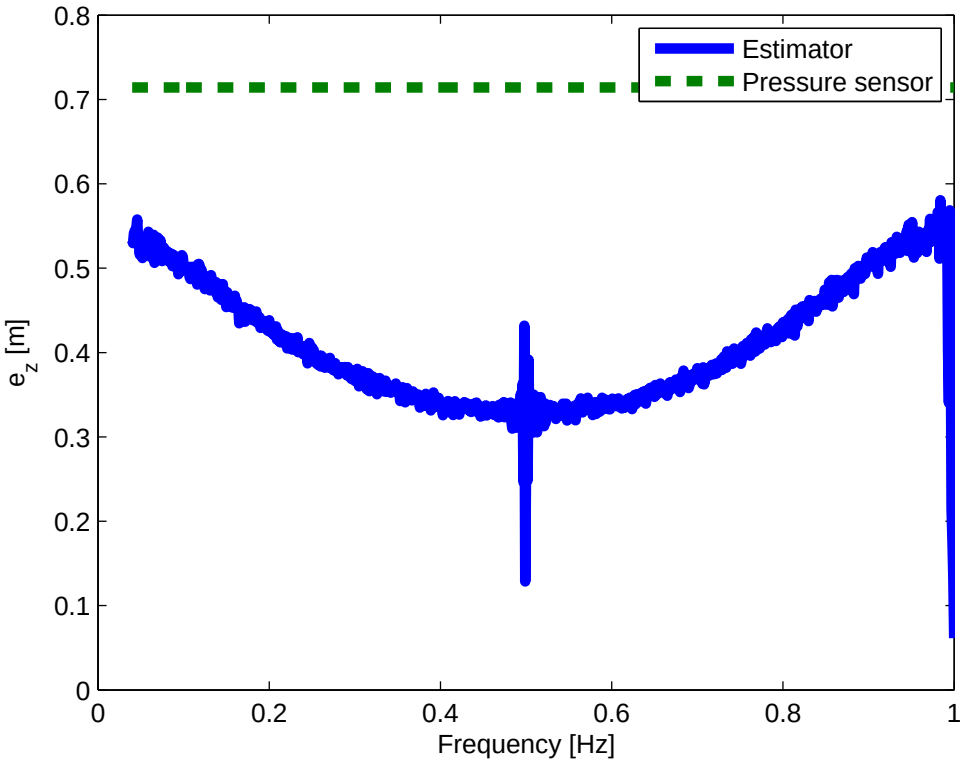

(b) DGMM

Figure 5.8: GMM: error for different frequencies. $S_{acc} = 1[\text{Hz}]$

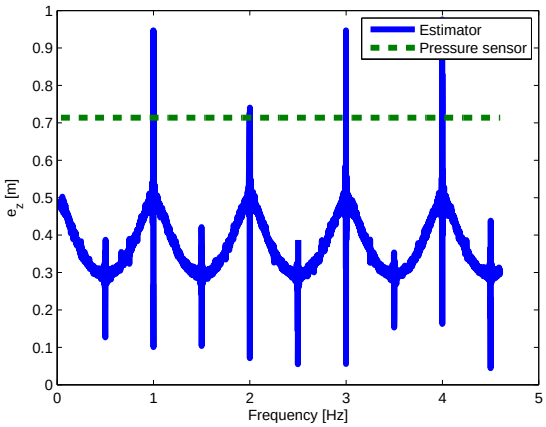

(a) Wide range of frequencies

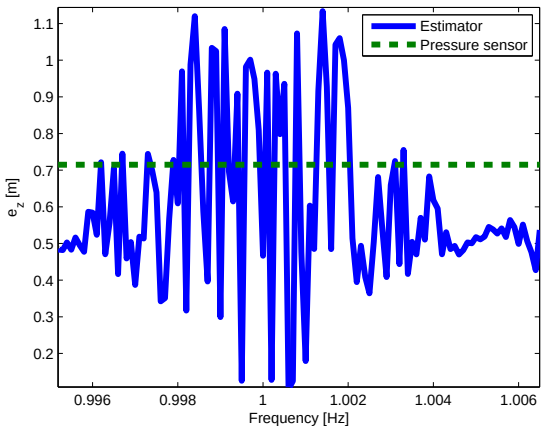

(b) μe_z dynamics close to spike

Figure 5.9: DGMM with $S_{pres} = 1[Hz]$

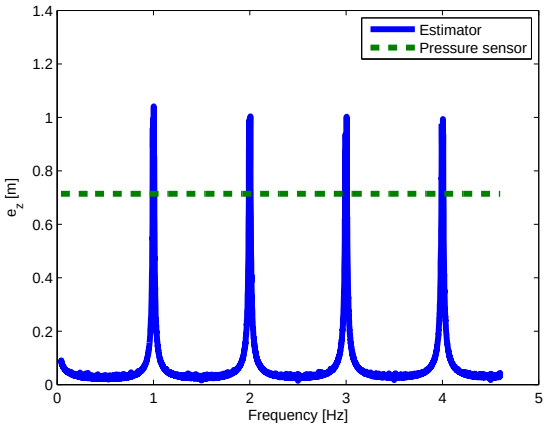

(a) Wide range of frequencies

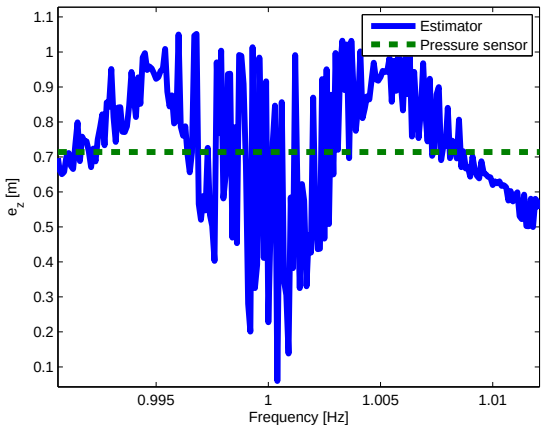

(b) μe_z dynamics close to spike

Figure 5.10: OGMM with $S_{pres} = 1[Hz]$

the frequency of the signal is no more. This pattern repeats itself as a result of aliasing. At a wave frequency of 0.5 [Hz] pressure measurement might not get the right information of the system dynamics. However in some cases that might be good for estimation, as the wave bias after all is noise.

Figure 5.11 illustrates how the phase relation between the wave bias and sampling rate might both increase and decrease the accuracy. These phase relations are simulated in figures 5.12 and 5.13. Due to phase, the best estimates should have an accuracy approximately the measurement noise (0.1[m]), while the worst will have an approximate accuracy of max wave bias amplitude (1[m]) plus/minus measurement noise. The spikes in figures 5.9 and 5.10 substantiate these claims.

A solution to the problem is to have the pressure sensor sampling frequency S_p high enough that the discussed phenomena do not occur, see figure 5.14. Although it needed not be that high, S_p was set to 10[Hz].

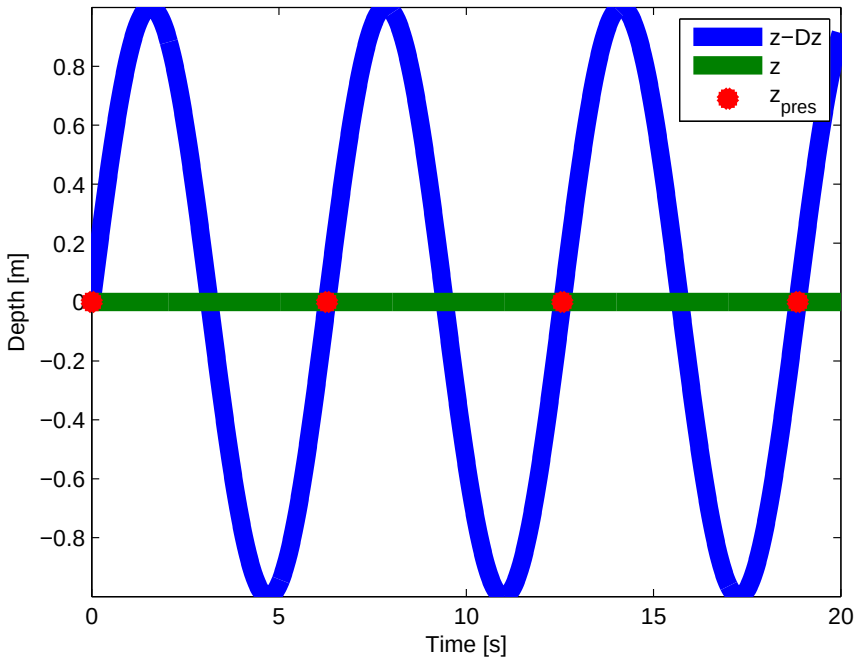

(a) Due to optimal phase alignment, the measurement is not affected by wave bias

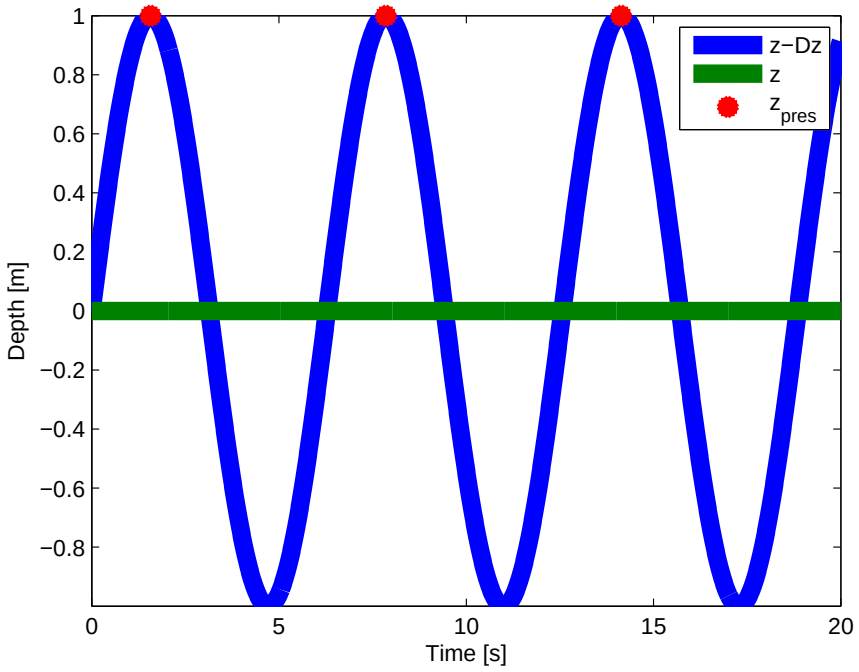

(b) Due to poor phase alignment, the measurement is erroneous without observing waves

Figure 5.11: GMM: When $S_{pres} = \omega$, the measurements are subjected to a constant bias. This can result in both poor and good estimates.

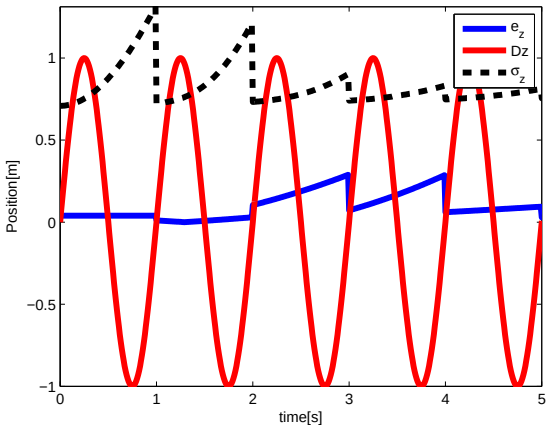

(a) Accurate estimates e_z, due to phase alignment

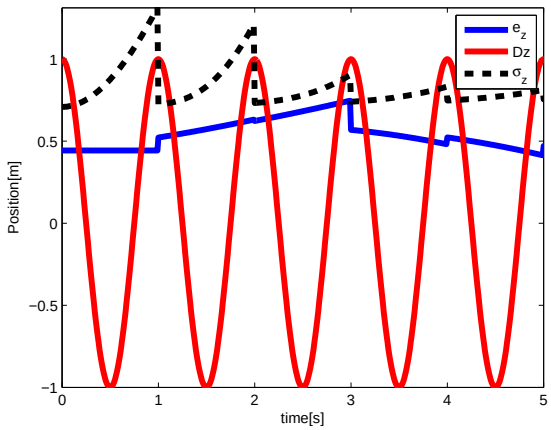

(b) Poor estimates e_z, due to phase alignment

Figure 5.12: The figures show the dynamics in figure 5.11 at work with DGMM on the simulation model

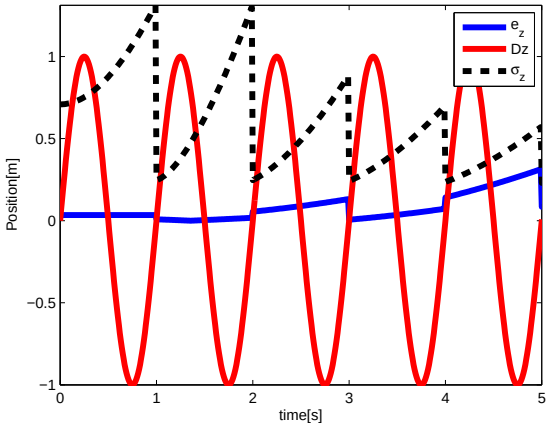

(a) Accurate estimates e_z, due to phase alignment

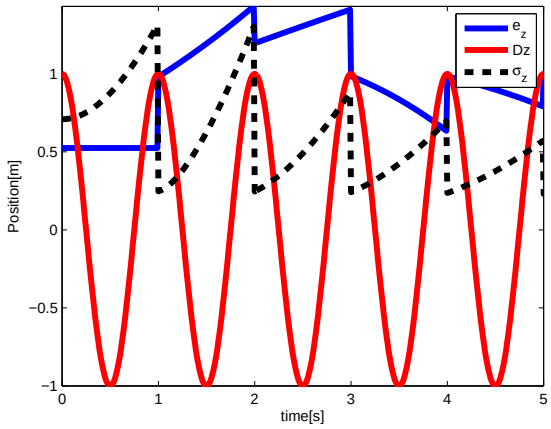

(b) Poor estimates e_z, due to phase alignment

Figure 5.13: The figures show the dynamics in figure 5.11 at work with OGMM on the simulation model

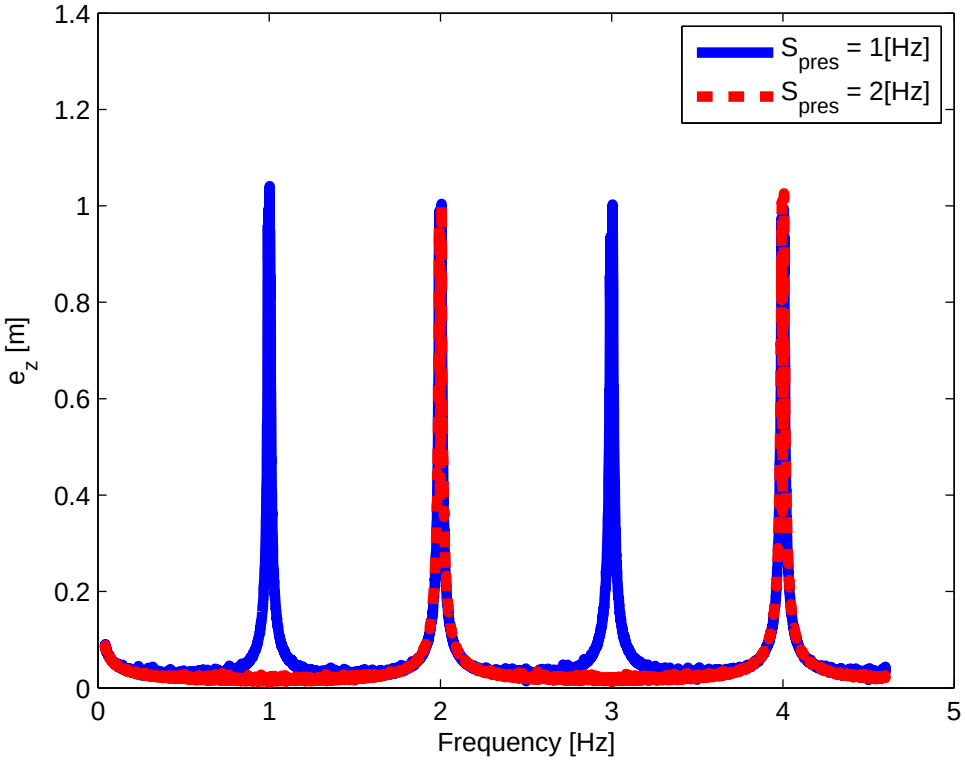

(a) GMM with optimal $\sigma_{w_{Dz}}$ and T_{Dz}

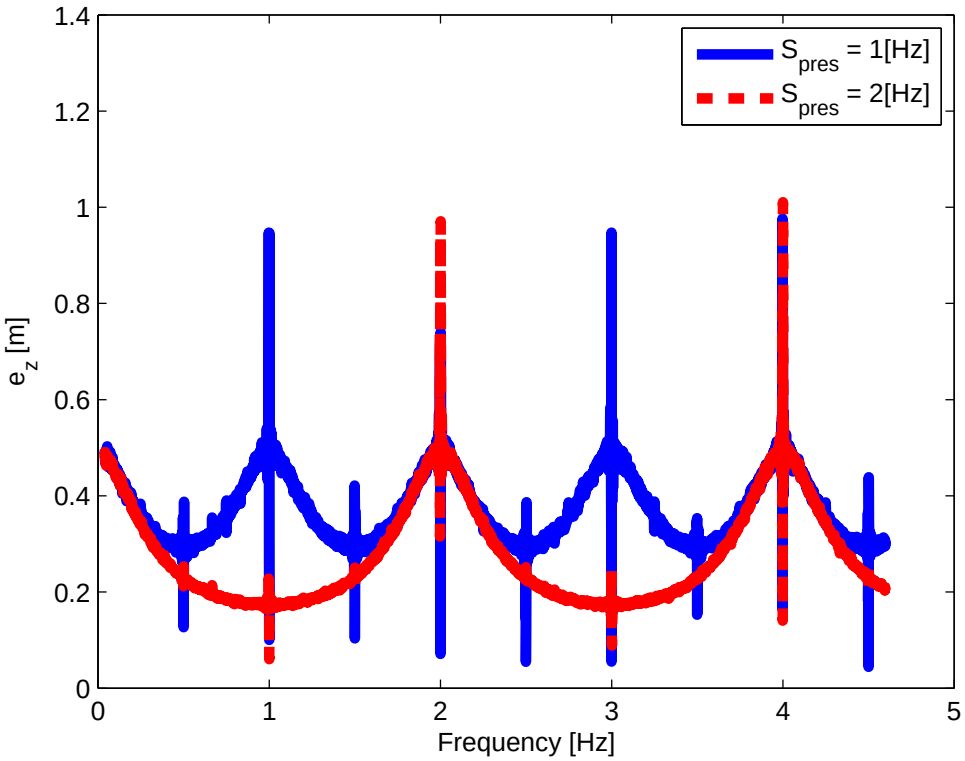

(b) GMM with default $\sigma_{w_{Dz}}$ and T_{Dz}

Figure 5.14: Estimators with S_{pres} 1 and 2 [Hz]

Chapter 6

Wave Bias Model 1

The model described in this chapter is similar to the GMM with one major difference: the process of the wave bias is modeled as an oscillatory function. Due to this it will be referred to as the *Wave Bias Model* (WBM). The model was developed in Haaland (2016) and its estimates were more accurate than those of the DGMM. However, the WBM was only tested on one set of data with one specific wave frequency. In this chapter the WBM will be implemented on the simulation data from chapter 4 so that it can be tested on different frequencies. In chapter 7 the model will be further developed so that it may estimate unknown frequencies accurately. To avoid confusion, the model in this chapter is referred to as WBM1, while the one in the next chapter is WBM2.

In order to model the wave bias Dz as an oscillatory function, the differential equation needs to be of second order. For the state space, that means adding an extra state: *wave bias velocity* ψ. The state vector of the WBM1 is:

$$\begin{bmatrix} z \\ v \\ b \\ Dz \\ \psi \end{bmatrix} \tag{6.1}$$

The process is given by 6.2. The measurement is expressed by equation 6.3, which is the

same as for GMM.

$$\dot{z} = v \tag{6.2a}$$

$$\dot{v} = a_{acc} + b + w_{acc} \tag{6.2b}$$

$$\dot{b} = -\frac{1}{T_{acc}} b + w_b \tag{6.2c}$$

$$\dot{Dz} = \psi \tag{6.2d}$$

$$\dot{\psi} = -\omega_A^2 Dz + w_{\dot{Dz}} \tag{6.2e}$$

$$z_{pres} = z - Dz + v_z \tag{6.3}$$

The system presented on state space form is:

$$\dot{x} = Ax + Bu + Ew \tag{6.4a}$$

$$y = Cx + v \tag{6.4b}$$

$$\begin{bmatrix} \dot{z} \\ \dot{v} \\ \dot{b} \\ \dot{Dz} \\ \dot{\psi} \end{bmatrix} = \underbrace{\begin{bmatrix} 0 & 1 & 0 & 0 & 0 \\ 0 & 0 & 1 & 0 & 0 \\ 0 & 0 & -(\frac{1}{T_{acc}}) & 0 & 0 \\ 0 & 0 & 0 & 0 & 1 \\ 0 & 0 & 0 & -\omega_A^2 & 0 \end{bmatrix}}_{\text{A}} \begin{bmatrix} z \\ v \\ b \\ Dz \\ \psi \end{bmatrix} + \underbrace{\begin{bmatrix} 0 \\ 1 \\ 0 \\ 0 \\ 0 \end{bmatrix}}_{\text{B}} a_{acc} + \underbrace{\begin{bmatrix} 0 & 0 & 0 \\ 1 & 0 & 0 \\ 0 & 1 & 0 \\ 0 & 0 & 0 \\ 0 & 0 & 1 \end{bmatrix}}_{\text{E}} \begin{bmatrix} w_{acc} \\ w_b \\ w_\psi \end{bmatrix} \tag{6.5}$$

$$z_{pres} = \underbrace{\begin{bmatrix} 1 & 0 & 0 & -1 & 0 \end{bmatrix}}_{\mathrm{H}} \begin{bmatrix} z \\ v \\ b \\ Dz \\ \psi \end{bmatrix} + v_z \tag{6.6}$$

$$Q = \begin{bmatrix} \sigma^2_{w_{acc}} & 0 & 0 \\ 0 & \sigma^2_{w_b} & 0 \\ 0 & 0 & \sigma^2_{w_\psi} \end{bmatrix} \tag{6.7a}$$

$$R = \sigma_{v_z} \tag{6.7b}$$

6.0.1 Parameters in WBM1

Most of the parameter values are explained in section 4.0.3. The parameters introduced by WBM1 are σ_{w_ψ} and ω_A.

σ_{w_ψ} This is the contribution of random noise in the wave bias. It is GWN with a standard deviation σ_{w_ψ} of 0.020[m]. This value was determined in Haaland (2016) through tuning.

ω_A WBM1 is dependent on an accurate estimate of the wave frequency. The assumed frequency, ω_A, is equal to that of the true wave frequency ω.

An overview of the current parameters and their values is detailed in table 6.1.

Table 6.1: WBM1 parameters

	Variable	Value	Unit	Explanation	Section
Wave-parameters	θ	0-2π	rad	Wave phase	4.0.3
	A_{max}	1	m	Max wave amplitude	4.0.3
Accelero-meter parameters	$\sigma_{w_{acc}}$	245,25	$\mu m/s^2$	STD GWN accelerometer	4.0.3
	σ_b	245,25	$\mu m/s^2$	STD bias accelerometer	4.0.3
	σ_{w_b}	5.78	$\mu m/s^{\frac{5}{2}}$	STD GWN accelerometer bias	4.0.3
	S_a	100	Hz	Sample rate accelerometer	4.0.3
	T_{acc}	3600	s	Time constant accelerometer	4.0.3
P. sensor parameters	S_p	10	Hz	Sample rate pressure sensor	5.2.4
	σ_{v_z}	0.1	m	STD GWN pressure sensor	4.0.3
WBM1	σ_{w_ψ}	0.020	m	STD GWN wave bias	6.0.1
	ω_A	ω	rad/s	Time constant wave bias	6.0.1

6.1 Linear Kalman Filter

In the same way as for the GMM, the estimation algorithm is a Linear Kalman Filter. The same requirements as in section 5.1 are checked for WBM1.

1. Process noise w_{acc}, w_b, w_ψ and v_z are all Gaussian and white. See sections 4.0.3 and 6.0.1.

2. Initial state z_0, v_0, b_0, Dz_0 and ψ_0 are, as detailed in section 4.0.1, Gaussian.

3. Linear system The state space form of both the WBM1 is detailed in equations 6.5 and 6.6. Neither of the process or measurement matrices contain any states. The system is therefore linear.

4. Observable system With equation 2.2 the observability matrix of WBM1 was checked.

Observability WBM1

$$\mathcal{O}_{WBM1} = \begin{bmatrix} 1 & 0 & 0 & -1 & 0 \\ 0 & 1 & 0 & 0 & -1 \\ 0 & 0 & 1 & \omega_A^2 & 0 \\ 0 & 0 & -(\frac{1}{T_{acc}}) & 0 & \omega_A^2 \\ 0 & 0 & (\frac{1}{T_{acc}})^2 & -\omega_A^4 & 0 \end{bmatrix} \tag{6.8}$$

$\mathcal{O}_{WBM1}$ has full rank for $\omega_A \neq 0$. Waves with a very low frequency and accelerometers with very high time constant could cause problems. However, with the T_{acc} value from section 4.0.3 and the ω_A is within the peak frequency spectrum defined in section 3.6, observability is ensured. The systems thereby satisfy the requirements for implementing a linear Kalman Filter.

6.2 Simulation

Like with the GMM, WBM1 was given input from the simulation generated by the simulation model presented in chapter 4. The discretization and estimation verification was conducted in the same fashion as for GMM, described in section 5.2. Figures 6.1 and 6.2 are from a single simulation with $\omega = 0.04 \cdot 2\pi$. Compared to GMM, see figure 6.2, it is apparent that the impact of the wave bias is much less on WBM1. This is in line with the findings of Haaland (2016).

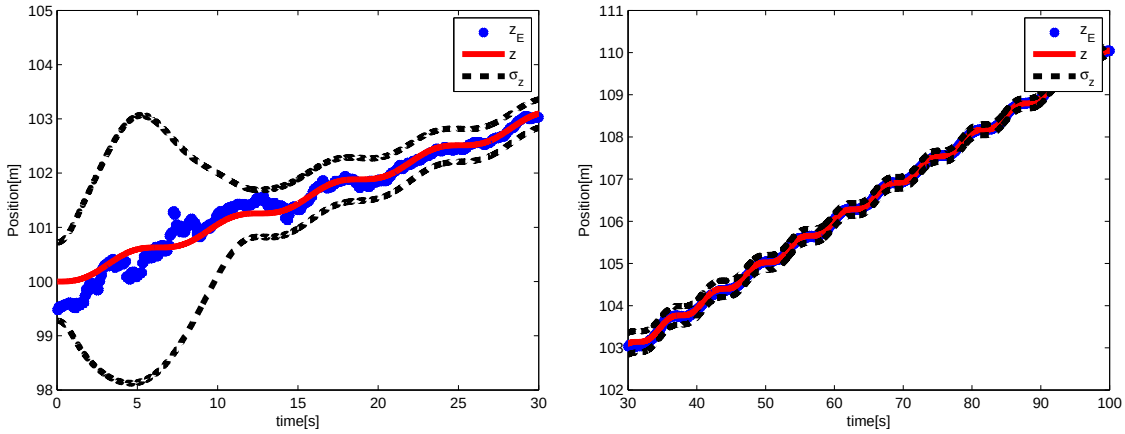

(a) Initiation (b) After initiation (note timespan)

Figure 6.1: WBM1: Estimated and true z

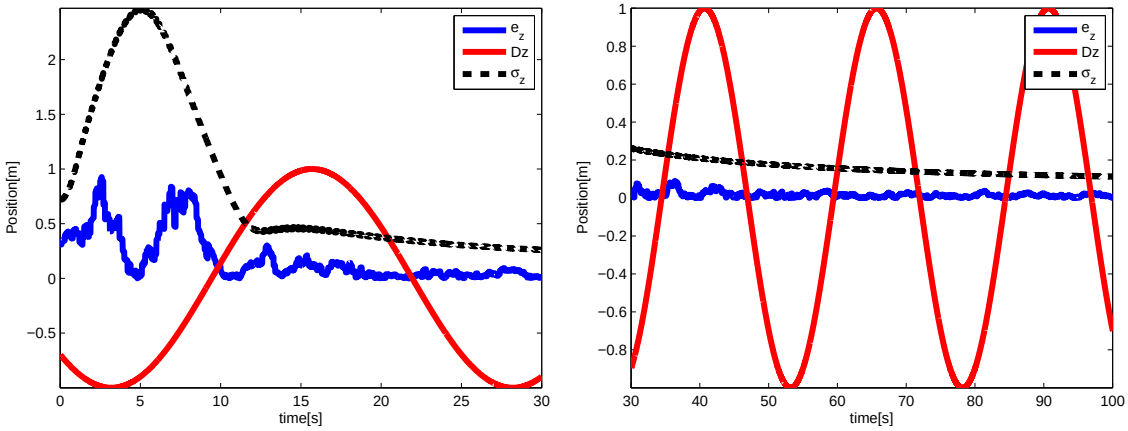

(a) Initiation (b) After initiation

Figure 6.2: WBM1: Error in z estimation (e_z)

6.2.1 Comparing WBM and GMM

Figure 6.2 shows that the estimation error is high during initiation. As with GMM, the accuracy of WBM1 will be considered from when the estimation error has reached a steady state. Figure 6.3 show e_z and σ_z over a 600[s] simulation. Values are plotted for both $\omega = 0.04 \cdot 2\pi$ [rad/s] and $\omega = 1.00 \cdot 2\pi$[rad/s]. As expected, the estimates reach steady state quicker when the frequencies are larger. For low frequencies the σ_z is at steady state approximately 200-250[s] into the simulation. When addressing the accuracy of the estimator models, the error will be calculated for 250[s] and onwards.

Figure 6.4 show WBM1 for frequencies of 0.04-1.00[Hz]. A comparison of the μe_z for test frequencies is noted in table 6.2. These values are approximates. It can be observed that the benefits of WBM1 compared to GMM are more pronounced at low frequencies. At $\omega/(2\pi) = 1$[Hz] the OGMM is about as accurate as WBM1.

Table 6.2: A comparison of approximate depth errors at different frequencies.

	STD $ez[m]$		
$\omega/2\pi$ [Hz]	OGMM	DGMM	WBM1
0.04	0.095	0.53	0.004-0.014
0.20	0.035	0.41	0.004-0.014
0.60	0.018	0.20	0.004-0.014
1.00	0.013	0.13	0.004-0.014

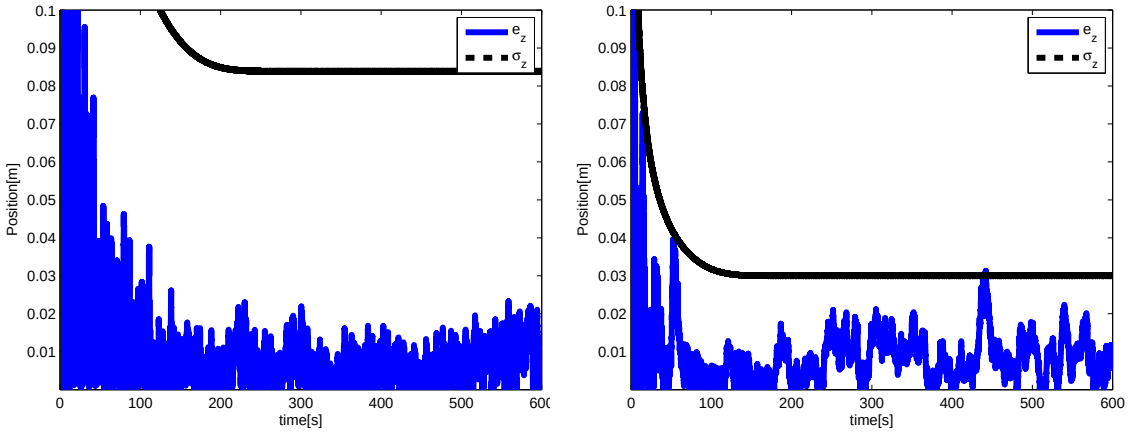

(a) $\omega = 0.04 \cdot 2\pi[rad/s]$ (b) $\omega = 1.00 \cdot 2\pi[rad/s]$

Figure 6.3: WBM for $\omega = \omega_A$

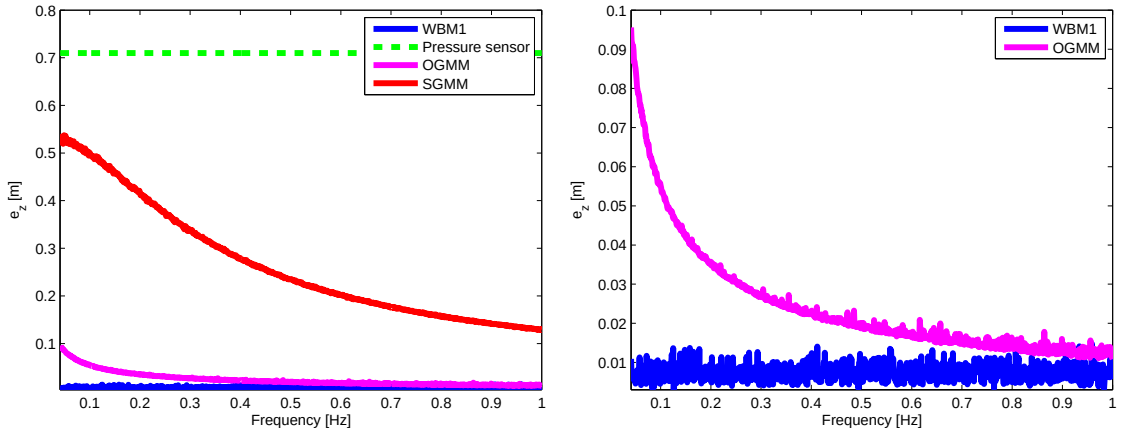

Figure 6.4: GMM: Mean estimation error μe_z at different wave frequencies

6.2.2 WBM1 for unknown ω

So far WBM1 has only been evaluated for $\omega_A = \omega$. As explained in chapter 1, one of the primary objectives is to create a model that works for unknown wave frequencies. In this section, the performance of WBM1 with unknown ω is explored. The performance of the model was compared to both and OGMM.

An overall plot of WBM1 for all reasonable values of assumed and true wave frequencies is shown in figure 6.5. Not surprisingly, the most accurate estimates are achieved when the assumed frequency equals the true. In the logarithmic plot, figure 6.5b, this relation is apparent.

So that the models could compare to the WBM, the OGMM and were plotted in figure 6.6. Note that these 3D-plots are actually the 2D-plots of figure 5.7 plotted for different ω_A. Since ω_A is not a part of the GMMs, the mean estimation error μe_z is the same for all ω_A.

Comparing plots are that show the difference in μe_z are presented in figures 6.7 and 6.8. The difference in figure 6.7a (Δe_D) is given by:

$$\Delta e_D = e_{z_{WBM}} - e_{z_{DGMM}} \tag{6.9}$$

In figure 6.8a, the difference (Δe_O) is defined as:

$$\Delta e_O = e_{z_{WBM}} - e_{z_{OGMM}} \tag{6.10}$$

A negative Δe means that for the given combination of ω and ω_A, the WBM1 is more accurate than the compared model (OGMM or DGMM). Figures 6.7b and 6.8b is a simple representation of Δe_D and Δe_O. The areas where WBM1 is more accurate is colored blue, the areas where the accuracy is approximately the same ($\pm$ 0.01[m]) is colored green, and the areas where WBM1 is less accurate is colored brown. Δe_D for all values of assumed and estimated ω, are negative. WBM1 does therefore seem to be a more accurate model than DGMM, even when ω_A is completely off.

This is not the case for Δe_O. The WBM is more accurate only when $\omega_A \approx \omega$. At medium to high frequencies, the difference between the two models is little. At low frequencies, with ω_A being off, the OGMM is much more accurate. However it is also at low frequencies that the potential benefit of WBM1 over the GMM is greatest. This, however, requires either that ω

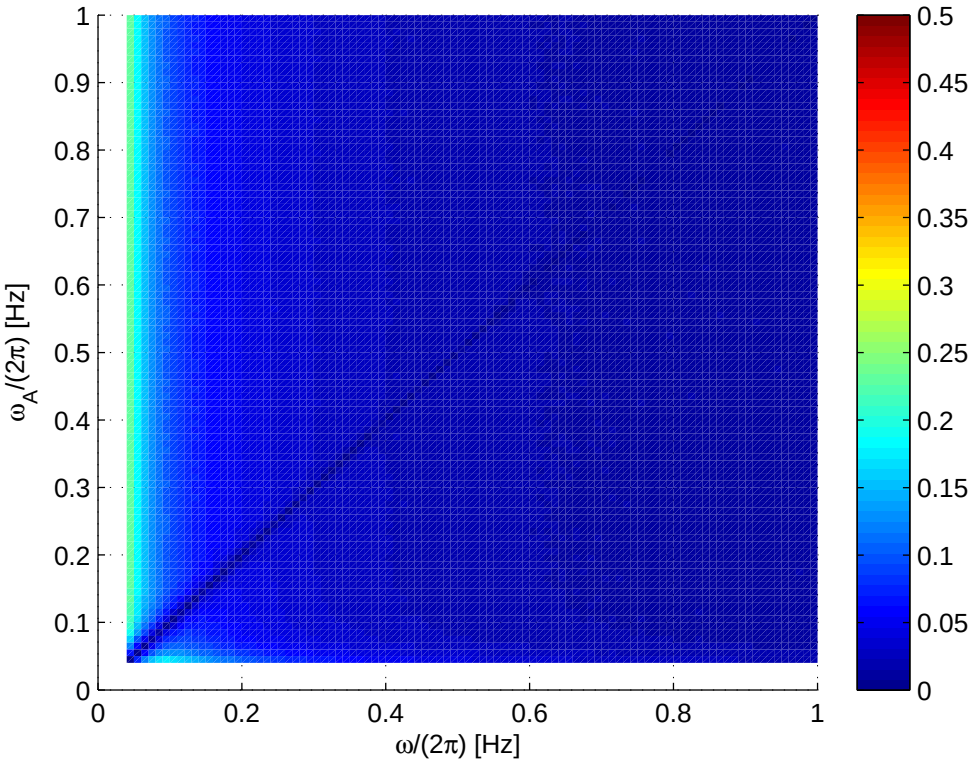

(a) Arithmetic scale

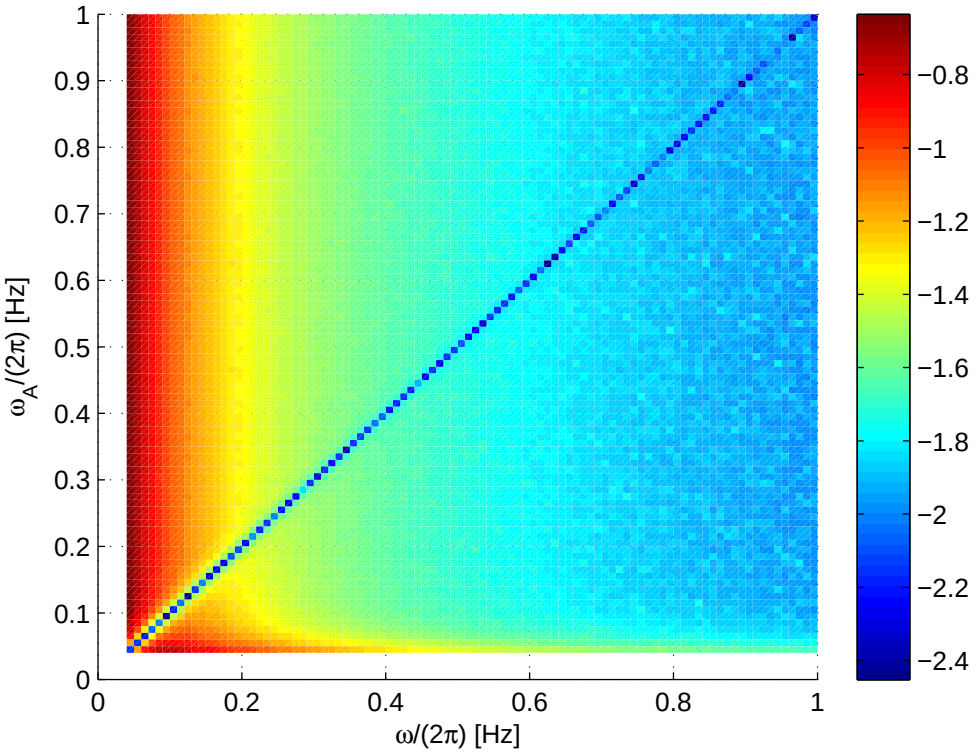

(b) Logarithmic scale

Figure 6.5: μe_z for WBM at different ω and ω_A

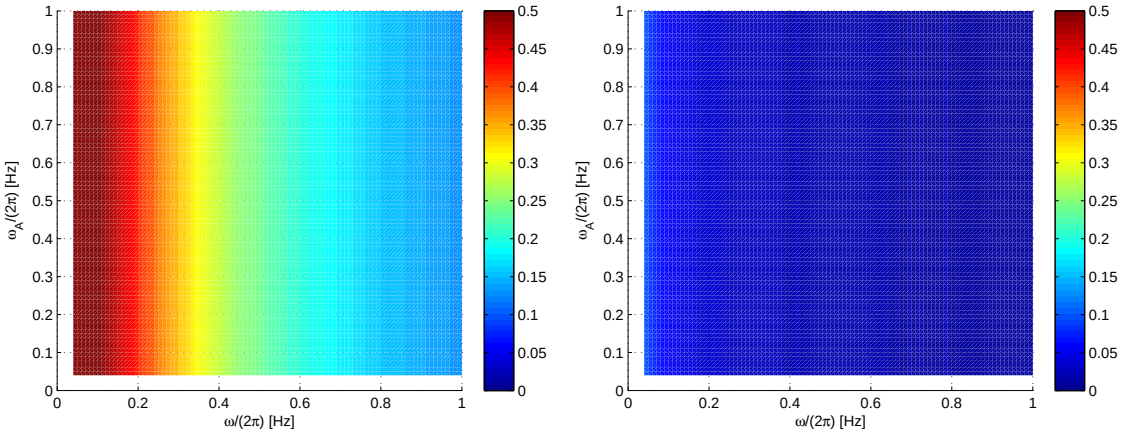

(a) DGMM (b) OGMM

Figure 6.6: GMM for different ω and ω_A

is known or that it can be estimated. Keeping with the objectives given in chapter 1, ω is not known. A model that estimates ω was therefore developed. This model is detailed in chapter 7.

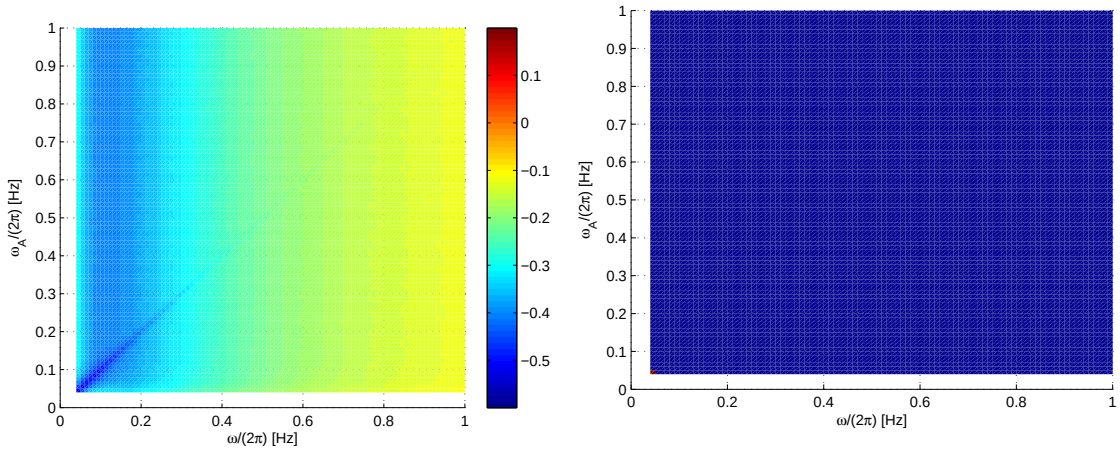

(a) Detailed Δe_D presentation

(b) Rough Δe_D presentation. Brown:Δe_D>0.01, Green:$\Delta e_D \pm 0.01$, Blue:Δe_D<-0.01

Figure 6.7: Difference in μe_z between the OGMM estimates and the GMM (Δe_D) for different true and assumed wave frequencies. $\Delta e_D = e_{z_{WBM1}} - e_{z_{DGMM}}$. WBM1 is more accurate than OGMM where the $\Delta e_D < 0$. OGMM is more accurate than WBM1 where $\Delta e_D > 0$

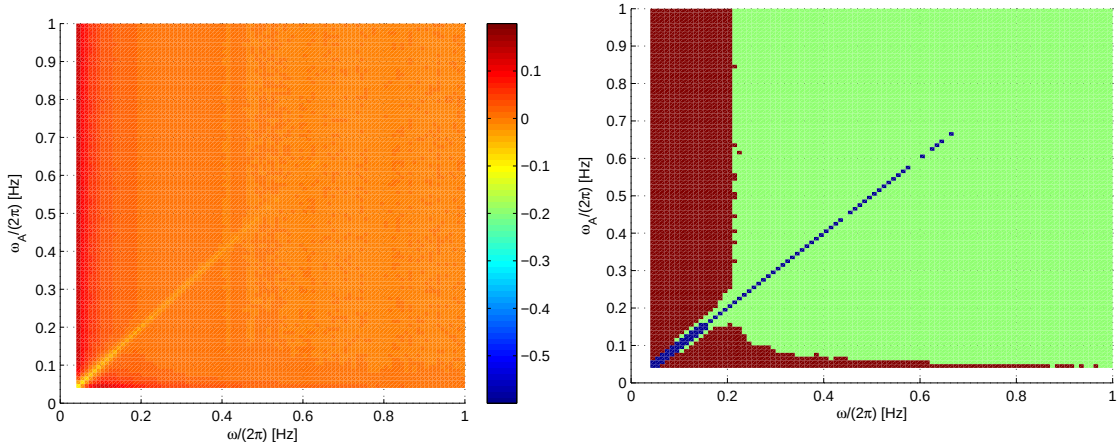

(a) Detailed Δe_O presentation

(b) Rough Δe_O presentation. Brown:Δe_O>0.01, Green:$\Delta e_O = \pm 0.01$, Blue:Δe_O<-0.01

Figure 6.8: Difference in μe_z between the OGMM estimates and the GMM (Δe_O) for different true and assumed wave frequencies. $\Delta e_O = e_{z_{WBM1}} - e_{z_{OGMM}}$. WBM1 is more accurate than OGMM where the $\Delta e_O < 0$. OGMM is more accurate than WBM1 where $\Delta e_O > 0$

Chapter 7

Wave Bias Model 2

As detailed in chapter 6, the depth estimate of WBM1 is most accurate when $\omega_A = \omega$. However, in chapter 1 it is specified that wave parameters are not known. Therefore, in this chapter, an expanded version of WBM1 is developed where the wave frequency is included in the state vector and estimated jointly with the other states. This model is referred to as WBM2 and its state vector is

$$\begin{bmatrix} z \\ v \\ b \\ Dz \\ \psi \\ \omega \end{bmatrix} \tag{7.1}$$

The process model is given by equation 7.2. The measurement is equal to that og GMM and WBM1. For the sake of convenience it is repeated in 7.3. As seen in equation 7.2f, omega is

modeled as a Gauss Markov process.

$$\dot{z} = v \tag{7.2a}$$

$$\dot{v} = a_{acc} + b + w_{acc} \tag{7.2b}$$

$$\dot{b} = -\frac{1}{T_{acc}} b + w_b \tag{7.2c}$$

$$\dot{Dz} = \psi \tag{7.2d}$$

$$\dot{\psi} = -\omega^2 Dz + w_\psi \tag{7.2e}$$

$$\dot{\omega} = \frac{1}{T_\omega}(\omega_M - \omega) + w_\omega \tag{7.2f}$$

$$z_{pres} = z - Dz + v_z \tag{7.3}$$

On state space form, the system is:

$$\dot{x} = Ax + Bu + Ew \tag{7.4a}$$

$$y = Cx + v \tag{7.4b}$$

$$\begin{bmatrix} \dot{z} \\ \dot{v} \\ \dot{b} \\ \dot{Dz} \\ \dot{\psi} \\ \dot{\omega} \end{bmatrix} = \underbrace{\begin{bmatrix} 0 & 1 & 0 & 0 & 0 & 0 \\ 0 & 0 & 1 & 0 & 0 & 0 \\ 0 & 0 & -(\frac{1}{T_{acc}}) & 0 & 0 & 0 \\ 0 & 0 & 0 & 0 & 1 & 0 \\ 0 & 0 & 0 & -\omega^2 & 0 & 0 \\ 0 & 0 & 0 & 0 & 0 & -(\frac{1}{T_\omega}) \end{bmatrix}}_{\text{A}} \begin{bmatrix} z \\ v \\ b \\ Dz \\ \psi \\ \omega \end{bmatrix} + \underbrace{\begin{bmatrix} 0 & 0 \\ 1 & 0 \\ 0 & 0 \\ 0 & 0 \\ 0 & 0 \\ 0 & \frac{1}{T_\omega} \end{bmatrix}}_{\text{B}} \begin{bmatrix} a_{acc} \\ \omega_M \end{bmatrix} + \underbrace{\begin{bmatrix} 0 & 0 & 0 & 0 \\ 1 & 0 & 0 & 0 \\ 0 & 1 & 0 & 0 \\ 0 & 0 & 0 & 0 \\ 0 & 0 & 1 & 0 \\ 0 & 0 & 0 & 1 \end{bmatrix}}_{\text{E}} \begin{bmatrix} w_{acc} \\ w_b \\ w_\psi \\ w_\omega \end{bmatrix} \tag{7.5}$$

$$z_{pres} = \underbrace{\begin{bmatrix} 1 & 0 & 0 & -1 & 0 & 0 \end{bmatrix}}_{\mathrm{H}} \begin{bmatrix} z \\ v \\ b \\ Dz \\ \psi \\ \omega \end{bmatrix} + v_z \tag{7.6}$$

$$Q = \begin{bmatrix} \sigma^2_{w_{acc}} & 0 & 0 & 0 \\ 0 & \sigma^2_{w_b} & 0 & 0 \\ 0 & 0 & \sigma^2_{w_\psi} & 0 \\ 0 & 0 & 0 & \sigma^2_{w_\omega} \end{bmatrix} \tag{7.7a}$$

$$R = \sigma_{v_z} \tag{7.7b}$$

7.0.1 Parameters in WBM2

Most of the parameters are the same as presented in section 4.0.3. The WBM2 parameters ω_M, σ_{w_ω}, σ_{w_ψ} and T_ω are detailed here.

ω_M Since the wave frequency is positive, the mean wave frequency cannot be zero. A more likely candidate, the *middle wave frequency* ω_M, is added to make sure the Gauss Markov process described in 7.2f goes towards a more likely, positive wave frequency. This parameter value will also serve as the initial estimate of the wave frequency ω. ω_M was set to $0.20 \cdot 2\pi$[rad/s]. The reasoning behind this value is explained in section 7.2.2.

w_ω The wave frequency is modeled so that it is subjected to GWN. Since the wave frequency is constant the standard deviation is given a low value: $\sigma_{w_\omega} = 10^{-3}$[rad/s]

w_ψ This parameter describes the random noise in the wave bias. This value proved to significantly influence the accuracy of the estimator. It will be detailed in section 7.2.2.

T_ω The time constant of the wave frequency was set very high. This is due to the wave frequency being constant. The value was set to: $T_\omega = 10^4$[s]. The reasoning behind a constant wave frequency is explained in section 3.6. An overview of all the parameter values for WBM2 is detailed in table 7.1.

Table 7.1: Model 2: WBM2 parameters

	Variable	Value	Unit	Explanation	Section
Wave-parameters	θ	0-2π	rad	Wave phase	4.0.3
	A_{max}	1	m	Max wave amplitude	4.0.3
Accelero-meter parameters	$\sigma_{w_{acc}}$	245,25	$\mu m/s^2$	STD GWN accelerometer	4.0.3
	σ_b	245,25	$\mu m/s^2$	STD bias accelerometer	4.0.3
	σ_{w_b}	5.78	$\mu m/s^{\frac{5}{2}}$	STD GWN accelerometer bias	4.0.3
	S_a	100	Hz	Sample rate accelerometer	4.0.3
	T_{acc}	3600	s	Time constant accelerometer	4.0.3
P. sensor parameters	S_p	10	Hz	Sample rate pressure sensor	5.2.4
	σ_{v_z}	0.1	m	STD GWN pressure sensor	4.0.3
WBM2	ω_M	0.20·2π	rad/s	Middle wave frequency	7.2.3
	σ_{w_ω}	10^{-3}	m	STD GWN wave frequency	7.0.1
	σ_{w_ψ}	Variable	m/s	STD GWN wave bias velocity	7.2.3
	T_ω	10^4	s	Time constant wave frequency	7.0.1

7.1 Extended Kalman Filter

The system described so far in this chapter satisfies requirement 1 and 2 from section 2.4.1. However equation 7.2e is not linear as it contains the term $\omega^2 Dz$. The Linear Kalman Filter that was implemented on WBM1 is therefore not applicable. An Extended Kalman Filter (EKF), as described in section 2.4.2 is used instead.

7.1.1 Linearization

The EKF requires that the process and measurements are linearized. Since the measurement is linear, the linearization can be omitted. The process was linearized before it is discretized, even though the reversed order has been proven to be exact (Grammont et al., 2014). This is

done since it is simpler to discretize a linear system. The linearization of $Ax + bu$ is denoted by $F(\tilde{x}(t), u(t), t)$, see equation 7.8a.

$$\delta\dot{x} = F(\tilde{x}(t), u(t))\delta x(t) + w(t) \tag{7.8a}$$

$$\delta z_{pres} = H\delta x + v_z(t) \tag{7.8b}$$

In the simulation, the linearization is done numerically. To control the numerical method, an analytical linearizaton was done, shown in 7.9. x denotes the states, while $\tilde{x}$ denotes the state values at the point of linearization.

$$F(\tilde{x}(t),u(t)) = \begin{bmatrix} \frac{\delta f_1}{\delta x_1} & \frac{\delta f_1}{\delta x_2} & \frac{\delta f_1}{\delta x_3} & \frac{\delta f_1}{\delta x_4} & \frac{\delta f_1}{\delta x_5} & \frac{\delta f_1}{\delta x_6} \\ \frac{\delta f_2}{\delta x_1} & \frac{\delta f_2}{\delta x_2} & \frac{\delta f_2}{\delta x_3} & \frac{\delta f_2}{\delta x_4} & \frac{\delta f_2}{\delta x_5} & \frac{\delta f_2}{\delta x_6} \\ \frac{\delta f_3}{\delta x_1} & \frac{\delta f_3}{\delta x_2} & \frac{\delta f_3}{\delta x_3} & \frac{\delta f_3}{\delta x_4} & \frac{\delta f_3}{\delta x_5} & \frac{\delta f_3}{\delta x_6} \\ \frac{\delta f_4}{\delta x_1} & \frac{\delta f_4}{\delta x_2} & \frac{\delta f_4}{\delta x_3} & \frac{\delta f_4}{\delta x_4} & \frac{\delta f_4}{\delta x_5} & \frac{\delta f_4}{\delta x_6} \\ \frac{\delta f_5}{\delta x_1} & \frac{\delta f_5}{\delta x_2} & \frac{\delta f_5}{\delta x_3} & \frac{\delta f_5}{\delta x_4} & \frac{\delta f_5}{\delta x_5} & \frac{\delta f_5}{\delta x_6} \\ \frac{\delta f_6}{\delta x_1} & \frac{\delta f_6}{\delta x_2} & \frac{\delta f_6}{\delta x_3} & \frac{\delta f_6}{\delta x_4} & \frac{\delta f_6}{\delta x_5} & \frac{\delta f_6}{\delta x_6} \end{bmatrix}_{x=\tilde{x}} \tag{7.9a}$$

$$F(\tilde{x}(t),u(t),t) = \begin{bmatrix} \frac{\delta v}{\delta z} & \frac{\delta v}{\delta v} & \frac{\delta v}{\delta b} & \frac{\delta v}{\delta Dz} & \frac{\delta v}{\delta \dot{D}z} & \frac{\delta v}{\delta \omega} \\ \frac{\delta(a_{acc}+b)}{\delta z} & \frac{\delta(a_{acc}+b)}{\delta v} & \frac{\delta(a_{acc}+b)}{\delta b} & \frac{\delta(a_{acc}+b)}{\delta Dz} & \frac{\delta(a_{acc}+b)}{\delta \dot{D}z} & \frac{\delta(a_{acc}+)b}{\delta \omega} \\ \frac{\delta(-\frac{b}{T_{acc}})}{\delta z} & \frac{\delta(-\frac{b}{T_{acc}})}{\delta v} & \frac{\delta(-\frac{b}{T_{acc}})}{\delta b} & \frac{\delta(-\frac{b}{T_{acc}})}{\delta Dz} & \frac{\delta(-\frac{b}{T_{acc}})}{\delta \dot{D}z} & \frac{\delta(-\frac{b}{T_{acc}})}{\delta \omega} \\ \frac{\delta \dot{D}z}{\delta z} & \frac{\delta \dot{D}z}{\delta v} & \frac{\delta \dot{D}z}{\delta b} & \frac{\delta \dot{D}z}{\delta Dz} & \frac{\delta \dot{D}z}{\delta \dot{D}z} & \frac{\delta \dot{D}z}{\delta \omega} \\ \frac{\delta(-\omega^2 Dz)}{\delta z} & \frac{\delta(-\omega^2 Dz)}{\delta v} & \frac{\delta(-\omega^2 Dz)}{\delta b} & \frac{\delta(-\omega^2 Dz)}{\delta Dz} & \frac{\delta(-\omega^2 Dz)}{\delta \dot{D}z} & \frac{\delta(-\omega^2 Dz)}{\delta \omega} \\ \frac{\delta(-\frac{\omega}{T_\omega})}{\delta z} & \frac{\delta(-\frac{\omega}{T_\omega})}{\delta v} & \frac{\delta(-\frac{\omega}{T_\omega})}{\delta b} & \frac{\delta(-\frac{\omega}{T_\omega})}{\delta Dz} & \frac{\delta(-\frac{\omega}{T_\omega})}{\delta \dot{D}z} & \frac{\delta(-\frac{\omega}{T_\omega})}{\delta \omega} \end{bmatrix}_{x=\tilde{x}} \tag{7.9b}$$

$$F(\tilde{x}(t),u(t)) = \begin{bmatrix} 0 & 1 & 0 & 0 & 0 & 0 \\ 0 & 0 & 1 & 0 & 0 & 0 \\ 0 & 0 & -(\frac{1}{T_{acc}}) & 0 & 0 & 0 \\ 0 & 0 & 0 & 0 & 1 & 0 \\ 0 & 0 & 0 & -\tilde{\omega}^2 & 0 & -2\tilde{\omega}\tilde{Dz} \\ 0 & 0 & 0 & 0 & 0 & -(\frac{1}{T_\omega}) \end{bmatrix} \tag{7.9c}$$

7.1.2 Observability

Another use of the analytical linearization in equation 7.9 is that it can be used to check for observability.

$$\mathcal{O} = \begin{bmatrix} 1 & 0 & 0 & -1 & 0 & 0 \\ 0 & 1 & 0 & 0 & -1 & 0 \\ 0 & 0 & 1 & \tilde{\omega}^2 & 0 & 2\tilde{\omega}\tilde{Dz} \\ 0 & 0 & -(\frac{1}{T_{acc}}) & 0 & \tilde{\omega}^2 & -(\frac{1}{T_\omega}) \\ 0 & 0 & \frac{1}{T_{acc}^2} & -\tilde{\omega}^4 & 0 & 2\tilde{\omega}\tilde{Dz}(\frac{1}{T_\omega^2} - \tilde{\omega}^2) \\ 0 & 0 & -(\frac{1}{T_{acc}^3}) & 0 & -\tilde{\omega}^4 & \frac{2\tilde{\omega}\tilde{Dz}}{T_\omega}(\tilde{\omega}^2 - \frac{1}{T_\omega^2}) \end{bmatrix} \tag{7.10}$$

The matrix 7.10 has full rank for all reasonable values of states and parameters. The system is observable.

7.2 Simulation

In the same way as the previous model, WBM2 was given input from the simulation model described in chapter 4. The discretization was carried out in the same way as for GMM in section 5.2.1. To see whether WBM2, estimates were inspected. Plots shown in figures 7.1 and 7.2 are from a single simulation with $\omega = 0.04 \cdot 2\pi$.

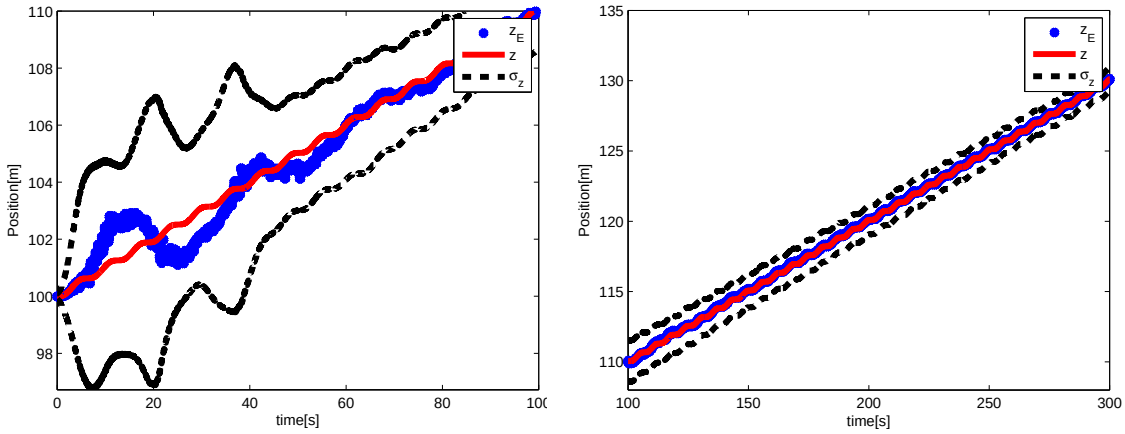

(a) Initiation (b) After initiation

Figure 7.1: WBM: Estimated and true z

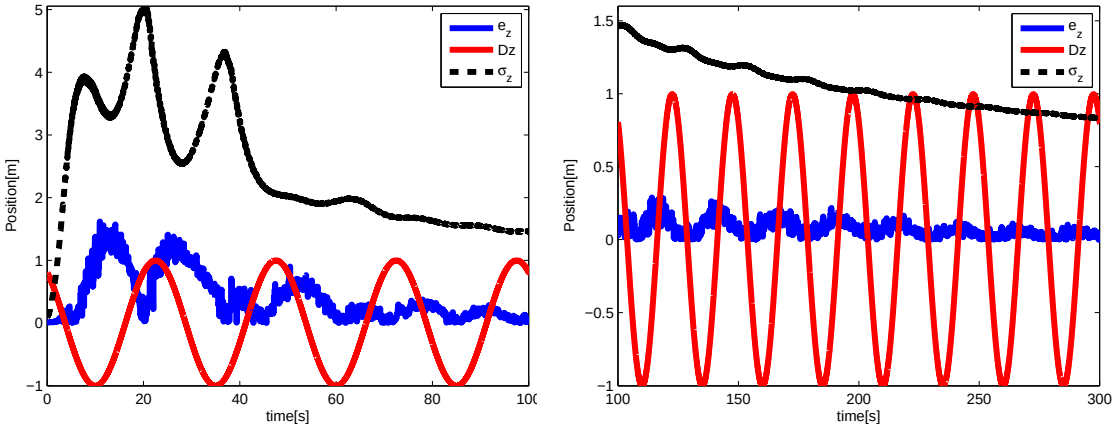

(a) Initiation (b) After initiation

Figure 7.2: WBM: Error in z estimation (e_z)

7.2.1 Evaluating WBM2

As expected, figure 7.2 show that accuracy is low during initiation. Like with GMM and WBM1, it is the stable state estimates that are of interest. Figure 7.3 show e_z and σ_z over a 2000[s] simulation. Values are plotted for both $\omega = 0.04 \cdot 2\pi$ [rad/s] and $\omega = 1.00 \cdot 2\pi$[rad/s]. The accuracy of the estimates will be considered from 1000[s] into the simulation.

Figure 7.4 show the accuracy of WBM2, OGMM and for the entire frequency specter. Approximate accuracies at test frequencies are detailed in table 7.2. WBM2 outperforms at all frequencies. OGMM however, is more accurate at high frequencies.

Table 7.2: A comparison of approximate depth errors at different frequencies.

	STD $e_z[m]$			
$\omega/2\pi$ [Hz]	OGMM	DGMM	WBM1	WBM2
0.04	0.095	0.53	0.004-0.014	0.02-0.03
0.20	0.035	0.41	0.004-0.014	0.015-0.045
0.60	0.018	0.20	0.004-0.014	0.01-0.08
1.00	0.013	0.13	0.004-0.014	0.02-0.11

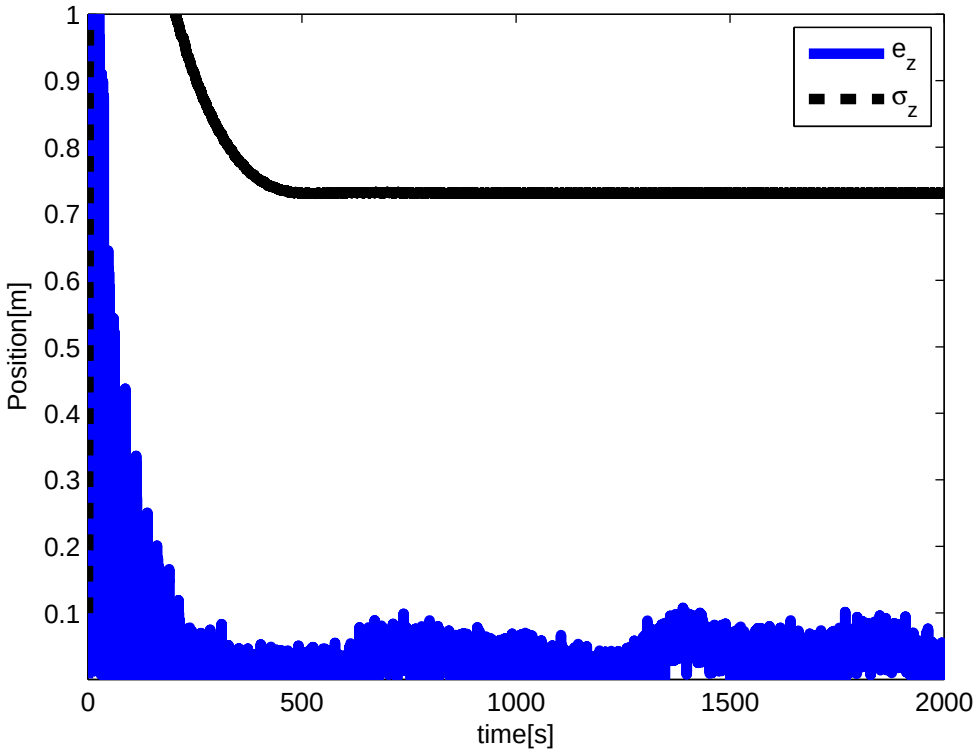

(a) $\omega = 0.04 \cdot 2\pi [rad/s]$

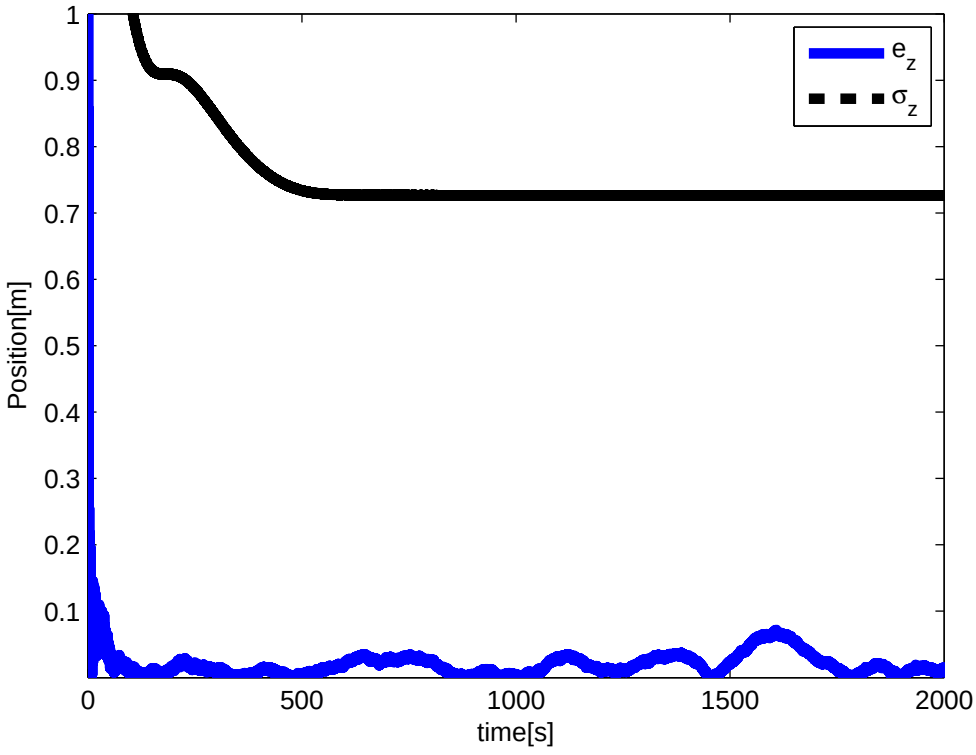

(b) $\omega = 1.00 \cdot 2\pi [rad/s]$

Figure 7.3: WBM for $\omega = \omega_M$

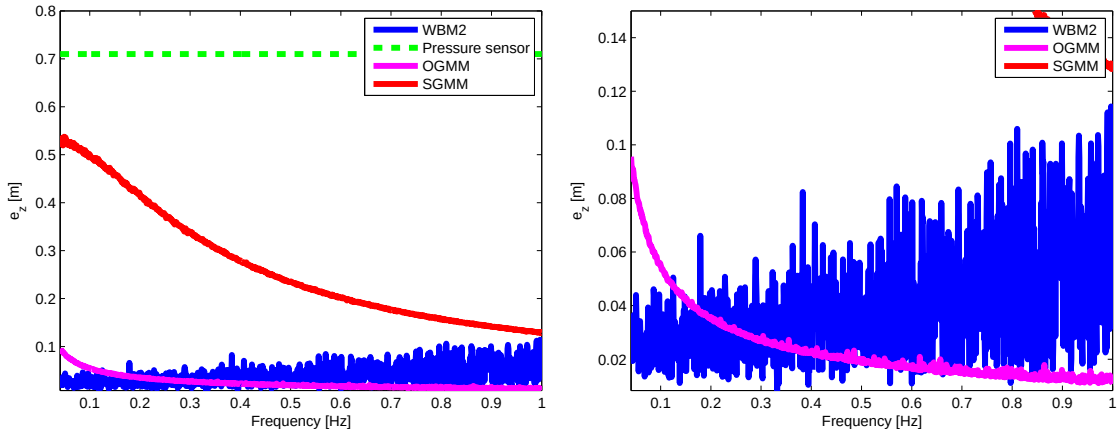

Figure 7.4: WBM2 compared to OGMM and

7.2.2 Wave Bias Velocity Noise

Most of the parameters of WBM2 were simple to estimate, see section 7.0.1. This was not the case for the standard deviation of the wave bias velocity noise, σ_{w_ψ}. It seemed to be connected to both wave frequency and amplitude.

Frequency Relation

Figures 7.5-7.8 show a relationship between the mean depth error μe_z and σ_{w_ψ} for test frequencies. For each sample of σ_{w_ψ}, ten simulations were conducted. The most accurate, least accurate and the average estimates were color coded and plotted. The average does not take into account outliers significance value of 0.05. The same plot is presented twice for each test frequency. This is to show that there is a big gap in μe_z at the same time as to present the most accurate range of σ_{w_ψ} values. These ranges are also shown in table 7.3. It is clear that there is a relationship between ω and σ_{w_ψ}. Because robustness is important, when talking of accuracy for an ensemble of estimations, it is the *Max* values in the plots that is considered.

One possible explanation to how σ_{w_ψ} relates to ω can be found through equation 7.2e, repeated here for convenience:

$$\dot{\psi} = -\omega^2 Dz + w_\psi$$

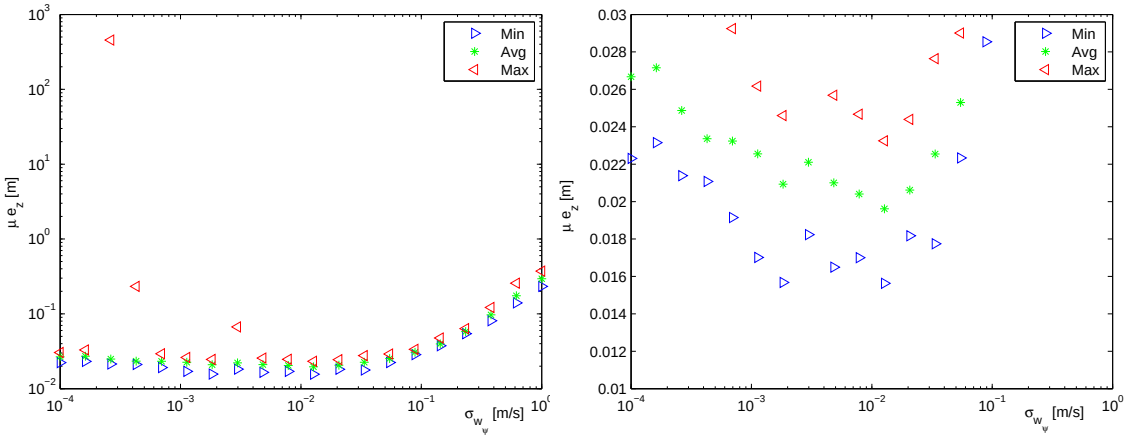

(a) σ_{w_ψ}: logarithmic error (b) σ_{w_ψ}: arithmetic error

Figure 7.5: $\omega_M/2\pi = \omega/2\pi = 0.04[Hz]$

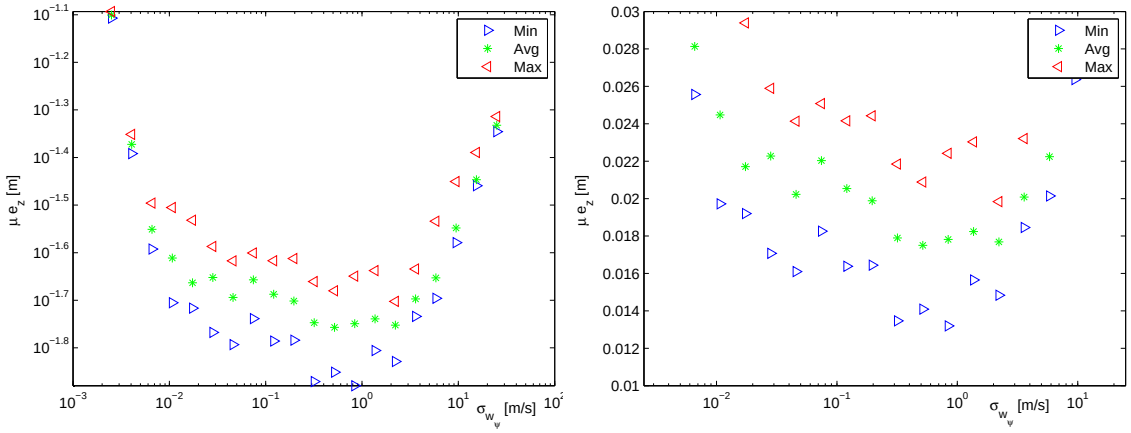

(a) σ_{w_ψ}: logarithmic error (b) σ_{w_ψ}: arithmetic error

Figure 7.6: $\omega_M/2\pi = \omega/2\pi = 0.20[Hz]$

Table 7.3: Most accurate $\sigma_{w_{\dot{D}z}}$ range for different ω

	σ_{w_ψ} [m/s]	
$\omega/2\pi$ [Hz]	Min	Max
0.04	0.001	0.04
0.20	0.1	4
0.60	2	60
1.00	3	200

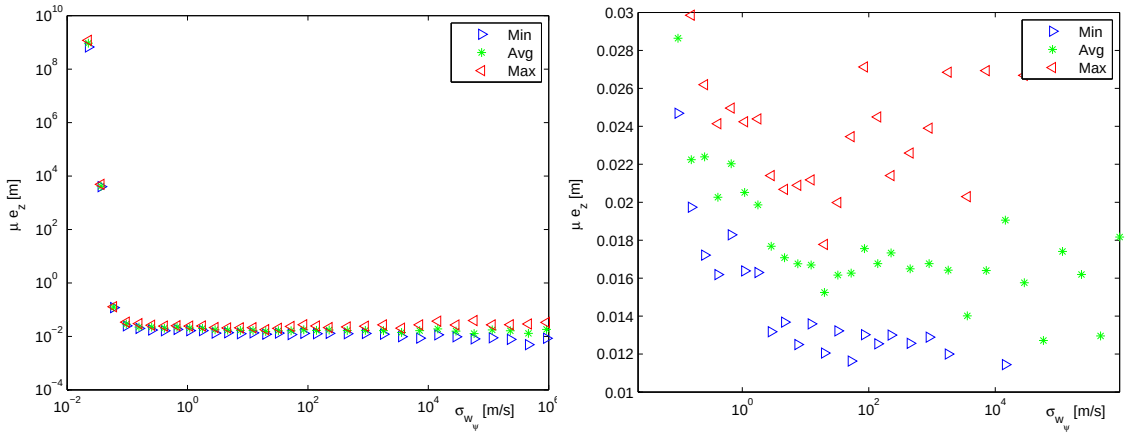

(a) σ_{w_ψ}: logarithmic error

(b) σ_{w_ψ}: arithmetic error

Figure 7.7: $\omega_M/2\pi = \omega/2\pi = 0.60[Hz]$

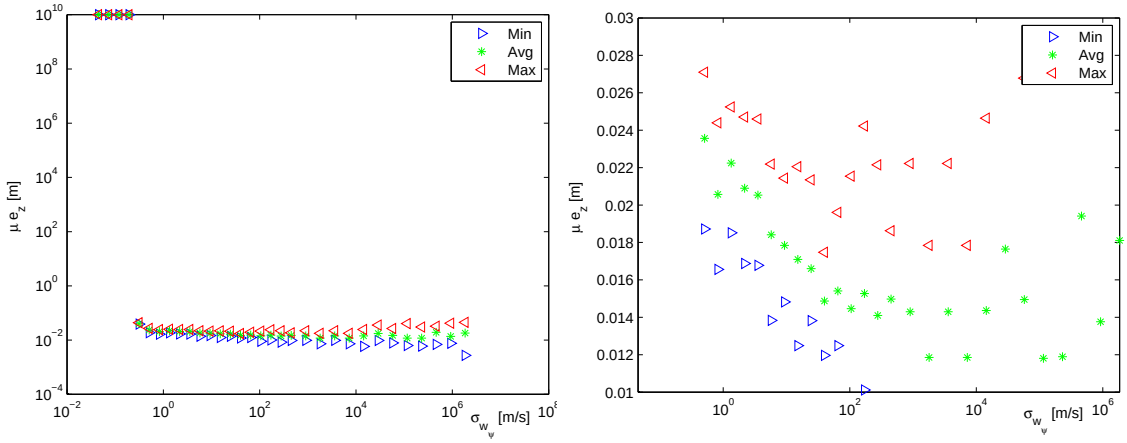

(a) σ_{w_ψ}: logarithmic error

(b) σ_{w_ψ}: arithmetic error

Figure 7.8: $\omega_M/2\pi = \omega/2\pi = 1.00[Hz]$

Table 7.4: C_{w_ψ}

	C_{w_ψ}	
$\omega/2\pi$ [Hz]	min	max
0.04	3.1	25
0.20	5	100
0.60	13.9	166.7
1.00	10	200

Here the contribution of the wave bias depends heavily on ω, while the noise is independent. One way of changing this is by defining σ_{w_ψ} as a function of ω:

$$\sigma_{w_\psi} = \omega^2 C_{w_\psi} \tag{7.11}$$

where $C_{w_{\dot{D}z}}$ is constant for all ω.

Figures 7.5-7.8 have all $\omega_M = \omega$. To test whether the relation in 7.11 can prevent deviation, there must exist a C_{w_ψ} and ω_M that for any ω within the given range, will produce an estimate that is reasonably accurate. To see whether these parameters exist, a new set of simulations were estimated with different values of C_{w_ψ}, ω_M and ω.

The test range of ω_M and ω is naturally given by the peak frequency spectrum. The test range of C_{w_ψ} is approximated by applying equation 7.11 on the accurate σ_{w_ψ} ranges presented in table 7.3. The result for different wave frequencies is shown in table 7.4. From these values, the range of C_{w_ψ} was initially set to 3-200. However, seeing that the accuracy was much higher at the lower end of that spectrum, the range was set to 0.01-40. Plots are shown in figures 7.9-7.12.

Some of the lowest values of $C_{w_{\dot{D}z}}$ gave more accurate estimates. However they were also more prone to diverge. A quick investigation found the most accurate of the robust parameter value combinations to be $\omega_M/(2\pi) = 0.20$ [Hz] and $C_{w_{\dot{D}z}} = 4$, see table 7.5. This prompted a more thorough inspection of the accuracy at $\omega_M = 0.20 \cdot 2\pi$, which found $C_{w_\psi} = 5$ to be an even better parameter value.

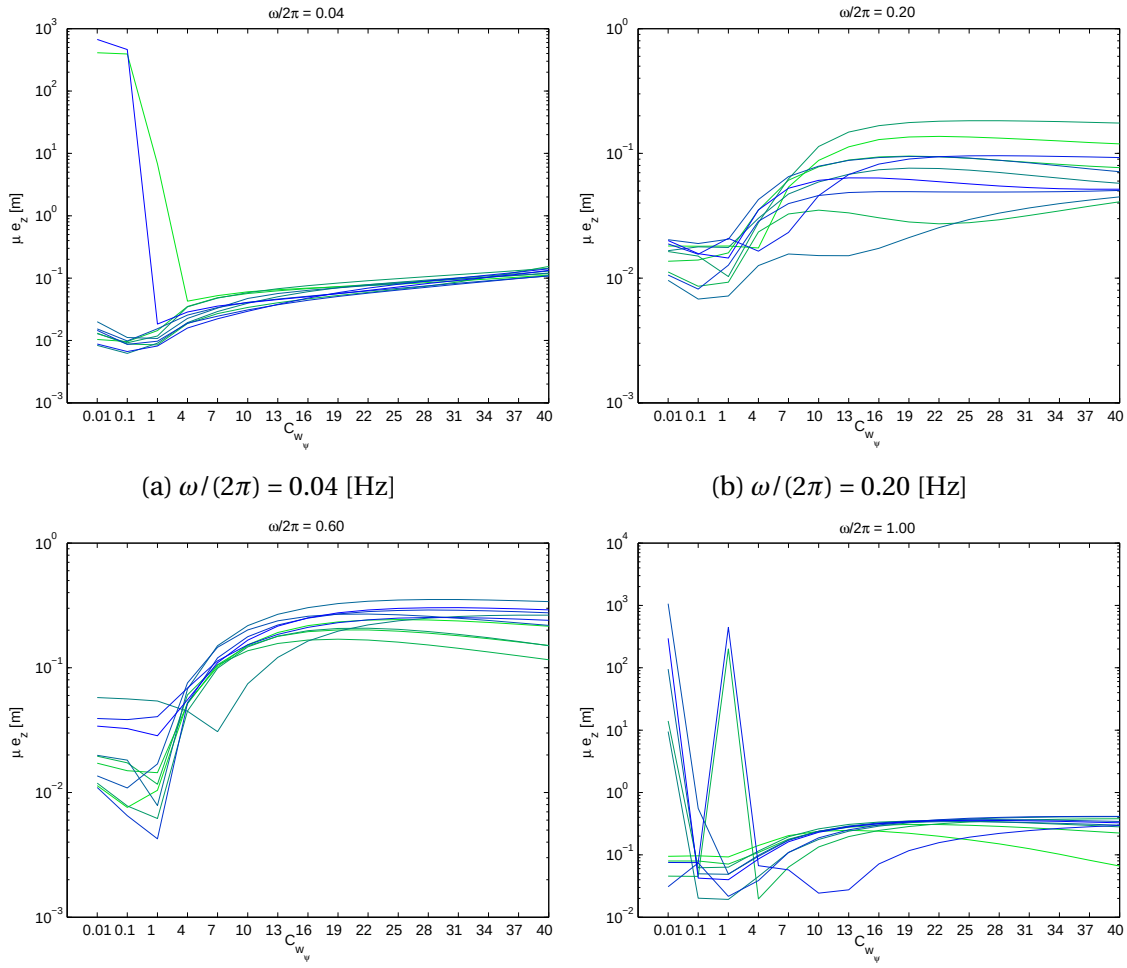

(a) $\omega/(2\pi) = 0.04$ [Hz]

(b) $\omega/(2\pi) = 0.20$ [Hz]

(c) $\omega/(2\pi) = 0.60$ [Hz]

(d) $\omega/(2\pi) = 1.00$ [Hz]

Figure 7.9: $\omega_M/2\pi = 0.04[Hz]$

Table 7.5: Finding the best ω_a and $C_{w_{\dot{D}z}}$

$\omega_a/2\pi$ [Hz]	Best $C_{w_{\dot{D}z}}$	max e_z [m]
0.04	4	0.141
0.15	7	0.081
0.20	4	0.073
0.30	4	0.088
0.40	4	0.089
0.60	1	0.084
1.00	1	0.084

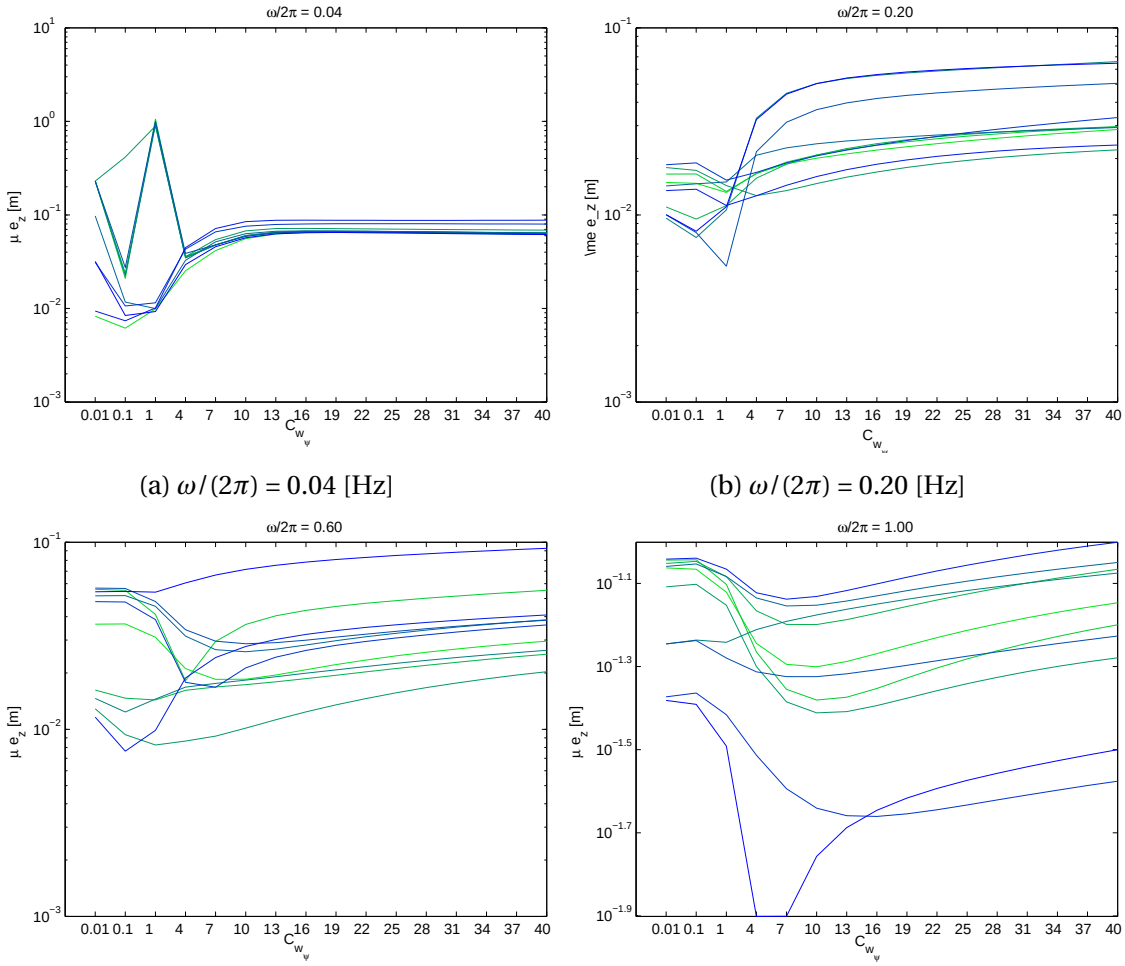

(a) $\omega/(2\pi) = 0.04$ [Hz]

(b) $\omega/(2\pi) = 0.20$ [Hz]

(c) $\omega/(2\pi) = 0.60$ [Hz]

(d) $\omega/(2\pi) = 1.00$ [Hz]

Figure 7.10: $\omega_M/2\pi = 0.20[Hz]$

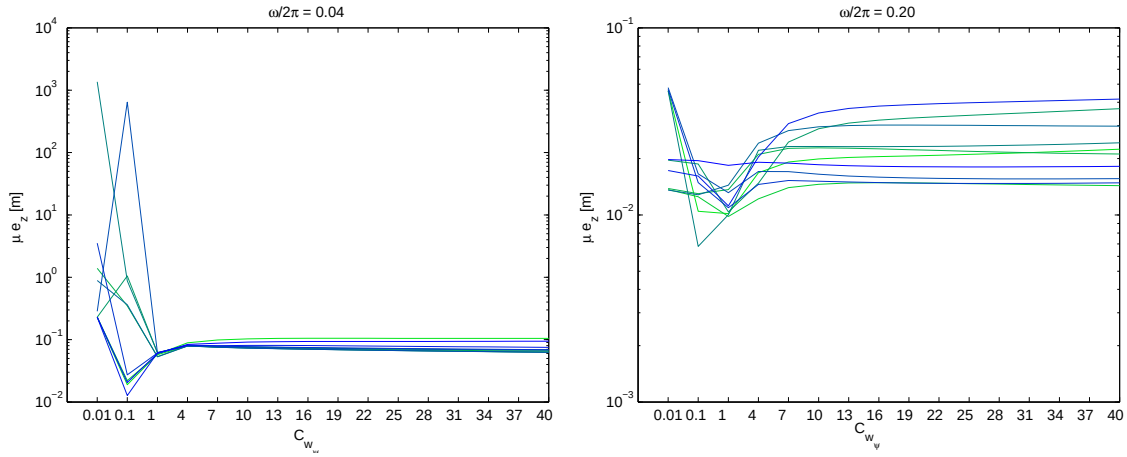

(a) $\omega/(2\pi) = 0.04$ [Hz]

(b) $\omega/(2\pi) = 0.20$ [Hz]

(c) $\omega/(2\pi) = 0.60$ [Hz]

(d) $\omega/(2\pi) = 1.00$ [Hz]

Figure 7.11: $\omega_M/2\pi = 0.60[Hz]$

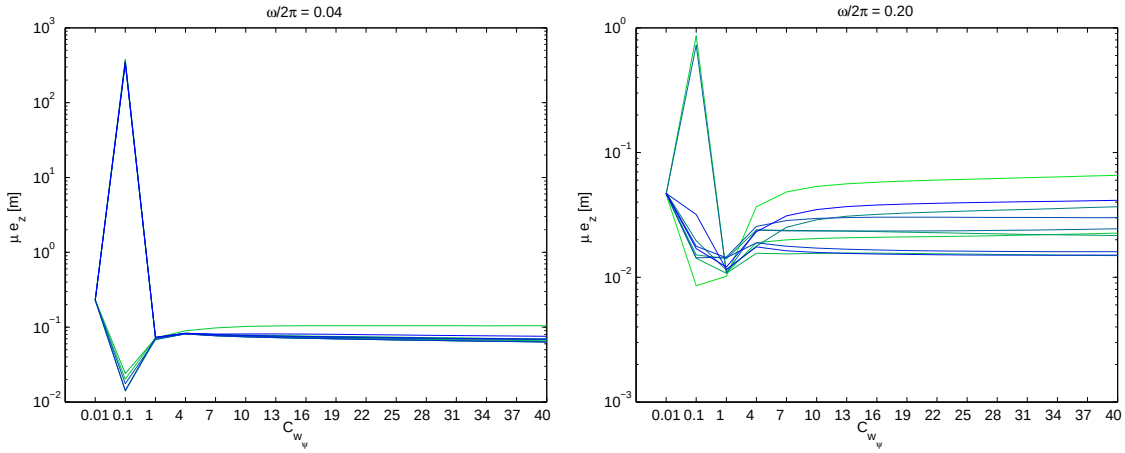

(a) $\omega/(2\pi) = 0.04$ [Hz]

(b) $\omega/(2\pi) = 0.20$ [Hz]

(c) $\omega/(2\pi) = 0.60$ [Hz]

(d) $\omega/(2\pi) = 1.00$ [Hz]

Figure 7.12: $\omega_M/2\pi = 1.00[Hz]$

Amplitude Relation

In addition to ω the wave bias velocity white noise, and by extension the constant C_{w_ψ}, was connected to the wave amplitude. Figure 7.13 shows this relation for a fixed frequency. Possible dependencies to amplitude were investigated but not implemented in the model. A large C_{w_ψ} value produced less accurate estimates for small amplitudes, while a small C_{w_ψ} value resulted in less accurate estimates of large amplitudes.

$C_{w_\psi} = 5$ was found to be a good parameter value with regards to frequency. Since the best C_{w_ψ}-value with regards to amplitude was not as clear, $C_{w_\psi} = 5$ was implemented in WBM2.

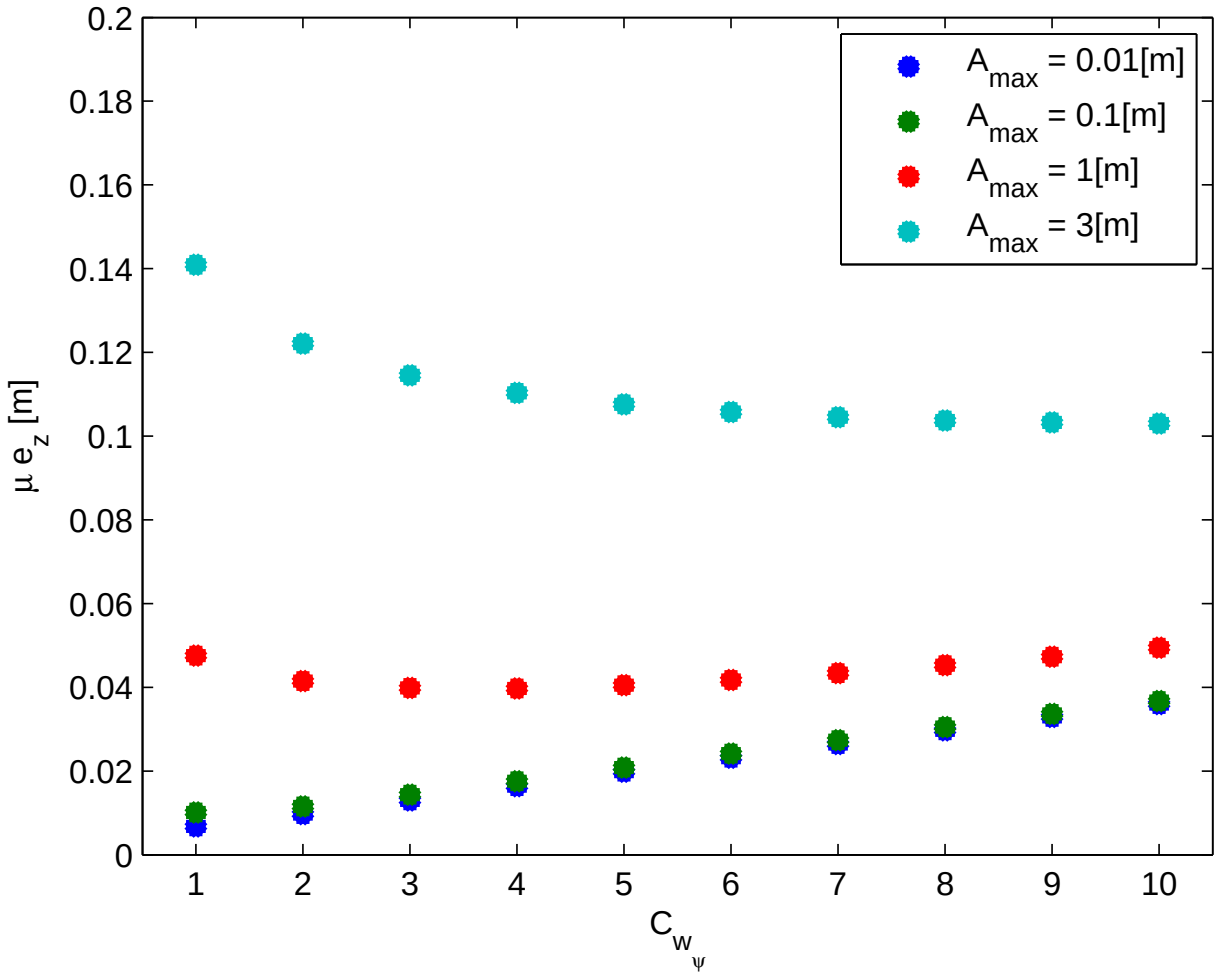

Figure 7.13: Each dot is the mean of 10 MC simulations for different amplitudes and with different values of C_{w_ψ}. All simulations were made with the same wave frequency ω. The figure shows that there is a relation between wave amplitude and C_{w_ψ}.

7.2.3 Test of ω_M

With $C_{w_\psi} = 5$, the performance of WBM2 at different combinations of ω and ω_M is plotted figure 7.14. Each pixel is a single simulation. In figure 7.14a μe_z is shown directly. To increase readability all values above 0.1[m] was set to 0.1[m]. To see whether or not an estimate is truly poor, see figure 7.14b. The color code is such that good estimates (μe_z<0.05[m]) are blue, less good estimates (μe_z>0.05) are colored green and bad/divergent estimates (μe_z>1[m]) are colored brown. These definitions of good and less good estimates are defined to highlight trends in the estimation accuracy. They have no relation with any industry standard.

The performance of WBM2 seems to get increasingly worse with higher wave frequencies, independent of the middle frequency ω_M. In addition an ω_M of less than $0.14 \cdot 2\pi$[rad/s] can cause some poor/divergent estimates. An ω_M larger than $0.60 \cdot 2\pi$[rad/s] gave some suboptimal estimates for low frequencies. All values in between 0.14 and 0.60 [Hz] had a similar performance. Since $\omega_M = 0.20 \cdot 2\pi$[rad/s] gave the most accurate estimates when tuned along with C_{w_ψ} (see table 7.5) it was implemented as thee parameter value of ω_M.

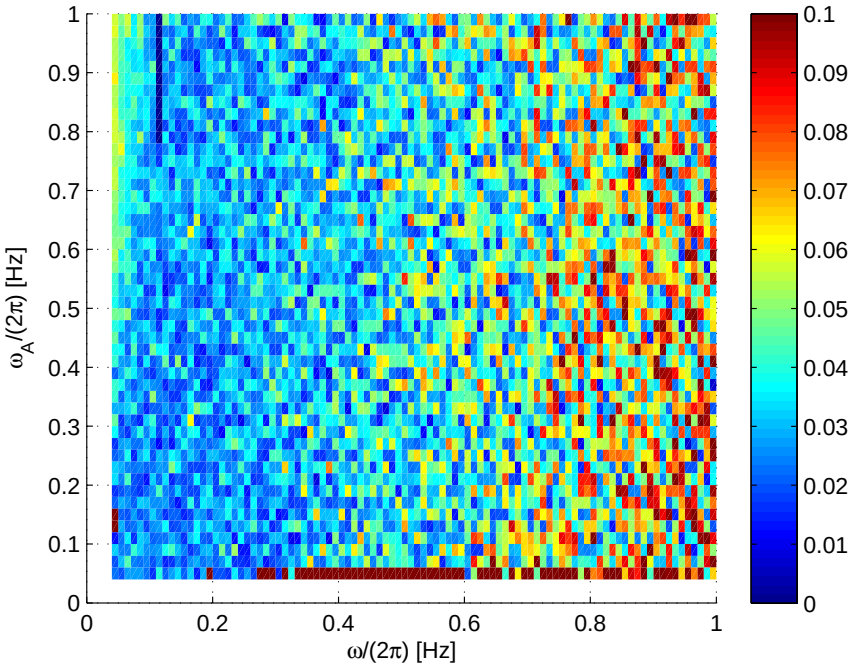

(a) The mean depth error μe_z represented by a color spectrum for values of 0.00-0.10[m]. μe_z>0.1[m] are colored as though they were 0.1[m]

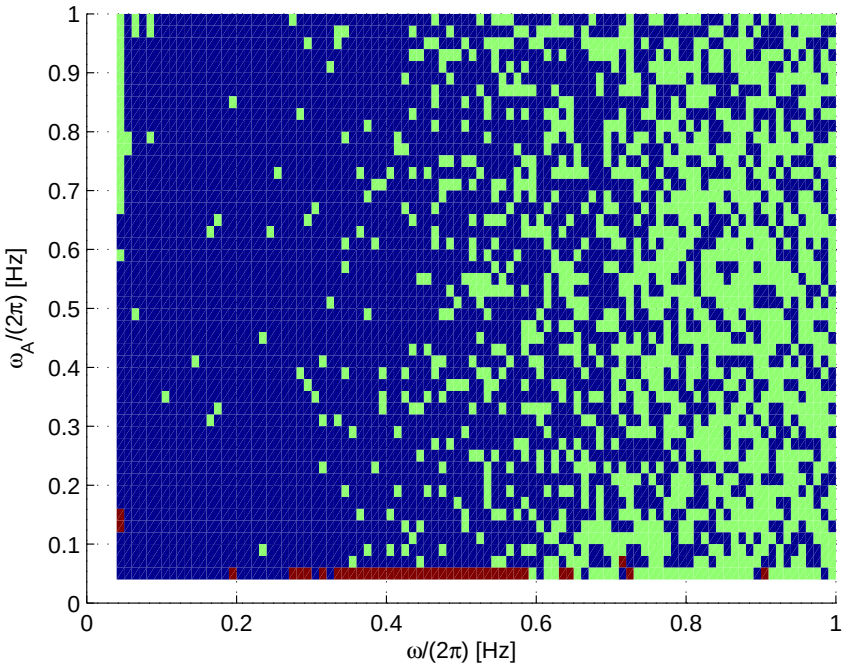

(b) The mean depth error μe_z represented by three colors: Accurate estimates (μe_z<0.05[m]) are blue, less accurate estimates (μe_z<0.05[m]) are green and estimates that deviate (μe_z>1.00[m]) are brown

Figure 7.14: WBM2: μe_z for different ω_M and ω

Chapter 8

WBM2 Performance on Experimental Data

The WBM2 has so far only been tested on simulated data. To verify whether the results generated in chapter 7 have practical implications, the WBM2 was given experimental data as input. This data originated from a previous experiment with an UV. The data represents the output generated by the pressure sensors and accelerometer as the UV was traveling and submerged.

8.1 Simulating the Experimental Data

To evaluate the validity of the simulation model, wave parameters from the experimental data was approximated and integrated in the model. The maximum amplitude A_{max} and the peak frequency ω_P of the experimental data set were approximated. Figure 8.1 show the estimated white noise from a smoothed DGMM on the experimental data. The PSD in figure 8.1b can be considered as a wave frequency spectrum with $\omega_P \approx 0.075 \cdot 2\pi$. The relation between the standard deviation σ and amplitude A of a sinusoidal function is given by:

$$A = \sqrt{2}\sigma \tag{8.1}$$

Since ω_P is so dominant, most of the estimated white noise can be attributed to wave disturbance. Adding estimated wave disturbance Dz to this, and the amplitude is derived: $A_{max} \approx 0.062[m]$. Table 8.1 shows the performance of the different estimators from chapter 5-7. The OGMM and WBM1 are the most accurate models. This is expected since they know the fre-

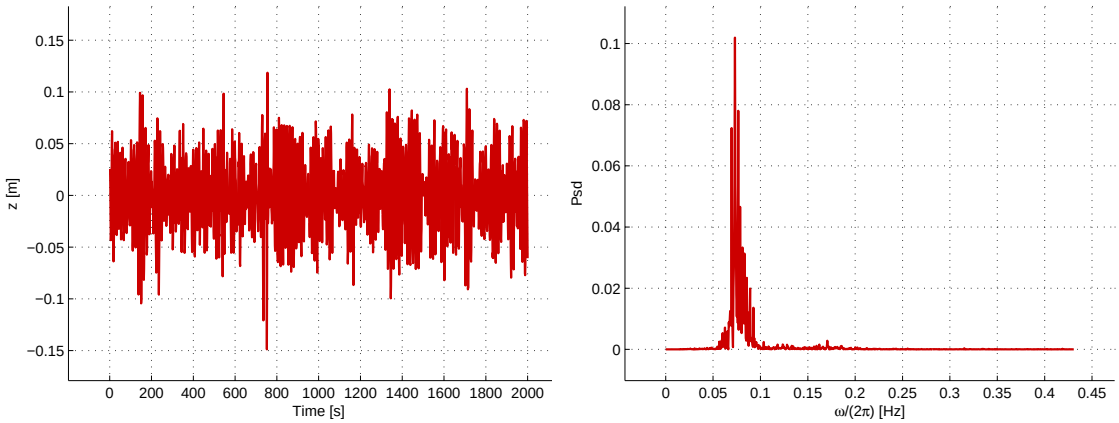

(a) Depth estimated white noise

(b) PSD in depth estimated white noise

Figure 8.1: As shown in this figure, the DGMM wrongly attributes wave induced noise as white noise. The peak wave frequency ω_P and maximum amplitude A_{max} can be approximated from this data.

Table 8.1: Mean estimate error of simulations with amplitude and wave frequency approximated from the experimental data. The values given here are the average of 10 MC simulations.

	μe_z [m]
DGMM	0.029
OGMM	0.009
WBM1	0.006
WBM2	0.020

quency and amplitude. The WBM2 is more accurate than the DGMM, but not to the extent as in figure 7.4. This can be explained by the wave induced noise being a less significant part of the noise since A_{max} is smaller.

8.2 Estimating Experimental Data

One of the benefits of the simulated data is that the true states are known. This is not the case with the experimental data. To evaluate the accuracy of the models, the smoothed estimates were used. However, the smoothed estimates will also differ with each estimator. Table 8.2 illustrates this. Here the real time estimates are compared to the smoothed. Since the WBM1 estimates were the most accurate in the simulated model, it is natural to assume that estimates are better the less they deviate from WBM1 in on the experimental data estimation. The smoothed

Table 8.2: Mean error μe_z between real time estimates and smoothed estimates for different estimators. The unit of μe_z is [m]

		Smoothed			
		DGMM	**OGMM**	**WBM1**	**WBM2**
Real time	**DGMM**	0.0244	0.1411	0.1412	0.1447
	OGMM	0.1375	0.0146	0.0181	0.0425
	WBM1	0.1391	0.0236	0.0116	0.0440
	WBM2	0.1686	0.0981	0.0988	0.0969

WBM1 values could therefore be assumed as true for the purpose of analysis. However, since the WBM1 and WBM2 share the same method of wave bias estimation, it is possible that their estimates will be prone to the same type of errors. In that way a DGMM with equal accuracy as a WBM1 may appear less accurate. For this reason both the OGMM and WBM1 smoothed estimates will be considered when evaluating the accuracy of estimates.

8.3 Results of the Estimation

Table 8.3 contains the values of interest from table 8.2. As seen in table 8.3 the real time estimates by WBM2 are more accurate than those of the DGMM estimates. As seen when comparing table 8.1 with 8.3 the performance of the WBM2 is different when subjected to the experimental data then that of the simulated data. It is therefore of interest to see whether the dynamics are the same for other parameter values.

Table 8.3: Mean error μe_z of real time DGMM and WBM2 compared with Smoothed OGMM and WBM1. The unit of μe_z is [m]

		Smoothed	
		OGMM	**WBM1**
Real time	**DGMM**	0.1411	0.1412
	WBM2	0.0981	0.0988

8.3.1 Tuning Parameters

The parameters of WBM2 as given in table 7.1 are repeated here for the sake of convenience:

1. Middle wave frequency $\omega_M = 0.20 \cdot 2\pi$[rad/s]
2. STD of the white noise of wave frequency $\sigma_{w_\omega} = 10^{-4}$[m]
3. Wave frequency time constant T_ω
4. The constant C_{w_ψ}, relating to the STD of the white noise of the wave bias velocity

The impact of parameters 1-3 can be summed up briefly:

ω_M This parameter is of little influence as long as it is within the defined spectrum of 0.04-1.00 $\cdot 2\pi$ [rad/s]. The same is true ω_0, though the estimates were a little less accurate with higher frequencies. This is in tune with observations on the simulation model, see figure 7.14.

σ_{w_ω} The accuracy is not significantly impacted as long as σ_{w_ω}-values are kept below 0.1 [rad/s].

T_ω For parameter values less than 0.1[s] the estimate deviates. Whether the value is 0.1 or 10^{20}[s] have little effect on the accuracy of the estimates.

Impact of C_{w_ψ}

More could be said about the effect of the constant C_{w_ψ} than the aforementioned WBM2 parameters. The estimate deviate when C_{w_ψ} is less than approximately 0.1. For values larger than 0.1 the mean estimate error μe_z has an almost linear relationship with C_{w_ψ}, see figure 8.2a. With the wave parameter values extracted from the experimental data, the simulation model has similar tendencies. See figure 8.2b.

However, this is not the case for all wave frequencies. In fact, converting figures 7.9-7.12 to arithmetic scale shows that for most frequencies, the relationship is not linear. Figure 8.3 shows how this can vary for different frequencies and different MC simulations.

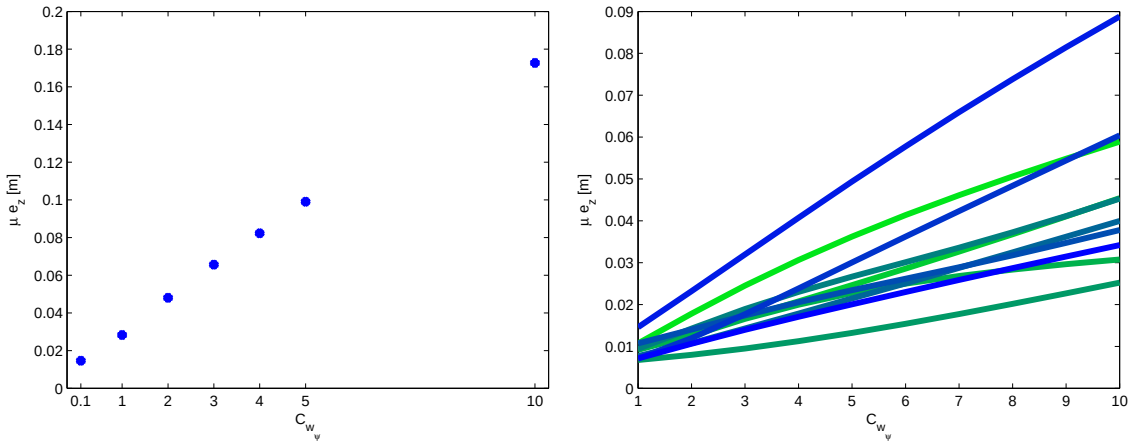

(a) Experimental dataset (b) Simulated data

Figure 8.2: The plots show the mean error in estimates for different values of C_{w_ψ} in the WBM2 estimator. OGMM is used as true state for the experimental data. For the simulated data, each line represent a single MC simulation with, estimated with different C_{w_ψ} values.

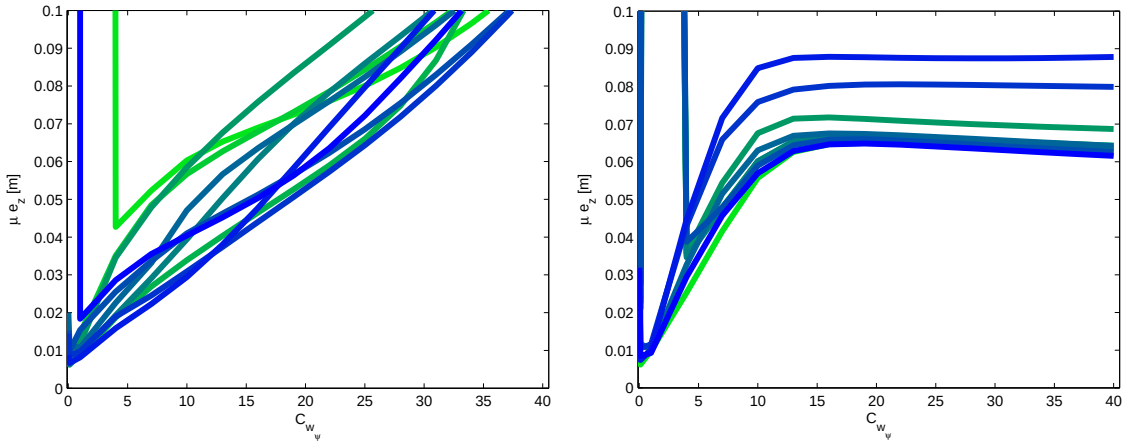

(a) $\omega = 0.04 \cdot 2\pi$[rad/s] (b) $\omega = 0.20 \cdot 2\pi$[rad/s]

Figure 8.3: Wave frequencies relate differently to C_{w_ψ}. These estimates are of the simulation model with the parameters described in chapter 4. The left figure shows a linear relation to C_{w_ψ}

8.3.2 WBM2 Performance

As explained, the only WBM2 parameter that could be tuned for a significant benefit to the accuracy of the estimates was the constant C_{w_ψ}. Table 8.4 shows a comparison between WBM2 estimates for the value derived at in section 7.2.3 (C_{w_ψ}=5) and the best value of C_{w_ψ} based on the tuning that was done on the experimental data. As the innovation of the WBM2 is in the estimation of wave bias Dz and wave frequency ω, these state estimates were compared for the two values of C_{w_ψ}.

In figure 8.4 a comparison is done for ω estimates. $\omega_{true} = 0.075 \cdot 2\pi$ is the peak frequency approximated from the PSD in 8.1b. With $C_{w_\psi} = 0.1$ the true frequency is estimated accurately. That is not the case for $C_{w_\psi} = 5$. Increasing the initial uncertainty, P_0, resulted in negative ω estimates or divergence.

The estimates for Dz are shown in figure 8.5, for $C_{w_\psi} = 5$, and in figure 8.6, for $C_{w_\psi} = 0.1$. The estimates in 8.5 do not resemble waves. From the close up it is apparent that for $C_{w_\psi} = 5$ the bias is only estimated during the measurement updates. The Dz estimates in figure 8.6, however, much more resemble waves. For that reason the Dz estimates for $C_{w_\psi} = 0.1$ can be compared to those of the OGMM and WBM1.

The standard deviation of the estimated Dz is 0.0160[m] for WBM2 with $C_{w_\psi} = 0.1$. For smoothed OGMM and WBM1, the STD of Dz is respectively 0.0339[m] and 0.0414[m]. This suggests that there is room for improvement in the Dz estimates. However, the DGMM estimated Dz has a STD of 0.002[m], compared to which the Dz estimates of the WBM2 is much more accurate.

Table 8.4: Mean error μe_z of real time DGMM and WBM2 compared with Smoothed OGMM and WBM1. WBM2 estimates are given for two values of C_{w_ψ}. The unit of μe_z is [m]

			Smoothed	
			OGMM	**WBM1**
Real time	**DGMM**		0.1411	0.1412
	WBM2	$C_{w_\psi} = 5$	0.0981	0.0988
		$C_{w_\psi} = 0.1$	0.0146	0.0134

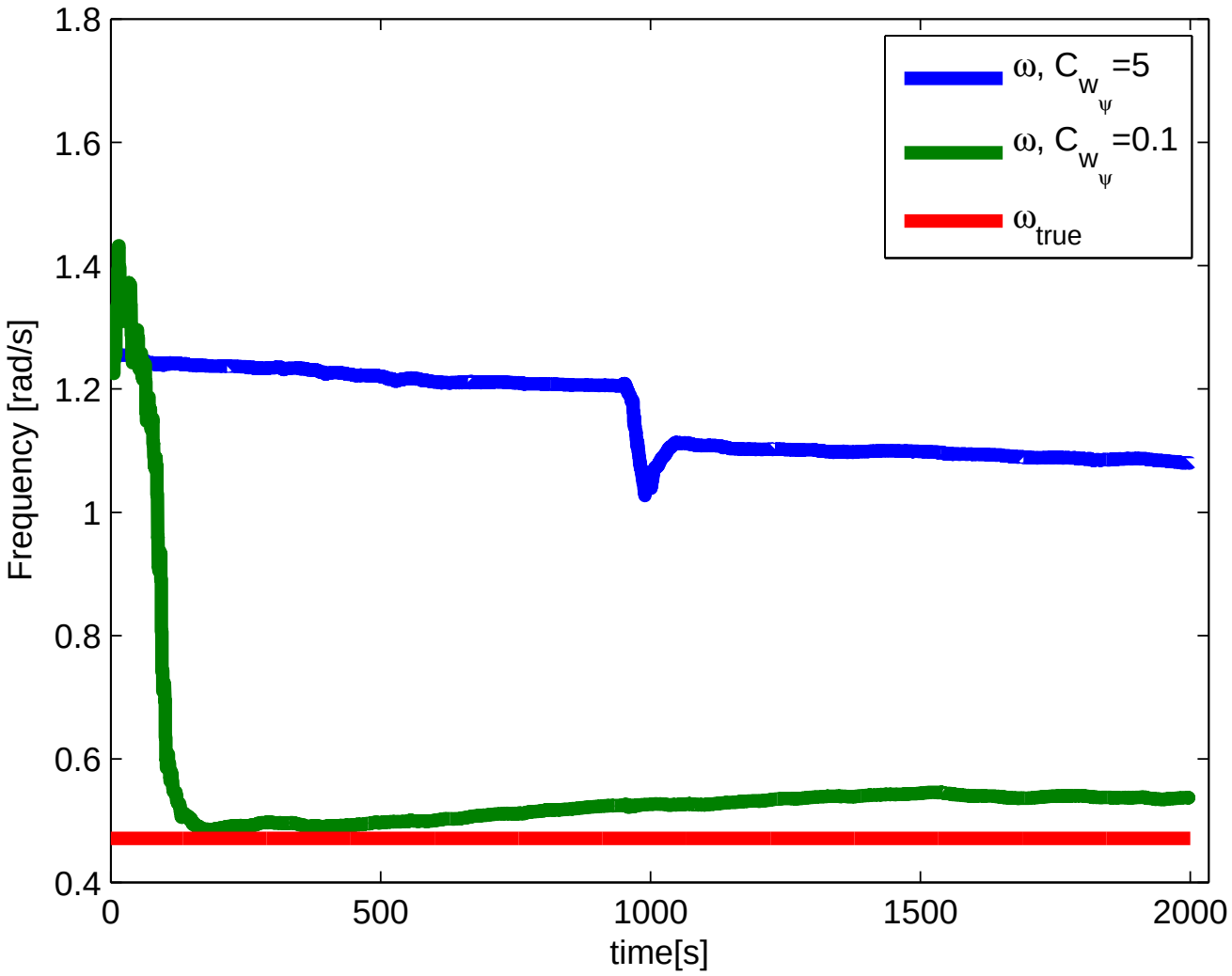

Figure 8.4: Estimation of wave frequency with different values for C_{w_ψ}. ω_{true} is an approximate value.

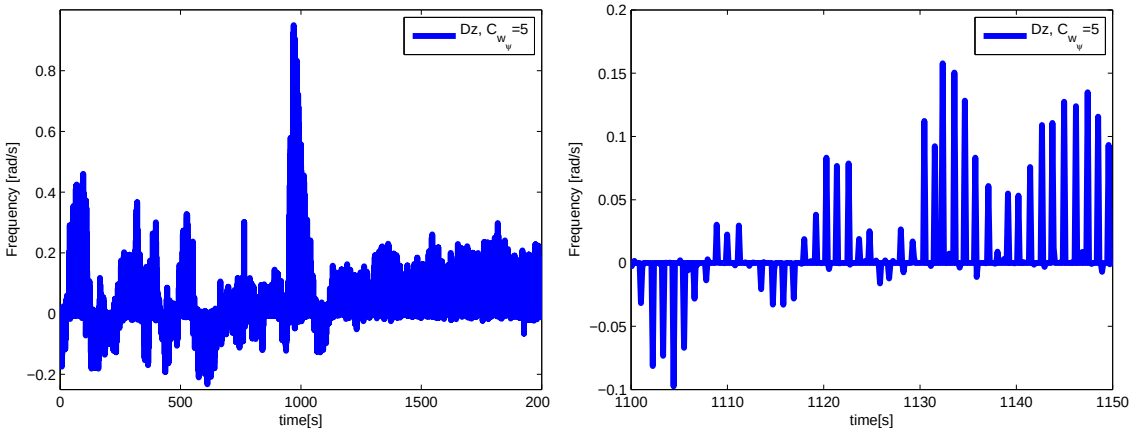

Figure 8.5: Wave bias estimate for WBM2 with $C_{w_\psi} = 5$. The figure to the right is a close up of the figure to the left.

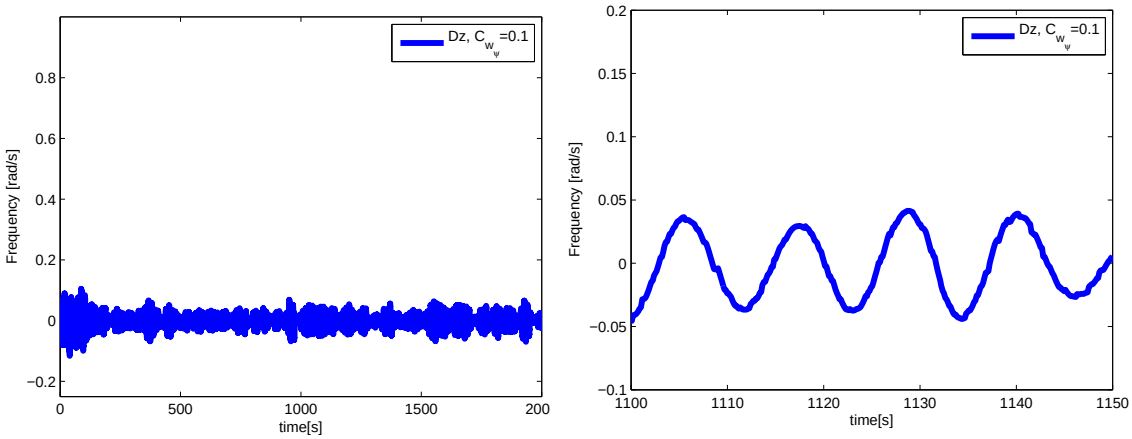

(a)

Figure 8.6: Wave bias estimate for WBM2 with $C_{w_\psi} = 5$. The figure to the right is a close up of the figure to the left.

Chapter 9

Summary and Recommendations for Further Work

9.1 Summary and Conclusions

Accurate real time depth approximation is important for navigation of and mapping by underwater vehicles (UV). Wave induced noise can cause a bias in the depth sensor of UVs. To improve the accuracy of depth measurements an estimator algorithm called Kalman Filter (KF) is applied. For the KF to produce accurate estimates it must have an accurate mathematical model of the noise. Previous work has demonstrated the benefit of modeling the wave induced noise as an oscillatory process, but came short of a model that could be implemented in real time estimation. The objective of this rapport was to develop such an oscillatory model that could be used in real time.

This model should not depend on prior knowledge of wave parameters, and should be able to estimate the noise contribution of most types of waves. A simulation model was therefore developed in chapter 4, so that the estimator model could be tested on different waves. The waves were simulated as single sinusoidal waves.

In chapter 5 an industry field tested model was introduced. With default parameter values, it was called *Default Gauss Markov Model* (DGMM). Based on prior knowledge of the wave parameters, the more accurate *Optimized Gauss Markov Model* was developed. Both models estimated data generated by the simulation model. This created a point of reference when it came to ac-

curacy, the DGMM being the minimum requirement for the oscillatory real time model. The estimations also uncovered some wave simulation difficulties regarding sinusoidal waves. The problem was solved by increasing the sampling frequency of the pressure sensor.

An estimator model with an oscillatory wave bias model was used as a base for the development of the oscillatory real time model. This model was dependent on prior knowledge of the frequencies of the waves it estimated. The base model was called *Wave Bias Model 1* (WBM1) and the oscillatory real time model was called *Wave Bias Model 2* (WBM2). In chapter 6 the WBM1 was introduced and tested on the simulated data.

The WBM2 was developed in chapter 7. There were two major differences from WBM1:

1. An extra state, wave frequency, was estimated.

2. The white noise in the wave bias process was given as a function of the wave frequency.

Compared to DGMM the wave bias produced more accurate estimates for all relevant true wave frequencies. The OGMM was more accurate for high frequencies, but less accurate for low frequencies.

In chapter 8, as a final test, the WBM2 was implemented on a set of real data from an experiment with an UV. Smoothed estimates of OGMM and WBM1 were treated as true state. With the parameter values arrived at in chapter 7, the WBM2 was able to produce more accurate depth estimates than DGMM. However, on further inspection the estimates of wave bias and wave frequency were quite poor. By reducing the noise in the wave bias process much more accurate estimates for depth, wave frequency and wave bias were obtained.

In conclusion, it seems likely that a real time oscillatory model with accurate depth estimates could be developed. Whether the WBM2 is such a model would require further testing.

9.2 Discussion

There are some clear limitations to the wave modeling. For instance, the wave bias in the simulation model is dependent on a dominant peak frequency. In a developing or decaying sea, several wave frequencies can be prominent. The presence of swells were also not considered.

Little emphasis was put on finding the best possible parameter values for WBM2. Test frequencies were used to describe the entire peak frequency spectrum. This simplification might have given a false or incomplete understanding of some parameter dynamics.

One parameter dynamic that was not well covered was the process wave bias white noise. This parameter was essential for accurate estimates. Too low values could sometimes cause the estimate to diverge. The mechanics of this divergence were not investigated.

In section 7.2.2 it was explained that some of the most accurate estimates were done with a small C_{w_ψ} values. However, these estimates also tended to diverge. The accurate WBM2 model in section 8.3.2 might therefore not be robust.

Another aspect of the estimates presented in 8.3.2 is that they are performed on a low frequency wave. As shown in figure 7.4 the WBM2 is more accurate on low frequencies, while the DGMM is more accurate on high frequencies. It is possible that the DGMM would have produced more accurate estimates than WBM2 if the wave frequency was higher.

The process model of the WBM2 is linearized. However, equation 7.11 for the process of the wave bias white noise is not linear. This conflicts with one of the requirements for an optimal Kalman Filter estimate.

9.3 Recommendations for Further Work

As an extension to the work presented in this rapport, I suggest the following investigations:

- Develop an oscillatory process model with multiple frequencies, possibly a frequency spectrum. Such a model might perform better for developing or decaying sea.
- The white noise of the wave bias velocity process proved crucial for the accuracy of the WBM2 estimates. A more thorough study into the parameters of this noise could result in a better estimator model. Among the things that should be investigated is the noise relation to wave frequency and amplitude.
- The models presented in figure 7.4 show that the Gauss markov models were better at high frequencies, while the wave bias models performed better at low frequencies.

- Figure 6.8 show that for wave data generated from the simulation model, WBM1 produces more accurate estimates than DGMM for all assumed frequencies within the peak frequency spectrum. I suggest a researching whether this is true for all real waves as well.

Appendix A

Acronyms and symbols

A.1 Acronyms

AINS Aided Inertial Navigation System

AUV Autonomous Underwater Vehicle

CKF Continuous Kalman Filter

DGMM Default Gauss-Markov Model

DKF Discrete Kalman Filter

ESKF Error State Kalman Filter

EKF Extended Kalman Filter

GPS Global Positioning System

GMM Gauss-Markov Model

GWN Gaussian White Noise

IMU Inertial Measurement Unit

INS Inertial Navigation System

JONSWAP Joint North Sea Wave observation Project

LRWM Linear Random Wave Model

LTI Linear Time Invariant

MCS Monte Carlo Simulation

MPD Mean Propagation Direction

OGMM Optimized Gauss-Markov Model

PDF Probability Density Function

PFS Peak Frequency Spectrum

PSD Power Spectral Density

ROV Remotely Operated Vehicle

SDGMM Smoothed Default Gauss-Markov Model

SOGMM Smoothed Optimized Gauss-Markov Model

STD Standard Deviation

TERT Total Error Real Time

TES Total Error Smooth

TF Test Frequencies

TME Total Measurement Error

UV Underwater Vehicle

WBM Wave Bias Model

WFS Wave Frequency Spectrum

A.2 Latin Symbols

A Wave amplitude

A_{max} Amplitude of the most significant frequencies.

b Accelerometer bias [m/s^2]

dz Depth error [m]

Dz Wave bias [m]

e_z Depth error [m]

f Frequency [Hz]

H_s Significant wave height

T Time constant [s]

v Depth velocity [m/s]

z Depth [m]

z_E Depth estimate

A.3 Greek Symbols

β Propagation Direction [rad]

μ Mean

ω_M Middle wave frequency [rad/s]

ω_E Estimated wave frequency [rad/s]

ω Wave frequency [rad/s]

ψ Wave bias velocity [m/s]

σ_z Modeled standard deviation in Depth [m]

Bibliography

(2012). Modelling and analysis of marine operations. Technical report, Det Norske Veritas.

(2017).

Brown, R. G. and Hwang, P. Y. C. (2012). *Introduction to Random Signals and Applied Kalman Filtering*. John Wiley & Sons, Inc.

Chen, C. T. (2013). *Linear System Theory and Design*. Oxford University Press.

Copley, J. (2014). Just how little do we know about the ocean floor? *The Conversation*.

Dunbar, B. (2007). Venus: Full view by magellan spacecraft. Technical report, North American Space Agency.

Gade (1997). Integrering av treghetsnavigasjon i en autonom undervannsfarkost. *Forsvarets Forskningsinstitutt*.

Gade, K. (2004). Navlab, a generic simulation and post-processing tool for navigation. *European Journal of Navigation*.

Grammont, L., Ahues, M., and D'Almeida, F. D. (2014). For nonlinear infinite dimensional equations, which to begin with: Linearization or discretization? *JOURNAL OF INTEGRAL EQUATIONS AND APPLICATIONS*.

Haaland, E. A. (2016). Modelling and estimation of ocean wave induced error in pressure measurement. Contact Haaland at eirik.a.haaland@gmail.com for access to document.

Hagen, O. K. and Jalving, B. (2017). Converting pressure to depth for underwater vehicles.

Olsen, O. A. (2015). *Industrielle Målemetoder*. Jubok As.

Stewart, R. H. (1997). *Introduction To Physical Oceanography*. Texas A & M University.

Techet, A. (2005). 13.42 design principles for ocean vehicles.

Thomson, R. E. and Emery, W. (2014). *Data Analysis Methods in Physical Oceanography*. Elsevier Science B.V.

Vik, B. (2014). Integrated satellite and inertial navigation systems.

Willumsen, A. B., Hagen, O. K., and Boge, P. N. (2007). Filtering depth measurements in underwater vehicles for improved seabed imaging.

Willumsen, A. B. and Hegernæs, y. (2009). The joys of smoothing.